



POLITECNICO
MILANO 1863

POLITECNICO DI MILANO

SCHOOL OF INDUSTRIAL AND INFORMATION ENGINEERING

MASTER'S DEGREE COURSE (LAUREA MAGISTRALE) IN
ENERGY ENGINEERING

**Design of Swept Wind Turbine Blades
for Passive Load Alleviation**

Master's Thesis

Supervisor:

Prof. Vincenzo DOSSENA, Politecnico di Milano

Author:

Alessandro ARTONI

Matr. 836652

Co-supervisor:

Prof. Filippo SPERTINO, Politecnico di Torino

External Supervisors:

Prof. Carlo L. BOTTASSO, TU München

M.Sc. Pietro BORTOLOTTI, TU München

Academic Year 2015 - 2016

STATEMENT OF AUTHORSHIP

I, Alessandro Artoni, confirm that the work presented in this thesis has been performed and interpreted solely by myself except where explicitly identified to the contrary. All verbatim extracts have been distinguished by quotation marks, and all sources of information have been specifically acknowledged. I confirm that this work has not been submitted elsewhere in any other form for the fulfillment of any other degree or qualification.

Milan, November 2016

SUMMARY

The success of renewable energy is driven by the development of innovative technologies that lower the cost of energy. Nowadays, thanks to the significant investments in R&D of the last few decades, wind power is already among the cheapest sources for electricity generation in many countries. The size of wind turbines has been constantly growing, with always larger rotors and higher towers in order to gain in energy harvesting capability and reduce the cost of energy, which is the most appropriate figure of merit when it comes to providing a competitive electricity generation from wind. However, machines of larger scale are subjected to relevant deformations and loads, thereby resulting in the need to increase the stiffness and mass of the turbine structural components.

One of the most studied topics in recent years is concerned with the development of advanced rotor control concepts that allow to mitigate the substantial forces and moments acting on the machine. The methods for load reduction can be categorized into two main families: active and passive. In particular, passive load mitigation techniques consist in designing structures that, when loaded, are able to adaptively deform so as to induce a load relief. This Master's thesis focuses on one of these passive methods, namely the swept blades concept, and its potential application on multi-MW wind turbines.

Sweep basically refers to the edgewise displacement of the blade outboard region in the plane of rotation. The adaptive structural behavior is based on bend-twist coupling effects that produce variations in the twist distribution as the blades bend due to aerodynamic loads, leading to a reduction in the angle of attack, hence resulting in lower loads. This technique enables a faster response to changes in wind conditions compared to the traditional pitch system and allows for a significant alleviation of both extreme loads and fatigue damage, thereby offering the possibility to use lighter and more flexible rotors.

The study begins with the parametrization of the sweep curve, which is characterized by three main variables: the distance of blade tip to the pitch axis, the starting position of the sweep curvature along the blade span, and the curve exponent. A preliminary sensitivity analysis is conducted to observe the impact of each sweep parameter on the main design factors. The most sensitive parameter is found to be the first one mentioned above, namely tip sweep; thus, major changes in the blade curvature have been applied mostly by varying this quantity.

Moreover, it is demonstrated that only backward sweep produces the desired load reduction, whereas forward sweep results in the increase of loads since the blades tend to twist to stall during operation, hence they are not interesting for load alleviation purposes. Therefore, the present work investigates the potential of backward swept blades only.

A more general sweep equation is introduced so as to consider the possibility of adding a certain extent of forward sweep in the inboard sections of the blade, thus creating a so-called boomerang shape. This advanced curvature is expected to make the blades more aeroelastically balanced and restrain the inherent increase in blade torsion deriving from sweep.

The potential benefits of this passive load alleviation technique are assessed for two different applications: a 2 MW onshore wind turbine and a 10 MW offshore conceptual machine.

Few studies in the literature investigate the impact of introducing sweep in the blade design process, but according to the author's knowledge, a full redesign of swept wind turbine rotors is still missing in the research.

In this thesis, a multidisciplinary design tool specifically developed for wind applications, called **Cp-Max**, has been used to perform the optimized design of wind turbines. The integrated code is built around the high-fidelity aero-servo-elastic simulator **Cp-Lambda** in a MATLAB environment and automatically interfaces with several other softwares. **Cp-Max** allows for the simultaneous optimization of both aerodynamic and structural aspects of the rotor, with the ultimate goal of finding the configuration that minimizes the cost of energy. All relevant design constraints, such as the ones related to frequency placement and maximum tip deflection for tower clearance, are taken into account throughout the optimization process, and control laws are updated at every iteration.

Two cost of energy models have been considered to account for the very different applicability range of the analyzed machines. The NREL cost model has been adopted for the 2 MW onshore wind turbine, whereas the INNWIND model is used for the offshore one. Parallel to the two cost models, a more detailed blade cost model has been implemented in the code to better account for the aero-structural trade-offs of the rotor, especially dividing blade cost into three terms considering material, labor, and equipment expenses.

Several corrections have been made to the MATLAB routines dedicated to the elaboration of geometric data in order to introduce the sweep curvature into **Cp-Max**, which can now simulate complex blade shapes including sweep and prebend simultaneously. Moreover, since the code had not been used to study swept blades before, it originally kept a fixed blade length instead of a constant rotor radius. Therefore, this feature has been modified to maintain the same rotor swept area for all the simulated configurations, which also allows to limit the inherent loss in annual energy production that occurs when sweeping the blades, due to the reduced angle of attack that drives load alleviation.

Swept blades are first applied to the 2 MW onshore wind turbine. The study begins with a detailed load analysis to understand the load reduction potential for different sweep curvatures, including boomerang-shaped blades. At this stage, only the effects on ultimate loads and fatigue are taken into account, without evaluating the consequences on power output and cost of energy. Hence, a full redesign of the machine is conducted using a **Cp-Max**, integrating the aerodynamic optimization of the twist distribution and the structural sizing loops so as to obtain the optimal configuration for each swept rotor. A reduced set of design load cases has been considered for the dynamic simulations, in order to take into account the most relevant situations that the machine is going to experience during its lifetime, following the standard certification guidelines.

Results show that operational loads can be effectively mitigated, leading to relevant blade mass reduction with respect to the unswept rotor with the same diameter. Generally, greater relief is achieved for larger tip sweep. However, the drop in blade cost is more limited and counterbalanced by losses in energy production below rated conditions, resulting in a slightly higher cost of energy when adding sweep. Furthermore, swept blades induce an inherent increase in torsional moments at the blade root, which can be successfully restricted by adding forward sweep in the inner sections of the blade, provided that the boomerang shape is properly designed.

The analysis of the 2 MW machine continues with the design optimization of larger rotors, showing that in this case using sweep may entail some benefits, since it is possible to gain in energy capture capability due to the expanded swept area for the same power rating, while maintaining similar blade mass and loads to the original wind turbine thanks to the passive load alleviation. It is observed that this method can lead to a reduced cost of energy, provided that such a complex shape does not imply particular issues in the blade manufacturing process.

Ultimately, the choice of a larger wind turbine rotor mainly depends on the design margins and requirements for the specific machine.

An initial investigation on the possible combination of sweep with prebend has also been conducted, as swept-prebent blades are expected to produce very light and flexible structures thanks to the load mitigation originating from sweep and the increased margin in tower clearance obtained with prebend.

Lastly, swept blades are tested on a large 10 MW conceptual machine, which is representative of the future generation offshore wind turbines. Initial results from the design optimization of a reduced set of swept configurations show that load reduction is more limited on this machine, especially for extreme loads, and no relevant blade mass reduction is observed.

The study on this offshore machine is still at a preliminary phase and there is a great need to investigate further the actual benefits from load alleviation with swept blades on large scale wind turbines, as well as the effects on power production losses and the overall impact on cost of energy.

La diffusione delle energie rinnovabili è guidata dallo sviluppo di tecnologie innovative che permettono di ridurre il costo dell'energia. Grazie agli importanti investimenti in ricerca e sviluppo degli ultimi anni, l'energia eolica è già oggi una delle forme più economiche di generazione elettrica in diversi paesi. La dimensione delle turbine ha subito un costante aumento, con rotori sempre più grandi e torri sempre più alte, che consentono di guadagnare in produzione di potenza e di ridurre il costo dell'energia; quest'ultimo parametro è la grandezza più adeguata da considerare per garantire la competitività dell'energia eolica. Tuttavia, macchine più grandi sono soggette a carichi e deformazioni maggiori, che rendono necessario un aumento in rigidità e peso dei componenti strutturali della turbina.

Uno dei temi più studiati nella ricerca recente concerne lo sviluppo di sistemi di controllo avanzato del rotore, che permettano di mitigare le ingenti forze cui la macchina è sottoposta. I metodi di riduzione dei carichi possono essere classificati in due principali gruppi: attivi e passivi. Le tecniche di controllo passivo, in particolare, consistono nel progettare strutture che si deformano quando sono soggette a carichi, adattando la propria forma a seconda delle condizioni operative e permettendo così di alleviare gli sforzi sulle pale. Questa tesi di laurea magistrale si concentra su uno di questi metodi passivi, ossia l'utilizzo di pale curve dette *sweep blades*, e studia la loro potenziale applicazione su aerogeneratori di grande taglia.

Con *sweep* si intende essenzialmente il dislocamento laterale della regione più esterna della pala all'interno del piano di rotazione. Il comportamento strutturale passivo è dato da effetti di accoppiamento flessio-torsionale, che producono variazioni nella distribuzione dell'angolo di twist lungo la pala, quando questa è sottoposta a carichi aerodinamici. Il risultato è una diminuzione dell'angolo d'attacco, che conduce a sua volta a carichi minori. Questa tecnica permette alla macchina di reagire più velocemente ai cambiamenti nelle condizioni del vento rispetto al sistema tradizionale di controllo di pitch, e può portare a benefici significativi in termini di riduzione dei carichi ultimi e della fatica dei componenti, offrendo quindi la possibilità di utilizzare rotori più leggeri e flessibili.

Lo studio ha inizio con la parametrizzazione della curva di *sweep*, che è caratterizzata da tre principali elementi: la distanza tra la punta di pala e il suo asse longitudinale, la coordinata radiale in corrispondenza della quale la pala inizia a inclinarsi e l'esponente della curva. Un'analisi di sensitività preliminare è stata poi condotta per osservare l'effetto dei vari parametri di *sweep* su alcune importanti variabili progettuali, da cui si può concludere che il parametro con il maggiore impatto è il primo di quelli descritti sopra, ossia il cosiddetto *tip sweep*. Per questo motivo, nel corso dello studio, la curvatura delle pale è stata modificata soprattutto cambiando questo parametro.

Viene dimostrato, inoltre, che solo una curvatura diretta verso il bordo di uscita della pala (*backward sweep*) produce gli effetti desiderati di riduzione dei carichi, mentre un'inclinazione della pala verso il bordo d'attacco (*forward sweep*) produce un aumento degli sforzi, a causa dell'anticipazione delle condizioni di stallo dovuta all'aumento dell'angolo di attacco, quindi non è interessante ai fini di alleviamento dei carichi. Perciò, lo studio si è concentrato solo sul potenziale di pale con *backward sweep*.

È stata poi definita un'equazione di curvatura più generale, che renda possibile aggiungere una certa quantità di *forward sweep* nella parte più vicina alla base di pala, creando dunque una cosiddetta forma “a boomerang”. Ci si aspetta che tale curvatura avanzata permetta di ottenere una pala più bilanciata in termini aeroelastici, al fine di ridurre l'inevitabile aumento dei momenti torsionali che avviene curvando le pale.

I potenziali benefici di questa tecnica di riduzione passiva dei carichi sono quindi analizzati per due diverse applicazioni: una turbina onshore da 2 MW e una macchina offshore da 10 MW, ancora in fase di studio. Solo alcune ricerche presenti in letteratura si occupano di analizzare le conseguenze dovute allo *sweep* nel processo di progettazione dei rotori eolici, ma una completa riprogettazione delle turbine con tali pale ricurve ancora non è disponibile, per quanto l'autore ne sia a conoscenza.

In questa tesi, il design ottimizzato degli aerogeneratori è stato eseguito con un codice di progettazione multidisciplinare, chiamato **Cp-Max**, specificatamente sviluppato per applicazioni in campo eolico. Questo codice è stato sviluppato su MATLAB e si basa sul simulatore aero-servo-elastico **Cp-Lambda**, oltre ad interfacciarsi automaticamente con diversi altri software. **Cp-Max** permette di effettuare simultaneamente un'ottimizzazione sia aerodinamica che strutturale del rotore, con lo scopo finale di trovare la configurazione che corrisponde al minimo costo dell'energia. Tutti i vincoli di progettazione, quali la massima deflessione della punta della pala per evitare il contatto con la torre e i vincoli di frequenza contro la risonanza, sono verificati durante l'intero processo di ottimizzazione, mentre le leggi di controllo sono aggiornate ad ogni iterazione.

Differenti modelli di costo dell'energia sono stati considerati per le due macchine analizzate, dal momento che esse operano in campi di applicazione molto diversi. Per l'aerogeneratore onshore è stato utilizzato il modello di costo NREL, mentre per la turbina offshore si adotta il modello INNWIND. In aggiunta, un modello di costo della pala più dettagliato è stato implementato nel codice di ottimizzazione per tenere conto di tutti gli aspetti aero-strutturali del rotore; in particolare, questo modello divide i costi in tre voci: materiali, manodopera e attrezzatura.

Diverse correzioni alle funzioni MATLAB del codice si sono rivelate necessarie per introdurre in maniera corretta la curva di *sweep* nei dati geometrici della pala. Ora **Cp-Max** è in grado di simulare forme rotoriche complesse, potenzialmente includendo sia *sweep* che *prebend* allo stesso tempo. Il codice non era mai stato usato prima per studiare le *swept blades*, quindi inizialmente considerava costante la lunghezza di pala invece di mantenere fisso il raggio del rotore. Perciò, quest'ultima caratteristica è stata modificata per mantenere la stessa area spazzata in tutte le configurazioni, permettendo oltretutto di limitare l'inevitabile perdita in energia prodotta che avviene quando si curvano le pale, a causa della riduzione dell'angolo di attacco.

Le *swept blades* sono quindi state testate sulla turbina onshore da 2 MW. Lo studio comincia con un'analisi dettagliata dei carichi per stimare il potenziale di riduzione degli stessi attraverso diverse curvature di pala, incluse le più complesse pale “a boomerang”. In questa fase sono stati analizzati solo gli effetti sui carichi ultimi e sulla fatica, senza valutare le conseguenze in termini di potenza prodotta e costo dell'energia. A partire da questi risultati, è stata condotta una completa riprogettazione della macchina con **Cp-Max**, integrando l'ottimizzazione aerodinamica dell'angolo di twist con il ridimensionamento dei componenti strutturali, con l'obiettivo di trovare la configurazione ottimale di ogni rotore. Per le simulazioni dinamiche è stato considerato un set ridotto di DLC (*Design Load Cases*), per tenere conto delle situazioni progettuali più rilevanti che possono avere luogo nella vita di una turbina eolica.

I risultati ottenuti mostrano che i carichi operativi possono essere alleviati in modo sostanziale, portando ad una rilevante riduzione di peso rispetto alla configurazione di riferimento, che consiste nel rotore con le pale dritte e lo stesso diametro. Si nota che, generalmente, una maggior diminuzione dei carichi avviene per *tip sweep* più grandi.

Tuttavia, la riduzione dei costi di pala è meno marcata e viene controbilanciata da una perdita in capacità di generazione di potenza, che produce un costo dell'energia leggermente più elevato per rotori con *swept blades*. Inoltre, la curvatura delle pale comporta un aumento dei carichi torsionali, che però può essere efficacemente limitato aggiungendo *forward sweep* nelle sezioni più vicine alla base, a condizione che la forma “a boomerang” venga progettata in modo adeguato.

L'analisi dell'aerogeneratore da 2 MW prosegue con la progettazione ottimizzata di rotori più grandi, dimostrando che, in questo caso, l'uso delle *swept blades* può risultare vantaggioso, dal momento che è possibile incrementare l'energia prodotta grazie alla maggiore area spazzata, al tempo stesso mantenendo carichi simili rispetto alla configurazione originale per mezzo dello *sweep*. Si osserva poi che questo metodo può portare ad un costo dell'energia minore, a patto che una forma più complessa delle pale non presenti particolari problematiche durante il processo di fabbricazione. In ogni caso, la scelta finale per un rotore più grande dipende fundamentalmente dai margini di progettazione e dai requisiti della specifica macchina.

La possibile combinazione dello *sweep* con il *prebend* viene quindi valutata attraverso uno studio preliminare, dal momento che una pala caratterizzata da entrambe queste caratteristiche potrebbe produrre una struttura molto leggera e flessibile, grazie alla riduzione dei carichi dovuta allo *sweep* e al maggior margine nella distanza torre-pala legata al *prebend*.

Infine, le *swept blades* sono state testate su un aerogeneratore da 10 MW, rappresentativo delle turbine offshore di futura generazione. I risultati ottenuti dalla progettazione ottimizzata di un numero ridotto di configurazioni rotoriche mostrano che questa macchina presenti possibilità di riduzione dei carichi più limitate, soprattutto per quanto riguarda i carichi ultimi, e non rivelano particolari vantaggi in termini di peso delle pale.

Lo studio della turbina eolica offshore è ancora in una fase preliminare ed è necessario investigare in modo più approfondito gli effettivi benefici derivanti dallo *sweep* sull'alleviamento dei carichi, così come gli effetti sulle perdite in produzione di potenza e l'impatto finale sul costo dell'energia.

CONTENTS

1	Introduction	1
1.1	Background	1
1.2	Project motivations and goals	1
1.3	Report structure	1
2	Wind turbine technology	3
2.1	Wind power	3
2.2	Horizontal-axis wind turbines	6
2.2.1	The power performance curve	7
2.3	Wind turbine loads	9
2.3.1	Damage equivalent load	10
2.3.2	The Campbell diagram	11
2.3.3	Design load cases	12
3	Load alleviation techniques	15
3.1	Active load alleviation methods	16
3.1.1	Individual pitch control	16
3.1.2	Variable diameter rotor	16
3.1.3	Active flow control	17
3.2	Passive load alleviation methods	18
3.2.1	Bend-twist coupled blades	18
3.2.2	Combined load alleviation concepts	20
3.3	Swept blades	21
3.3.1	Sweep curve parametrization	22
3.3.2	Backward vs. forward swept blades	23
3.3.3	Preliminary sensitivity analysis	24
4	Wind turbine design algorithm	27
4.1	Integrated optimization of wind turbines	27
4.2	Aero-servo-elastic simulator	28
4.3	General code structure	30
4.3.1	Aerodynamic optimization	31
4.3.2	Structural optimization	32
4.3.3	Global sizing	33
4.4	Cost of energy models	34
4.5	Code modifications to account for sweep	37
5	2 MW wind turbine	41
5.1	Baseline wind turbine	41
5.2	Detailed load analysis	44
5.2.1	Maximum tip displacement	44
5.2.2	Ultimate loads	45

5.2.3	Fatigue loads	46
5.2.4	Conclusions of the load analysis	47
5.3	Design optimization	48
5.3.1	Optimal twist distribution	48
5.3.2	Ultimate loads	49
5.3.3	Fatigue loads	50
5.3.4	Design constraints analysis	51
5.3.5	CoE comparison	51
5.3.6	Conclusions of the design optimization	52
5.4	Larger rotor design	53
5.4.1	Ultimate loads	53
5.4.2	Fatigue loads	53
5.4.3	CoE comparison	55
5.4.4	Comparison with larger unswept rotor	56
5.5	Combined swept-prebent rotor design	57
6	10 MW wind turbine	59
6.1	Baseline wind turbine	59
6.2	Design optimization	61
6.2.1	Ultimate loads	61
6.2.2	Fatigue loads	61
6.2.3	CoE comparison	63
6.2.4	Conclusions of the design optimization	63
7	Conclusion	65
7.1	Outlook	66
	List of Figures	67
	List of Tables	69
	Bibliography	71

ABSTRACT

Since the first developments of modern wind power technology, the evolution in turbine size has experienced a constant shift towards larger rotors and higher towers in order to enhance energy capture and reduce the cost of energy. However, machines of greater scale are characterized by an increase in the loads acting on the blades, thereby resulting in the need for thicker and heavier structural components. This thesis analyzes one of the passive load alleviation methods, namely swept blades, which consists in the edgewise displacement of the blade outboard region in the plane of rotation. The study focuses on the full redesign of swept rotors for two different machines: a 2 MW onshore wind turbine and a 10 MW next generation offshore concept. An integrated design code that allows for the simultaneous optimization of blade aerodynamics and structural sizing has been used for the analysis, with the ultimate goal of finding the configuration that minimizes the cost of energy. The results of the design optimization show that by adopting swept rotors it is possible to achieve substantial load mitigation, leading to a reduction in terms of blade mass and cost. However, this technology entails a loss in the annual energy production, resulting in a slight increase in cost of energy. It is then demonstrated that significant benefits may be obtained by expanding the rotor swept area, so that power generation can be improved while maintaining similar loads to the original straight blades thanks to sweep.

Keywords: Wind energy, Rotor design optimization, Passive load alleviation, Swept blades

SOMMARIO

Fin dai primi sviluppi della moderna tecnologia eolica, la dimensione delle turbine ha subito un costante aumento in termini di diametro del rotore e altezza della torre, con lo scopo di migliorare la capacità di produzione di potenza e ridurre il costo dell'energia. Tuttavia, macchine sempre più grandi sono caratterizzate da maggiori carichi sulle pale, i cui componenti strutturali devono quindi aumentare di spessore e di peso. Questa tesi si propone di studiare uno dei metodi passivi per alleviare i carichi agenti sulla turbina, che consiste nell'utilizzo di *swept blades*, ossia di pale curvate all'interno del piano di rotazione nella loro parte più esterna. Lo studio si concentra sulla completa riprogettazione di tali rotori eolici per due macchine diverse: una turbina onshore da 2 MW e una offshore da 10 MW, rappresentativa delle macchine di futura generazione. In entrambi i casi è stato utilizzato un codice di design che permette di integrare la massimizzazione delle prestazioni aerodinamiche con il dimensionamento ottimizzato dei componenti strutturali del rotore, per trovare la configurazione corrispondente al minimo costo dell'energia. I risultati dell'analisi mostrano che adottando rotori *swept blades* è possibile ridurre i carichi in maniera significativa, portando a vantaggi in termini di massa e costo delle pale. Tuttavia, dal momento che con questa tecnologia l'energia prodotta subisce un leggero calo, il costo dell'energia aumenta. Viene dimostrato quindi che particolari benefici possono essere ottenuti espandendo l'area spazzata dal rotore, in modo da incrementare la generazione di potenza mantenendo carichi simili alla configurazione originale grazie all'utilizzo di pale curve.

Parole chiave: Energia eolica, Progettazione ottimizzata di rotori eolici, Riduzione passiva dei carichi, Swept blades

Introduction

1.1 Background

The international commitment to mitigate the effects of climate change, together with rising concerns on the sustainability of the world energy system, have caused a significant increase in the demand for wind energy. Thanks to the substantial investments of the last decades, wind power is already among the cheapest sources for electricity generation in several countries. This widespread success was primarily achieved thanks to innovations aimed at the optimization of wind turbines, with the ultimate goal of minimizing the cost of energy. The size of the machines has been continuously growing, with always bigger rotors and higher towers to gain in energy capture and lower the cost of power production from wind. However, larger turbines are subjected to relevant loads and deformations, demanding a greater stiffness and weight of the blades. The need to limit the increase in rotor mass has led to the development of load alleviation technologies that allow for the use of larger rotors to produce more energy, while keeping the loads within the structural limits of the materials.

1.2 Project motivations and goals

The present thesis focuses on the analysis of a passive load alleviation technique, consisting in blade sweeping, which would enable to reduce the loads on a wind turbine by adapting the shape of the blades to the occurring wind conditions. Few studies in the literature investigate the impact of introducing sweep in the blade design, but according to the author's knowledge, a full redesign of swept wind turbine rotors is still missing in the research.

Therefore, several sweep curvatures have been defined and each new configuration has been optimized, both aerodynamically and structurally, using a multidisciplinary simulation and design tool specifically developed for wind turbine applications. The main goal of this study is to thoroughly analyze the consequences of sweeping the blades on relevant loads acting on the main turbine components, as well as the impact on power output and cost of energy. The potential benefits of swept blades are evaluated for two different machines: a 2 MW onshore wind turbine and a conceptual 10 MW offshore one.

1.3 Report structure

This Master's thesis is organized according to the following structure. First, a brief introduction into the topic of wind turbines is provided in Chapter 2, describing their functioning and the main features that are needed to be considered as a basis for discussing the present work.

Next, a general overview on load mitigation methods is given in Chapter 3, distinguishing between active and passive techniques. In particular, the concept of swept blades is described here, followed by the parametrization of the sweep curve and the results from a preliminary sensitivity analysis on the sweep parameters.

The simulation and design environment used for the analyses conducted in this study is introduced in Chapter 4, where the general characteristics of the integrated wind turbine design tool are defined. The overall architecture of the code is described in detail, together with the main optimization algorithms and the considered cost models.

Then, in Chapter 5, the potential of swept blades is evaluated by analyzing the effects on loads and cost of energy when adopting this particular blade design on a 2 MW onshore wind turbine. Finally, Chapter 6 reports an initial assessment on the use of this technology on a conceptual 10 MW offshore machine.

The report is closed by Chapter 7, where conclusions are drawn and an outlook on future developments is presented.

Wind turbine technology

2.1 Wind power

The world energy system is arguably experiencing the greatest transformation since the discovery of hydrocarbons. Nowadays, trends in energy supply and consumption are not sustainable, not only environmentally but also economically and socially. Without substantial action, energy-related greenhouse gas emissions could more than double by 2050 [1], and increased fossil fuel demand will raise concerns on security of supply. There is a pressing need to foster the development of low-carbon energy technologies in order to address the challenges of global warming and sustainable progress, limiting the environmental impact of human activities.

The energy transition is predicted to further accelerate in the next decade as a consequence of the global commitment to mitigate climate change after the Paris Agreement [2]. In order to restrain the global mean temperature increase to 2 °C above pre-industrial levels, a range of technology solutions should be promoted: energy efficiency, renewables, nuclear power, and the near-decarbonization of fossil fuel-based power generation. The International Energy Agency has developed several scenarios to account for different policies of electricity generation (see Fig. 2.1).

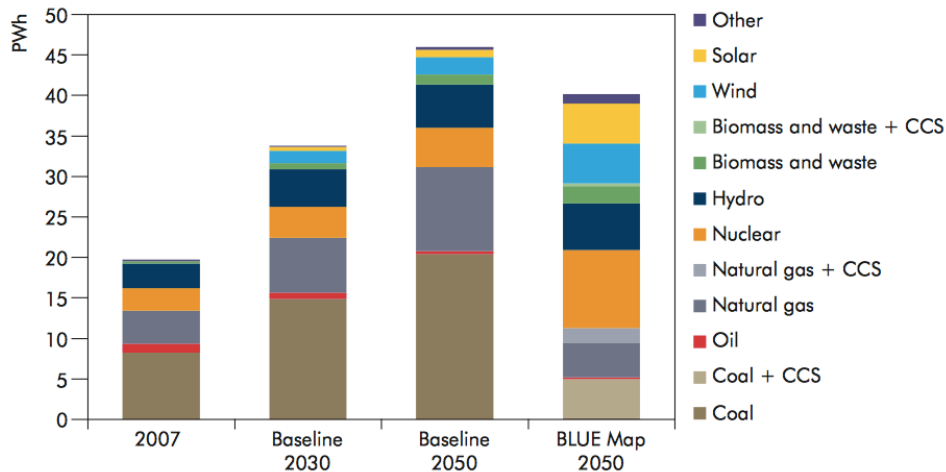


Figure 2.1: Global electricity production by source and by scenario [3]

Wind power already is and most likely will be one of the key players toward the development of the new energy system. Wind, like other renewable resources, is widely available all over the world; hence, it can contribute to enhance security of supply by reducing energy import dependence. Wind power improves the energy mix and can stabilize the cost of electricity generation against the price volatility typical of fossil fuels. Wind energy produces no direct greenhouse gas emissions and does not emit any other pollutants; additionally, it entails no water consumption. The main drawback of wind turbines is that, compared to most conventional generators, they can produce energy only in response to the resource (i.e. wind) that is immediately available, since it is not possible to store it in significant amounts for later use. Moreover, the output of a wind turbine follows the wind conditions, thus it is inherently fluctuating.

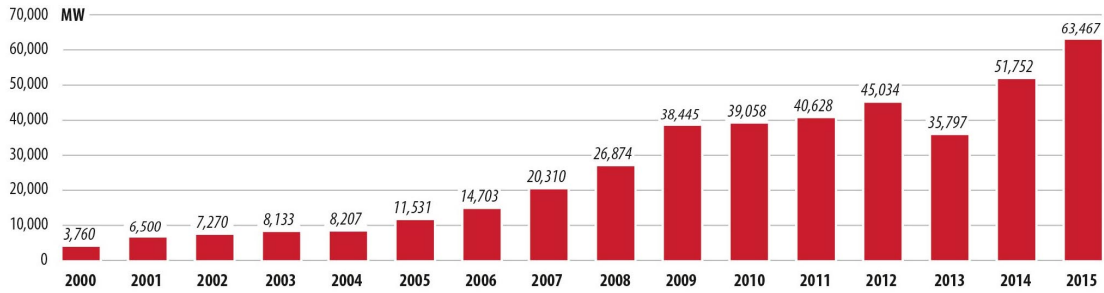


Figure 2.2: Global annual installed wind capacity, 2000-2015 [4]

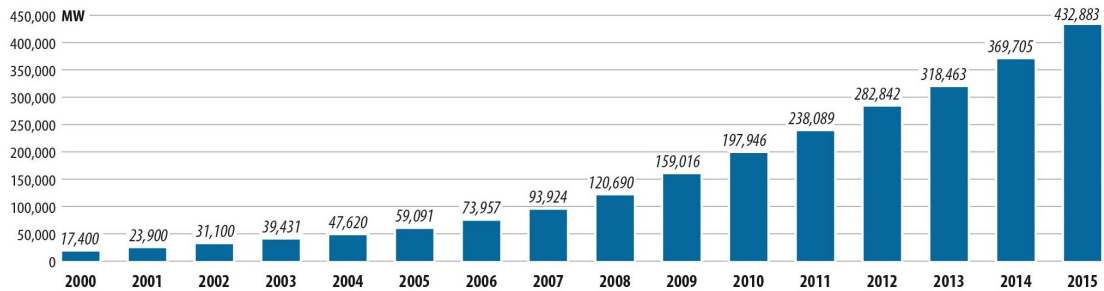


Figure 2.3: Global cumulative installed wind capacity, 2000-2015 [4]

In the last few decades, wind energy has turned from niche sector into mainstream industry, as clearly shown in Fig. 2.2 and 2.3. A great number of countries in the world now have significant wind generating capacity and are expected to heavily invest on new wind farms in the near future. According to the Global Wind Energy Council [4], wind power could supply up to 20% of global electricity by 2030, attracting annual investments of about €200 billion.

Europe has given a particular contribution to the wider use of wind energy in the last decades. Fig. 2.4 shows that wind power installations have been greater than any other electricity generating technology in the last twenty years [5]. Moreover, wind is a major export industry for Europe, which is still the world leader in wind technology development. The European manufacturing industry has a 40% share of all wind turbines sold globally and Europe leads the growing offshore sector with over 90% of current wind farms [6].

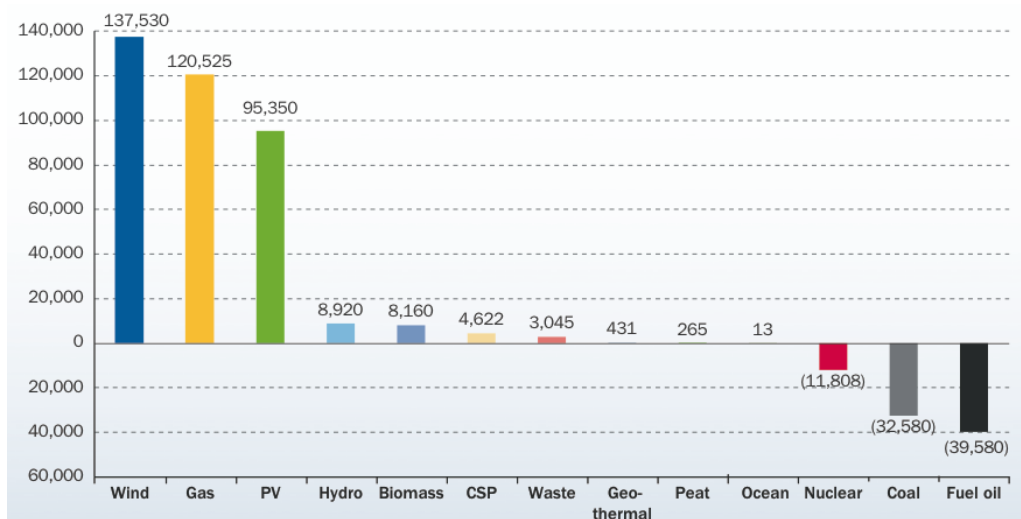


Figure 2.4: Net electricity generating installations in the EU, 1995-2015 [5]

At the end of 2015, wind energy had a 15% share of the installed power generation capacity in the European Union and accounted for almost half of all new power installations. There are currently around 146 GW of wind energy capacity installed in Europe. In 2015, almost one third of all power demand in the EU was produced from renewables, and 11% was covered by wind energy, overtaking hydropower as the third largest source of electricity generation. WindEurope, formerly known as EWEA (European Wind Energy Agency), has foreseen that wind power has the potential to secure 28% of electricity demand by 2030 [6]. In a few European countries, such as Denmark, Spain, and Portugal, it already provides 15% to 30% of total electricity supply. This is supported by the fact that onshore wind, thanks to the significant investments of the last decades, is now one of the cheapest forms of new power generation capacity in Europe, while also offshore wind costs are rapidly falling. In a number of countries, wind turbines are now being deployed without specific financial incentives. In fact, wind power is currently the most invested clean energy technology in Europe, as clearly reported in Fig. 2.5.

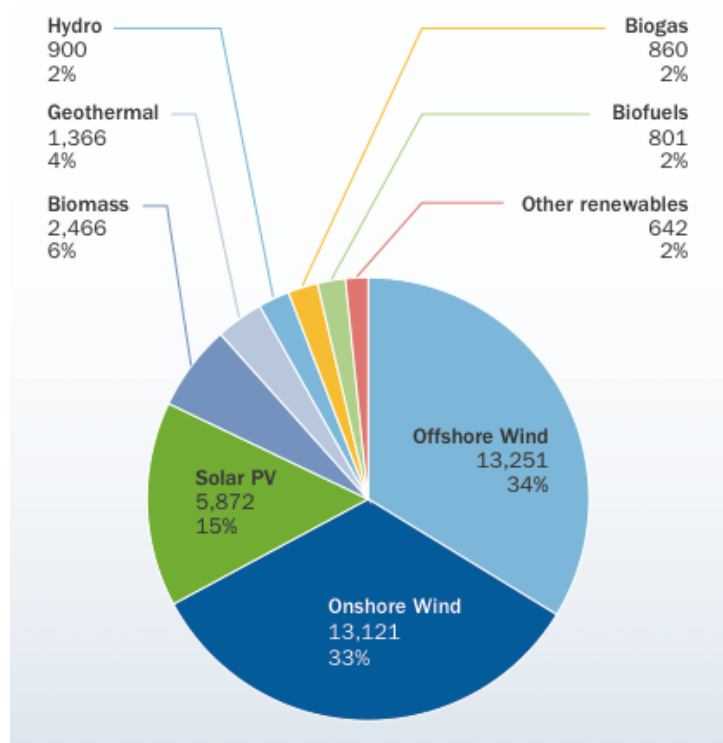


Figure 2.5: Clean energy investments in Europe, 2015 [5]

Since the first development of modern wind power technology, the evolution in turbine size has been evident (see Fig. 2.6), with always larger swept areas and higher towers to enhance energy capture and lower the cost of energy. Nowadays wind turbines are multi-MW machines, with rotor diameters and tower heights often exceeding 100 meters. Further enlargement of onshore turbines is limited by several constraints, such as logistics and noise regulations. Hence, more benefits are expected from offshore up-scaling. A great number of current R&D projects focus on the feasibility and development of 10 MW and 20 MW offshore wind turbines [7].

The size of these new rotors, together with the use of lightweight materials and smart technologies aimed at saving part of the manufacturing costs, entails relevant loads and deformations. Thus, great efforts have been put into the control and mitigation of loads, in order to reduce blade mass and cost while limiting the increase in cost of energy, possibly improving it. The main goal of this thesis is to describe one of the methods for load alleviation and analyze its potential on two different wind turbines.

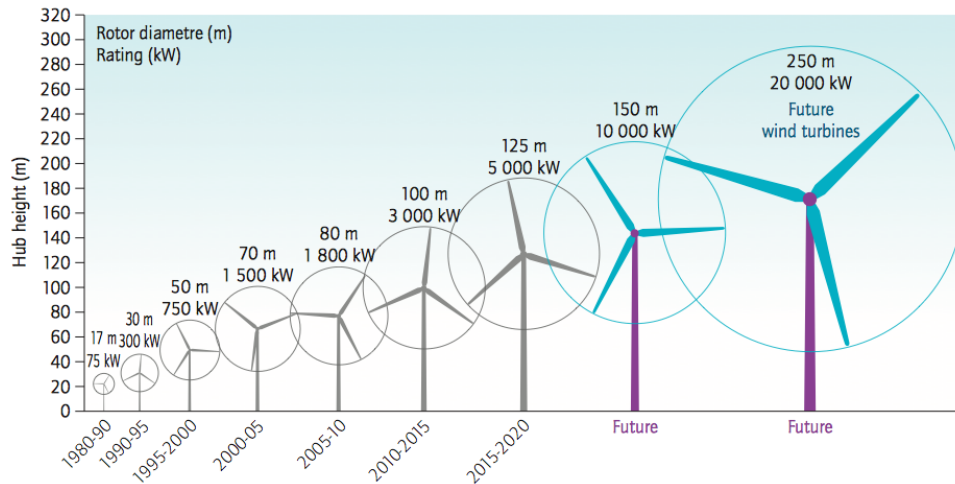


Figure 2.6: Growth in size of modern wind turbines [1]

Depending on the specific application, there exist various small scale horizontal-axis and vertical-axis wind turbines, usually designed to supply local grids or isolated power utilities. However, the present work focuses on larger multi-MW size horizontal-axis wind turbines, often installed in groups in the so-called wind farms, which are conceived to supply power to regional or national grids. This type of wind turbines has already reached a good level of standardization and worldwide diffusion. A brief description of the main features of a typical horizontal-axis wind turbine is provided in the next section.

2.2 Horizontal-axis wind turbines

A wind turbine is basically a machine able to convert the energy in the wind into electricity. The actual conversion process can be summarized as follows: wind generates the basic aerodynamic force of lift that induces a net torque on the rotating shaft, which results in the production of mechanical energy that is then transformed to electricity by the generator [8].

Horizontal-axis wind turbines (HAWT) have the axis of rotation parallel to the ground. The main components of a typical wind turbine are shown in Fig. 2.7 and include: the rotor, consisting of the blades and the supporting hub; the nacelle, containing the generator, the drivetrain, gearbox, and brake assembly; the tower and its foundation.

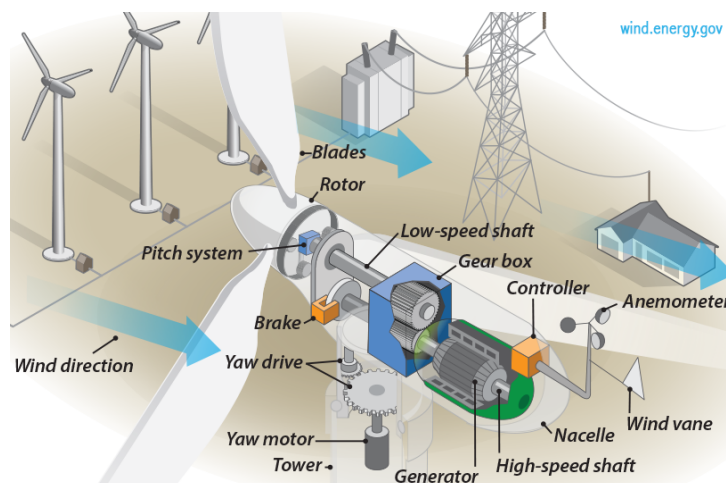


Figure 2.7: Main components of an upwind HAWT [9]

In order to constantly keep the machine at the optimal value of efficiency, thus maximizing the power extracted from the wind, while limiting the torque experienced by the drivetrain and the fatigue damage of the components, all multi-MW wind turbines today feature three different types of active control:

- yaw drive, to make the hub rotate with the wind;
- generator torque, to control the rotational velocity of the machine;
- blade pitch, to rotate the blades about their axis.

The hub is connected by means of the main bearing to the fixed structural part of the nacelle. The rotor is coupled to the generator either through a gearbox, which is able to raise the rotational speed in order to cope with the characteristics of the electric generator, or directly in a direct-drive configuration, if permanent magnets are used. The nacelle and rotor assembly is mounted on top of the tower, typically made of steel. The tower foundation is made of reinforced concrete in the case of onshore plants, whereas concrete-metallic floating or non-floating bases are used for offshore turbines.

Given the large size and relatively low mass of its components, the motion of a wind turbine is characterized by relevant deformations. Furthermore, the action of the wind is spatially non-uniform and unsteady, hence the resulting overall motion can be rather complicated. To limit this non-uniformity, turbines are usually designed to work aligned with the incoming flow in an upwind configuration, meaning that the wind reaches the rotor before the tower. However, this configuration is unstable as the rotor assembly tends to be twisted around the tower axis towards a stable downwind condition by the action of the aerodynamic forces. Thus, a yaw actuator is installed on the bearing connecting the nacelle to the rest of the tower, keeping the rotor always oriented towards the incoming wind flow in order to ensure maximum power generation and maintain symmetric loads on the three blades and drive shaft.

The majority of turbines today have upwind rotors with three blades, whereas downwind and/or two-bladed rotors are currently studied mostly for special applications, such as regions with monsoon climate. Most manufacturers now use pitch control, whereas smaller stall-controlled machines were widely used in the past. The rotor blades are usually made of composites, especially fiberglass or carbon fiber, but sometimes also wood/epoxy laminates are adopted. Blade mass depends primarily on the selected materials and the internal structure of the blade. The present work is focused on upwind, pitch-controlled, three-bladed wind turbines.

2.2.1 The power performance curve

In order to determine the power extracted from the wind flow, a simple model can be used [10]. The power associated to an air stream can be expressed with the following formula:

$$P_{\text{wind}} = \frac{1}{2} \rho A V^3 \quad (2.1)$$

where ρ is the air density, A is the rotor swept area, and V is the velocity of the wind. The power extracted by the turbine can be defined as:

$$P = \frac{1}{2} \rho A V^3 C_P \quad (2.2)$$

where C_P , namely the power coefficient of the wind turbine, expresses the amount of power that a specific turbine with radius R is able to extract from a wind flow with speed V , given a certain operating condition with rotor speed Ω and blade pitch β . In fact, the characteristic power coefficient of a given turbine can be defined as a function of the tip speed ratio $\lambda = \frac{\Omega R}{V}$ and of the blade pitch β , as shown in Fig. 2.8.

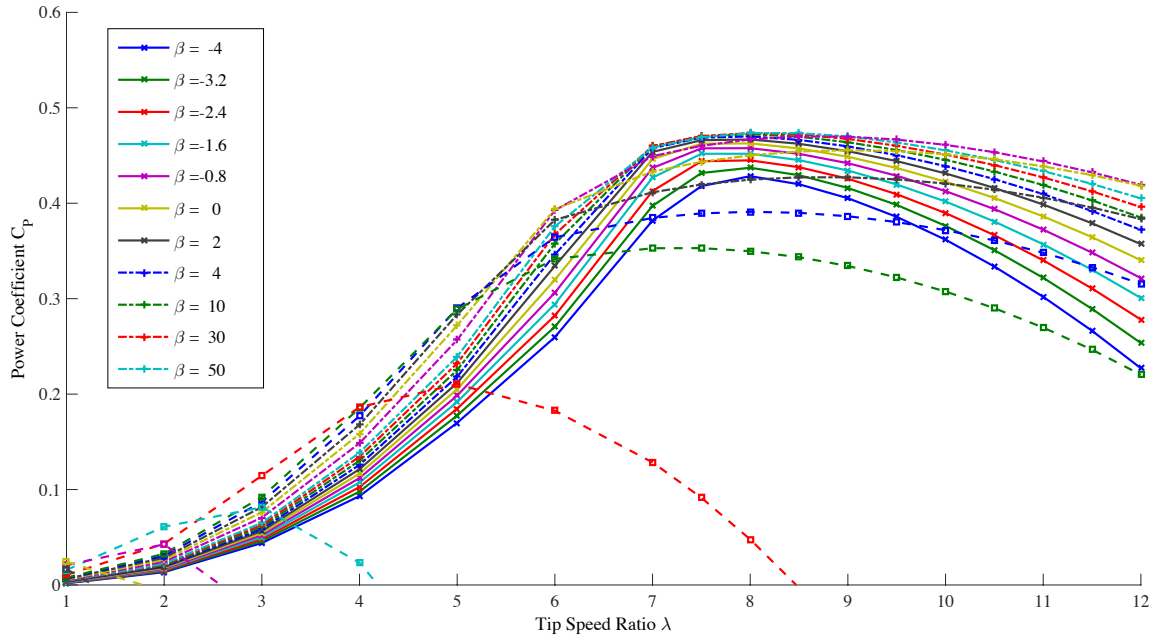


Figure 2.8: Power coefficient as a function of TSR and β for a given wind turbine

It can be shown that the maximum C_P , also called Betz limit, has the following upper boundary [11]:

$$C_{P,\max} = \frac{16}{27} = 0.5926 \quad (2.3)$$

In practice, the Betz limit cannot be achieved due to three main effects:

- finite number of blades and related tip losses;
- rotation of the wake behind the rotor;
- aerodynamic drag.

Top C_P values for existing turbines are usually located in the range of 0.45–0.50.

The power output of a wind turbine varies with wind speed and every machine has a characteristic power curve. This curve provides the electrical power output as a function of the wind speed at hub height. An example of a typical power curve is represented in Fig. 2.9.

Variable-speed wind turbines are regulated according to different policies depending on the wind speed intensity [12]. There are basically three key points on the velocity scale:

- cut-in wind speed, that is the minimum speed at which the machine delivers useful power, since below it the turbine efficiency is too low due to friction and dispersion effects;
- rated wind speed, at which the rated power (i.e. the maximum power of the electrical generator) is reached;
- cut-out wind speed, namely the maximum operating wind speed, limited by design and safety constraints.

Usually, two power production regimes are identified. The wind turbine is said to work in region II when wind speed ranges between cut-in and rated, while region III extends from rated to cut-out wind speed.

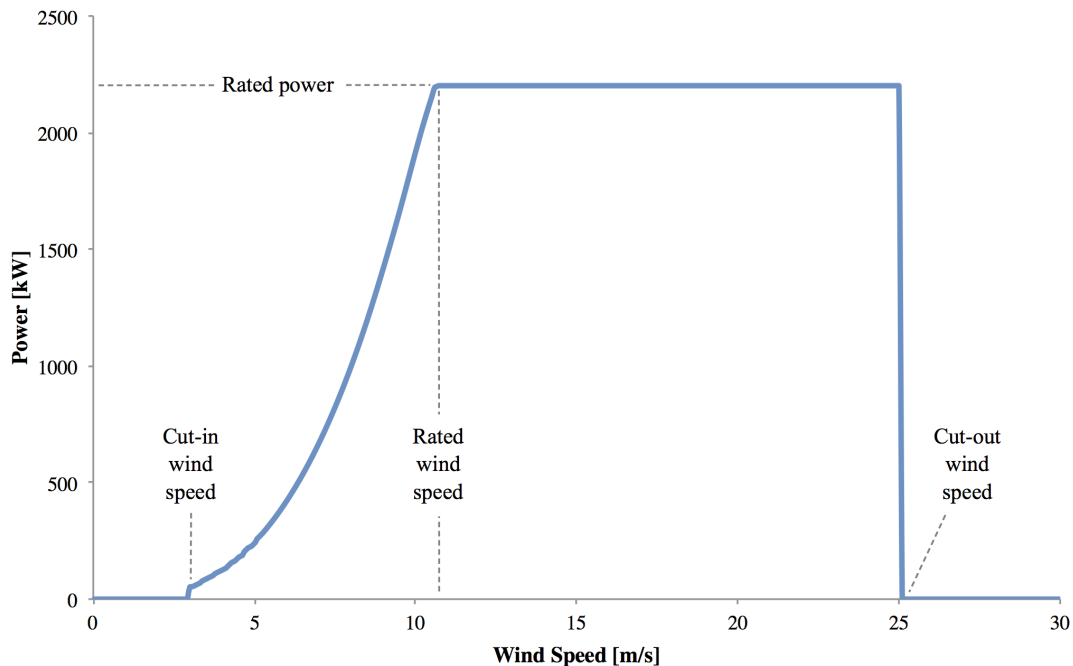


Figure 2.9: Example of a wind turbine power curve

In region II, the machine is operated at maximum C_P by maintaining a constant tip speed ratio; hence, for increasing wind speed, rotor speed linearly increases. This is achieved by setting blade pitch at the value corresponding to $C_{P,\max}$ while adjusting generator torque so as to obtain the desired rotor speed. In region III, the turbine is kept at constant rotor speed and torque in order for the power output to be constant and equal to the rated value. This is possible by pitching the blades so as to adjust the aerodynamic torque for varying wind speeds.

For larger turbines with noise constraints, it is easy to find a transition operating regime, called region $II^{1/2}$. Since noise can be easily correlated with the blade tip speed [13], it is common practice for modern wind turbines to place a limit on rotor speed, because this is directly related to tip speed for a given rotor radius. Region $II^{1/2}$ is essentially a sub-part of region II extending from a given wind speed up to the rated, where the turbine operates at rated rotational speed but below rated power.

2.3 Wind turbine loads

The aim of wind turbine design is not only to be effective in terms of energy production. A crucial step in the structural design process of a wind turbine is the assessment of the loads that the machine must be able to withstand. A load is an externally applied force or moment acting on the turbine or any of its components. The nature of wind turbine loads is various.

Steady loads are the ones that do not vary significantly over time, such as those due to the average wind speed, the weight of the machine on the tower, and the centrifugal forces acting on the rotating blades. Turbulence in the wind gives rise to stochastic loads that depend on small random wind speed fluctuations causing rapidly varying aerodynamic forces on the rotor. Temporary external events like the starting and stopping of the machine may generate transient loads arising from time-varying oscillations, too.

Other loads occur due to the rotation of the rotor and are referred to as cyclic because they vary in a regular manner, for instance due to wind shear or tower shadow. Periodic loads may also arise from mass or pitch imbalances. A particular type of cyclic loads is represented by resonance-induced loads, which result from the dynamic response of a structural component

being excited at one of its natural frequencies. As this condition may produce loads of very high magnitude and is to be avoided whenever possible, resonance-induced loads will be discussed in greater detail in Section 2.3.2.

Wind turbine elements are typically designed for two main kinds of loads: ultimate loads and fatigue. Ultimate loads correspond to the maximum loads applied to the component, multiplied by a safety factor. On the other hand, fatigue refers to the ability to withstand loads of varying magnitude applied repeatedly. While the former type is rather straight-forward to figure, it is better to describe fatigue more thoroughly, together with one common way to compute it.

2.3.1 Damage equivalent load

Fatigue occurs when a material undergoes repeated loading and unloading within its elastic limit. The stress values that produce fatigue damage are usually much lower than the ultimate stress limit of the material. A simplistic description of the causes underlying this phenomenon is that, when a composite material is loaded above a certain threshold, microscopic cracks begin to form at some stress concentration points in the structure. With each load cycle, these cracks grow a little until one reaches a critical size; the crack will then suddenly propagate, leading to structural failure [14].

Due to the very nature of their functioning, wind turbines are subjected to cyclic loading, hence fatigue assessment is particularly important for these machines. Many techniques for fatigue damage estimation that were first developed for metals have now been extended to composites, which are the primary materials used for blade fabrication. One of the most widely used models for fatigue is the so-called Damage Equivalent Load. The advantage of the fatigue DEL concept is that it translates a long history of random fatigue loads into one number, making it easy to compare different load situations and design configurations.

Damage equivalent load is defined as the constant amplitude load that for some arbitrary number of cycles N_{eq} (e.g. one million cycles) would produce the same fatigue damage as the variable amplitude load spectrum, meaning all actual loads combined. Even if a component undergoes fewer load cycles than would lead to failure, it will still suffer damage. Therefore, if a given load is applied n times and the number of cycles before failure for that specific amplitude is N , then a fraction d of the component life has been used, which corresponds to partial damage:

$$d = \frac{n}{N} \quad (2.4)$$

According to Miner's rule, the cumulative damage D is defined as the sum of the damages due to load cycles of m different amplitudes. Component failure is deemed to occur when total damage D is equal to unity.

$$D = \sum_{i=1}^m d_i = \sum_{i=1}^m \frac{n_i}{N_i} \quad (2.5)$$

The number of allowable load cycles at a given amplitude can be defined as follows:

$$N_i = \left(\frac{M_{\text{applied},i}}{M_{\text{ultimate},i}} \right)^{-m} \quad (2.6)$$

where $M_{\text{applied},i}$ is the load (e.g. a moment) actually applied to the material and $M_{\text{ultimate},i}$ is the maximum load before failure of the component. Finally, applying the equations stated above, the damage equivalent load M_{eq} for N_{eq} cycles can be obtained:

$$M_{\text{eq}} = \left(\frac{\sum (M_{\text{applied},i})^w n_i}{N_{\text{eq}}} \right)^{\frac{1}{m}} \quad (2.7)$$

where w is the inverse of the S-N curve, which relates stress amplitude with the number of cycles.

2.3.2 The Campbell diagram

In order to avoid significant energy dissipation in the system resulting from resonance, a wind turbine consists of a number of lightly damped components that are excited by numerous forcing factors, such as wind turbulence, wind shear, tower shadow, and other dynamic effects. Structures may have significant dynamic responses in the frequency range of the rotor rotation and its harmonics.

The control system of a wind turbine needs to be carefully designed so as to hinder the occurrence of resonant conditions. Sometimes, however, wind turbine operation near one of the natural frequencies of the system cannot be avoided, since response to turbulence may inevitably excite some parts of the structure to significant vibrations and, possibly, to resonance. This situation may occur during the start-up or shutdown phase, or at specific rotor speeds.

Thus, it is important to identify the possible points of interception between natural frequencies and external excitation from the rotor. For this purpose, a Campbell diagram is generally used. A typical Campbell diagram for a wind turbine is reported in Fig. 2.10. The plot represents the most significant natural frequencies of the turbine as a function of its rotation regime, corresponding to a variety of turbine modes.

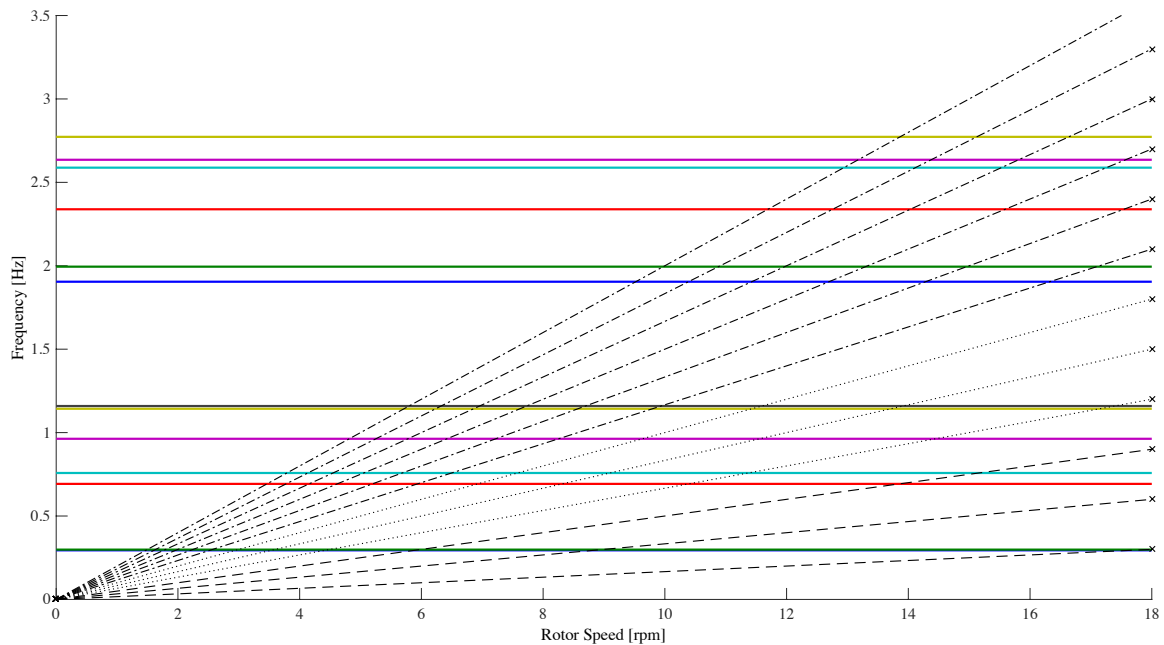


Figure 2.10: Example of a Campbell diagram for a wind turbine

For instance, a Campbell diagram generally includes:

- tower bending modes, both fore-aft and side-side;
- blade flapwise¹ and edgewise² bending modes;
- hub rolling and yawing modes.

On the other hand, the dashed lines starting from the origin correspond to the rotor rotation frequency and its harmonics. The most relevant ones are the rotation frequency ($1P$) and the blade-passing frequency ($3P$), where P is an abbreviation for *per revolution*.

¹Flapping moments cause the blade to bend upwind or downwind.

²Edging moments induce blade motion in the plane of rotation.

The Campbell diagram analysis is fundamental to understand if the rotor operates at rotational speeds associated to resonant conditions. Resonance occurs when one of the eigenfrequencies intercepts the rotor speed curve or multiples of it. Obviously, not all possible crossing points are equally dangerous for the system. For example, if a single natural frequency crosses one of the harmonics, external excitation affects the response of the system and strong oscillations potentially leading to fatigue damage may be experienced. Especially, wind turbine blades should be designed in such a way that no crossing with the three lower harmonics (i.e. from $1P$ to $3P$) is present, since they are the most energetic ones. Resonance can be partially prevented by increasing the component's stiffness in order to raise its natural frequency, however this translates into having a heavier structure, therefore a trade-off needs to be found. Intersections between different modes should also be avoided since they would result in the energy transfer from one dynamic response to the other.

2.3.3 Design load cases

Wind turbines are designed with reference to a range of conditions, corresponding to the numerous situations in which the machine may have to operate. Proper design is required to ensure that the turbine is able to withstand with no particular damage during normal operation, where most of the energy production occurs, as well as in extreme conditions, such as storms or possible electrical or control system faults.

In order to demonstrate the turbine's capability to perform in the whole range of operating states, a set of conditions has been codified by the International Electrotechnical Commission under the IEC 61400-1 Design Requirements [15]. In the IEC 61400-1, turbines are classified in terms of mean wind speed into four standard classes, as reported in Table 2.1. Additionally, the standard classes are divided into high and low turbulence intensity classes A and B.

Wind turbine class	I	II	III	IV
Annual average wind speed [m/s]	10	8.5	7.5	6

Table 2.1: Wind turbine classes

The life of a wind turbine can be represented by a set of design situations covering the most relevant conditions that the machine is going to experience during its lifetime. Design load cases (DLCs) are used as standards to ensure the adequacy of critical components. They are defined for eight different situations [16]:

1. Power production
2. Power production plus occurrence of fault
3. Start-up
4. Normal shutdown
5. Emergency shutdown
6. Parked (standing still or idling)
7. Parked plus fault
8. Transport, assembly, maintenance, and repair

Usually, each design situation presents more than one DLC. In the present study, structural simulations have been performed for the following design load cases:

-
- DLC 1.1: the turbine is running and connected to the grid; loads result from atmospheric turbulence occurring during normal operation.
 - DLC 1.3: same as DLC 1.1, but resulting from extreme turbulent conditions.
 - DLC 2.1: the occurrence of a fault during power production is considered.
 - DLC 6.1: the rotor is at standstill or idling; transient oblique inflow of up to $\pm 15^\circ$ for the steady extreme wind speed model, or a mean yaw misalignment of $\pm 8^\circ$ using the turbulent extreme model.
 - DLC 6.2: grid failure at an early stage in the storm with the extreme wind situation; yaw error of up to $\pm 180^\circ$ is considered.
 - DLC 6.3: extreme wind with a recurrence period of one year is imposed together with an extreme yaw misalignment.

Load alleviation techniques

The constant growth of the wind energy industry in the past decades has been made possible by the continuous decrease in the cost of energy (CoE). There are many ways to lower this figure, but the most straight-forward approach consists in expanding the rotor swept area to improve energy capture, as power extracted depends on the square of the rotor radius. However, a simply larger rotor would result in the increase of loads on the wind turbine, thereby raising its costs due to longer and heavier blades. A widely discussed topic in the recent literature has been the development of advanced rotor control concepts, which would enable the increase in rotor diameter to produce more energy for a given power rating and within the original load envelope.

The methods for load reduction fall into two main categories: active and passive. The classification of load control techniques is reported in Fig. 3.1, together with some examples. Typically, the control of turbine loads (and power) can be addressed by acting on four main parameters:

- flow velocity, adjusted by using a variable-speed rotor;
- blade incidence angle, controlled by varying the pitch and/or twist angle;
- blade section aerodynamics, implementing active flow controls;
- blade size, using variable blade length.

An overview of the different techniques that have been proposed and adopted for load mitigation is given in the following. Section 3.1 will deal with active control, whereas Section 3.2 will be dedicated to passive load alleviation methods, with a focus on bend-twist coupling through fiber rotation. Finally, in Section 3.3 the characteristics of swept blades will be thoroughly described.

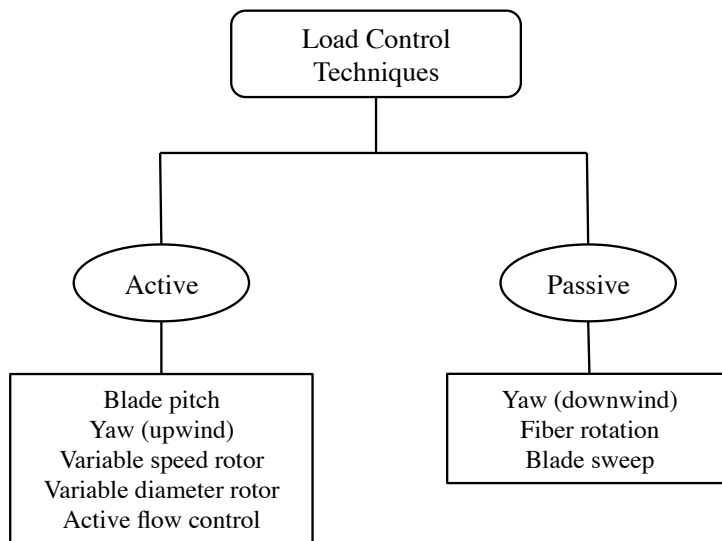


Figure 3.1: Active and passive load control techniques

3.1 Active load alleviation methods

Active load control techniques aim at reducing loads by actively controlling the machine, meaning that external power is required for their actuation. Therefore, a necessary condition to their use is that the increase in energy output offsets the auxiliary energy needed for load control [17]. Traditional methods of active control include rotor yawing, collective blade pitching, and variable-speed rotors, which are all commonly adopted in modern wind turbines and were briefly described in Section 2.2. Recently, a considerable amount of research has been performed in the area of advanced active controls, such as individual pitch and a number of active flow control concepts, which will be discussed in the following.

3.1.1 Individual pitch control

Most wind turbines nowadays are equipped with mechanisms that allow for pitch control to rotate each blade around its spanwise axis so as to change the angle of attack to the wind. However, blades are usually pitched either collectively, with all blades pitching to the same extent simultaneously, or cyclically, as a function of the azimuth angle. On the contrary, individual pitch control allows the machine to react to yaw errors and asymmetric loads caused by wind turbulence across the rotor, offering additional possibilities for load reduction [18, 19]. The goal is to create a combined pitch control system consisting of both collective and individual pitch, each of them being independent, where collective pitching is used to maintain rated power in region III (see Section 2.2.1) based on mean wind speed and the individual pitch regulator is actuated to minimize loads without affecting the power output.

Obviously, more sophisticated and suitably designed control algorithms are required for the blades to respond to asymmetric loading quickly enough to relieve the oscillating loads due to wind gusts, while limiting complexity and costs. Few control system models for individual pitching have been already developed [20, 21]. It has been demonstrated that, especially for larger wind turbines operating within regions of the upper atmospheric boundary layer characterized by coherent vortices, the use of individually pitch-controlled blades could effectively reduce blade root fatigue loads [22], at the expense of an increase in pitch activity.

3.1.2 Variable diameter rotor

This concept consists in using extendable blades that are divided into a main part and a tip part that can be extended and retracted (see Fig. 3.2) independently of the pitching mechanism, which is still used for power regulation, to vary the rotor radius. Variable diameter rotors would enhance energy capture in low wind speeds thanks to a larger swept area, while reducing loads in high wind speed conditions by decreasing the length of the blades [23]. The challenges for the successful implementation of this design include complex control strategies, increased blade weight, and the need to ensure a high enough aerodynamic performance.

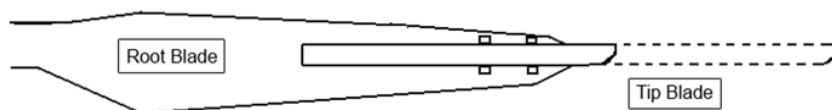


Figure 3.2: Illustration of the variable length blade concept [17]

Variable blade length rotors have recently risen interest for offshore applications [24]. In an offshore wind farm, turbines are inevitably in each other's wake, which results in a loss of energy because most machines are not operating at their full design capacity. By varying the rotor diameters along the wind farm, a significant increase in the overall power plant performance may be obtained.

3.1.3 Active flow control

Active flow control consists in techniques for the control of the local airflow surrounding the blade, which can be helpful for peak load mitigation as well as for improving the aerodynamic performance of an airfoil. Ailerons, which have long been used in fixed-wing aircraft applications, may be used to reduce the lift coefficient and increase the drag coefficient along the blade. Ailerons do not require actuators as powerful as the ones needed for pitch control [8], but the need to separate the blade into articulated parts and provide actuation inside the blade considerably affects rotor design and would entail significant complexity and costs.

Several innovative approaches that are more tailored to wind energy applications have been developed in recent years. These active load control devices, often referred to as “smart” blade technologies [25], include trailing edge flaps, microtabs, plasma actuators, vortex generators, tip brakes, pitchable tips, and spoilers. Smart devices require sensors located along the blade span to perceive variations in the local airflow conditions, together with microprocessors and distributed actuators that allow to respond quickly to alleviate loads by adjusting the sectional lift coefficient and/or the local angle of attack. Active flow controls are based on different principles but have several characteristics in common. For instance, smart devices must be small in size so that they can be distributed to allow for flow control at different sections along the blade span. They also need to be easily replaceable for maintenance and blade manufacturing complexity should not be drastically affected. Moreover, power requirements for the actuators must be low enough to be fully compensated by the improved energy capture of the wind turbine.

Trailing edge flaps are similar to ailerons but have no sudden change on the blade surface or openings that would disturb the airflow over the blade or generate noise. Adaptive devices have also been proposed where deformable flaps are attached with no hinge to the main airfoil and quickly deflected by piezoelectric actuators [26, 27]. This type of smart rotor control has been the subject of considerable research efforts and some developed concepts have shown good load reduction capability [28], although they have hardly been tested on full-scale wind turbines.

Microtabs consist in small tabs located near the trailing edge of the blade. When unused they are retracted into the blade, otherwise microtabs are deployed approximately perpendicular to the airfoil surface, reaching a thickness on the order of the boundary layer on the pressure side of the blade [29, 30]. The slight movement of microtabs affects the aerodynamics of the airfoil by shifting the flow separation point, leading to lift enhancement or mitigation when they are deployed on the pressure or suction side of the blade, respectively.

Plasma actuators operate by creating an electric field between two electrodes, generating an auxiliary airflow called “ionic wind” near the surface of the blade, which modifies the profile of the boundary layer and delays separation [31]. Vortex generators are simply solid tabs located on the blade surface to promote airflow mixing and alleviate boundary layer separation [32].

Finally, tip brakes and pitchable tips are used to contribute with negative torque to the rotor, whereas spoilers basically disrupt the airflow around the blade, considerably increasing drag and limiting lift. The basic functioning of these aerodynamic drag devices is represented in Fig. 3.3.

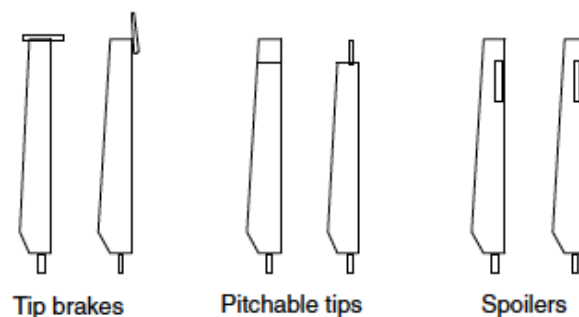


Figure 3.3: Illustration of aerodynamic drag devices [33]

3.2 Passive load alleviation methods

As described in Section 3.1, there are many active load controls under development. Even though it has been shown that these techniques have the potential to offer benefits in load reduction and aerodynamic performance, they present several drawbacks, namely added complexity, possible reliability problems, and additional power requirements. On the contrary, passive structures can improve the performance of a wind turbine by adapting their shape in response to changes in the operating environment. In this sense, passive load alleviation methods possess the following characteristics:

- no actuators/sensors present, reducing the risk of failure and the need for maintenance;
- no power supply required as the blades react passively to varying wind conditions;
- considerable reduction in fatigue damage, possibly increasing components lifetime;
- relatively fast response to variations in turbulent wind conditions;
- in most cases, blades are not made of several components but of a single part, where changes are either internal or in the blade shape.

All these features are very interesting for wind turbines, where simplicity, low maintenance, and high reliability are crucial factors for their widespread use. Thanks to the significant load reduction that can be obtained with passive techniques, the rotor diameter may be increased to boost energy capture and reduce the cost of energy.

The most studied technologies for passive load control are bend-twist coupling from fiber offset and blade sweep, whereas free-to-yaw rotors are typical of downwind applications and are not going to be discussed in this work. Swept blades will be described in detail in Section 3.3, since they are the principal topic of the present thesis.

3.2.1 Bend-twist coupled blades

Passive load mitigation techniques are based on the idea of having a structure that, under loading, passively deforms so as to alleviate loads. This structural behavior can be achieved by designing blades with some degree of bend-twist coupling (BTC), so that the twist distribution changes as the blades bend due to aerodynamic loads, leading to a reduction in angle of attack, which in turn results in lower loads. Moreover, since the blade adaptively twists according to the wind conditions, BTC allows to reduce pitch activity, which may be beneficial in terms of control system design and maintenance costs.

Bend-twist coupling was initially developed for stall-controlled rotors [34], where the blades were twisted with the goal of anticipating stall conditions by increasing the angle of attack. This twist-to-stall concept allowed for a reduction of peak loads, however fatigue loading substantially increased.

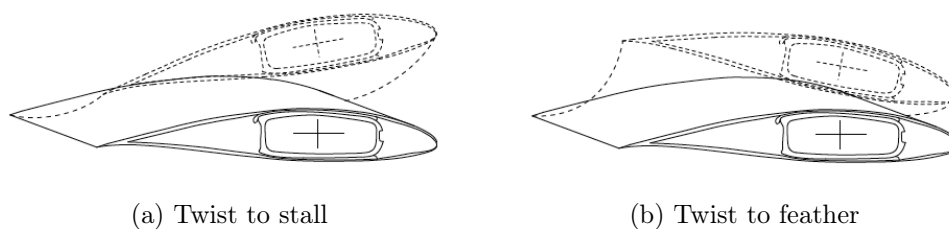


Figure 3.4: Response of bend-twist coupled blades to bending loads [35]

For modern wind turbines using pitch-controlled rotors, the opposite approach is adopted, making the blades twist towards feather in order to reduce the angle of attack, thereby alleviating fatigue as well as extreme loads [36]. At low wind speeds, when loads are rather small, the angle of attack does not vary significantly compared to the uncoupled blade. At higher values of wind speed, however, bend-twist coupled blades present a lower angle of attack, since the increase in blade bending due to gust loads makes the blade twist to feather. A representation of both the BTC approaches is shown in Fig. 3.4.

Aeroelastically tailored blades are an extensively studied solution for passive load control. In the case of fiber offset, BTC is obtained by rotating the composite material fibers away from the pitch axis, hence exploiting the anisotropic mechanical properties of these materials [37, 38]. When the fibers of a lamina are offset from its longitudinal axis and the plate is pulled, it deforms not only by extension but also by shear deformation, as shown in Fig. 3.5a. Similar coupling effects can be obtained for composite beams. Fibers in the horizontal walls are symmetrically biased so that when a bending moment is applied to the beam, the top side is in tension while the bottom one is compressed (see Fig. 3.5b). This principle can be applied to wind turbines to induce coupled blade response under bending loads.

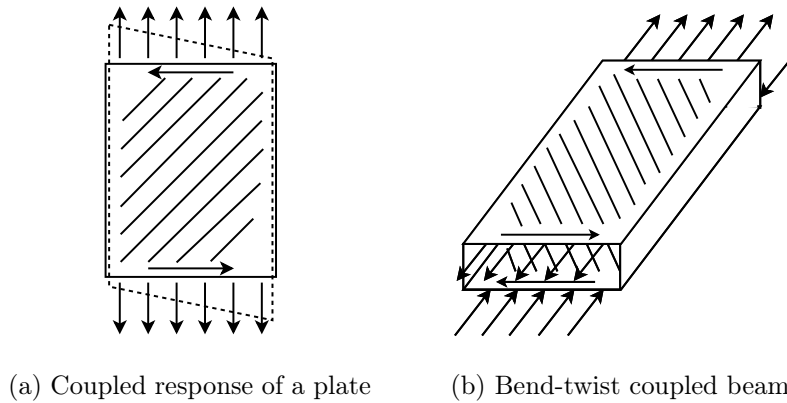


Figure 3.5: Coupling mechanisms in composite plates and beams

A good insight into the potential benefits on CoE reduction from the use of this technological solution is clearly shown in many studies in the literature [39]. Parametric analyses have been performed to understand the trade-offs between material cost and coupling effects, varying the material used, such as carbon fibers instead of fiberglass [40], and the amount of fiber offset [41]. By suitably designing fiber rotation in the spars [42], it would be possible to tailor the blade elastic response to aerodynamic pressure, improving energy capture below rated conditions and mitigating gust loads at rated power.

The synergistic use of inclined fibers in the skin and spar caps has been demonstrated to be beneficial in terms of weight, which is often increased in BTC solutions due to the need to satisfy the frequency placement and maximum tip deflection constraints by rising bending stiffness [43]. In fact, biased fibers in the skin allow for limited rotation in the spars, which would otherwise result in higher thickness to counter the loss in bending stiffness. This way, the adoption of better performing materials like carbon fiber can be avoided. Moreover, the use of partially coupled blades, with off-axis fiber starting only from a certain outboard section, may further limit the increase in structural thicknesses to satisfy fatigue constraints near the blade root.

The benefits of BTC with fiber offset may be accompanied by undesirable effects, such as a mass increase and the need for more complex manufacturing, possibly leading to higher cost. A viable solution to some of these issues can be obtained by combining together different load alleviation techniques, thereby limiting the inherent drawbacks of each technology. Some alternatives will be briefly discussed in the next section.

3.2.2 Combined load alleviation concepts

Combined bend-twist coupling and individual pitch control

As discussed in Section 3.1.1, changing the pitch of each blade independently through individual pitch control (IPC) results in the reduction of asymmetric loads due to wind turbulence fluctuations, at the expense of more expensive actuators and higher maintenance costs. On the other hand, bend-twist coupled (BTC) blades allow for more limited pitch activity thanks to the passive reaction to wind gusts. This means that the pitch control system can respond less aggressively compared to uncoupled blades, resulting in a reduced effort for the actuator duty cycle. Therefore, a combined BTC-IPC technology may lead to higher load reductions than it would be possible by adopting the single techniques separately, while making IPC more economically viable due to the reduced complexity and cost for the actuators [43].

Combined fiber offset and sweep

The combination of material (i.e. off-axis fiber orientation) and geometric (i.e. blade sweep) coupling has the potential to dramatically reduce both fatigue damage and extreme loads, allowing for lightweight structures and, ultimately, significant benefits in terms of cost of energy, especially if bigger rotors are used. Only few studies have tackled this solution so far [44]. With such combined adaptive load alleviation, it would be possible to restrain the increase in bending stiffness that is inherent to BTC from fiber offset, while limiting the amount of tip sweep to keep the blade envelope within viable bounds for transportability.

Spar cap offset

An alternative way to induce bend-twist coupling behavior in a blade is represented in Fig. 3.6 and consists in displacing the spar cap on the suction side towards the leading edge, and the one on the pressure side towards the trailing edge [45]. Additional couplings may be achieved by combining spar cap offset with fiber rotation. While the resulting design shows important benefits in terms of blade mass and load attenuation when compared to the uncoupled configuration, this solution also entails a significant loss in energy harvesting performance, allowing for a net reduction in the cost of energy only if the rotor radius is increased.

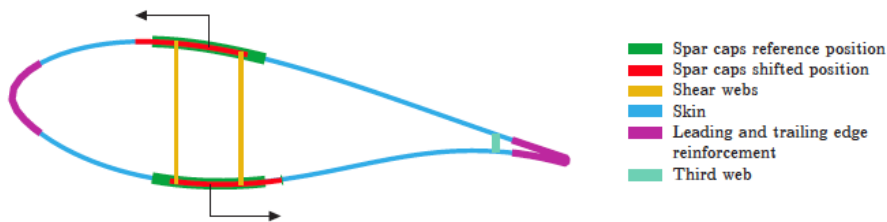


Figure 3.6: Representation of the blade sectional topology with spar cap offset [45]

Passive load control devices

A novel concept for the alleviation of loads on wind turbines consists in passive aero-elastic devices, such as flaps or pitching blade tips, which respond automatically to oppose blade vibrations, driven by their aerodynamic or inertial characteristics [46, 47]. Compared to active flow control devices, such as active flaps, this solution is easier to implement because it requires neither sensors nor actuators, with expected benefits in manufacturing and maintenance costs due to the reduced complexity.

3.3 Swept blades

Blade sweep consists in the edgewise displacement of the blade outboard region in the plane of rotation. The swept blade concept is regarded as a passive load mitigation technique because, when a sudden change in wind speed occurs, increased aerodynamic loads at the tip introduce a moment about the blade axis [48]; with enough blade torsional flexibility, the tip twists to feather, decreasing the angle of attack and hence reducing loads. Blade twisting due to sweep has a faster response compared to the traditional pitch system.

The alleviation of extreme loads and fatigue would allow for a substantial decrease in rotor cost by reducing the required materials and maintenance needs. This can be achieved when backward swept blades are used, meaning that the blade outboard region is curved in the opposite direction to the sense of rotation. The concept functioning is represented in Fig. 3.7.

On the other hand, by adopting forward sweep the blade tip twists to stall, so the angle of attack increases when the rotor is loaded, increasing the loads even further. This is the reason why the present study is going to focus primarily on backward swept blades. In Section 3.3.2, it will be better demonstrated why forward swept blades are not an interesting solution with respect to the goal of CoE reduction.

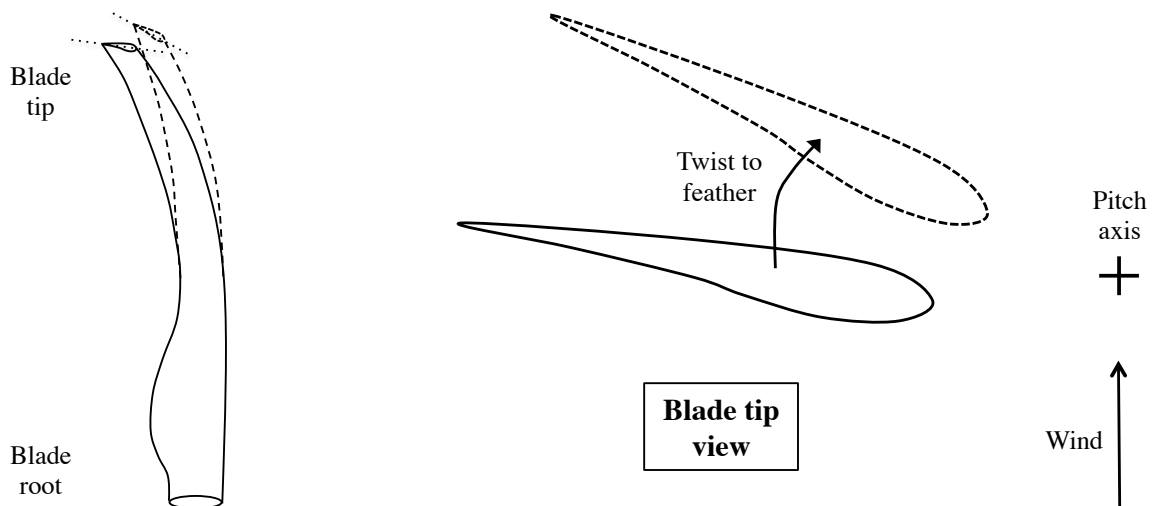


Figure 3.7: The swept blade concept: solid lines correspond to unloaded situation, while dashed lines represent the loaded blade with tip twisting to feather

Swept blades were originally proposed by Liebst [49] with the idea of applying to wind turbines a technique that had already been developed in the aerospace industry, in order to lower the loads from wind gusts for a given rotor diameter. The swept blade concept was then described by Zuteck [50] as an alternative to bend-twist coupling from off-axis fiber orientation, showing that to provide sufficient twisting for load relief it would be necessary to decrease torsional rigidity, which Zuteck achieved using carbon fiber in the spar caps. Starting from Zuteck's work, the STAR program developed a swept-twist adaptive rotor prototype [51]. The project included the design and manufacturing of swept blades for a 750 kW wind turbine, introducing the possibility to increase the rotor diameter so as to obtain benefits in terms of cost of energy thanks to load alleviation.

A parametric study of swept blades was conducted by Verelst [52] on a 5 MW wind turbine, investigating 120 variations in the sweep parameters and showing the positive effects on load reduction that can be achieved with this technology. Similar results were reported by Larwood [53] with the design of swept rotors for multi-MW wind turbines of different sizes. Swept blades have also started to be adopted on a commercial level; for example, in 2012, Siemens began large-scale production on a 3 MW machine using swept blades [54].

The major drawback that is inherent to swept rotors is a drastic increase in the blade root torsional loads, caused by the geometric shape of sweep. This induces an external torque that is transferred to the blade pitch system, potentially leading to additional wear in the pitch actuators. Moreover, given the torsional deformation of the blade under loading, the geometric twist distribution is not the same as the initial (optimal) one; this effect, together with the reduction in angle of attack, results in a power loss below rated wind speed. Recently, a method to provide an appropriate benchmarking of swept wind turbines rotors with comparable power curves has been proposed in Ref. [55]. Additionally, in order to compensate the decrease in angle of attack, the authors evaluated the possibility to pitch the blades towards stall with respect to the baseline blade so as to achieve a similar power output.

Several studies in the literature have also found that swept rotors in machines of very large size may exhibit aerodynamic instabilities, such as flutter [53], which are being extensively analyzed in the wind energy field due to the trends towards larger rotors.

Another drawback of swept blades is that they might be more difficult to manufacture compared to unswept rotors, because more complicated manufacturing processes or *ad-hoc* tooling may be required for fabrication. Furthermore, a larger blade envelope affects the transportability of the blade, especially for onshore applications; in fact, a limit on blade geometry variations like sweep is usually set as the maximum chord envelope.

3.3.1 Sweep curve parametrization

Backward swept blades

In the present study, the parametrization of swept geometries was performed using the formula introduced by Zuteck [50] and reported below:

$$y = d_{\text{tip}} \left(\frac{x - x_{\text{start}}}{L_{\text{blade}} - x_{\text{start}}} \right)^\gamma \quad (3.1)$$

where y is the local distance from pitch axis to sweep curve, x is the radial coordinate along the pitch axis, L_{blade} is the length of the unswept blade, d_{tip} is the distance of blade tip to pitch axis, x_{start} is the start position of sweep, and γ is the sweep curve exponent. The last three variables are the main parameters defining a swept shape; an example is reported in Fig. 3.8.

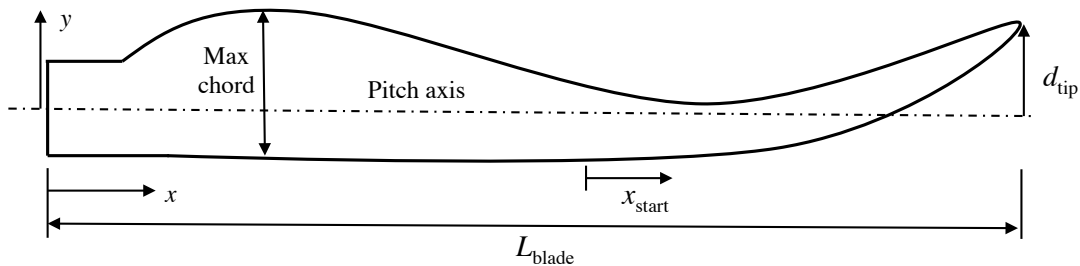


Figure 3.8: Backward swept blade geometry

An alternative sweep curve may be defined using a 3rd order polynomial equation [56]:

$$y(x) = \begin{cases} 0 & \text{if } 0 < x \leq x_{\text{start}} \\ \sum_{i=0}^3 a_i \cdot x^i & \text{if } x_{\text{start}} < x \leq L_{\text{blade}} \end{cases}$$

where a_i is the polynomial coefficient and all the other parameters are defined as in Eq. 3.1. However, this formula has not been used here.

Boomerang-shaped blades

As already mentioned, a major consequence of adopting swept blades is a dramatic increase in the blade root torsional loads, both fatigue and ultimate. Several swept rotor studies in the literature suggest using boomerang-shaped blades to limit this issue [52], but an actual design of wind turbine rotors with such advanced shape has not been described before to the author's knowledge, except for a load analysis performed in Ref. [57] simultaneously to the present work.

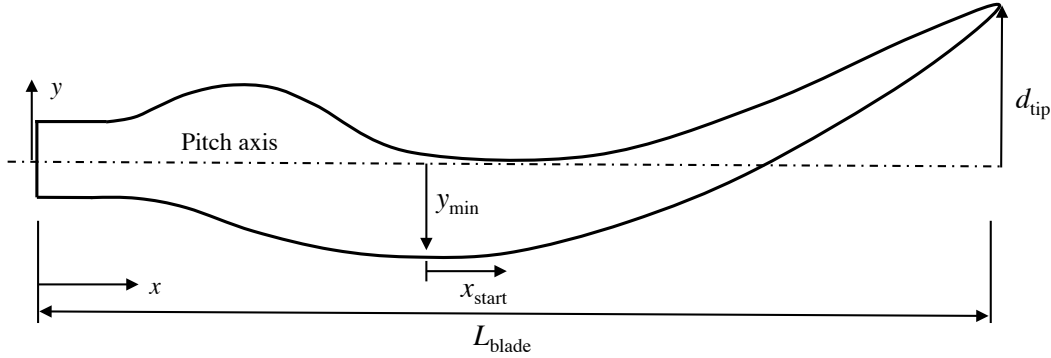


Figure 3.9: Boomerang-shaped blade geometry

With boomerang-shaped blades, the inner sections are forward swept in the opposite direction with respect to the outer part. This would produce a more aeroelastically balanced shape, as represented in Fig. 3.9. Hence, the previous sweep curve equation (Eq. 3.1) has been modified to account for the new particular shape in the design process:

$$y = (d_{\text{tip}} - y_{\text{min}}) \left(\frac{x - x_{\text{start}}}{L_{\text{blade}} - x_{\text{start}}} \right)^{\gamma} - y_{\text{min}} \quad (3.2)$$

where y_{min} is the distance from pitch axis at the maximum forward sweep location in the in-board sections of the blade, and x_{start} now corresponds to the radial position associated to y_{min} . Therefore, an additional sweep parameter needs to be considered to account for the novel shape, thereby raising the number of possible design combinations for swept blades manifold.

3.3.2 Backward vs. forward swept blades

An initial study has been conducted to show that dissimilar results are to be expected between backward and forward swept blades. For a better visualization of the different swept shapes, the former is represented in Fig. 3.10a, while the latter is depicted in Fig. 3.10b.

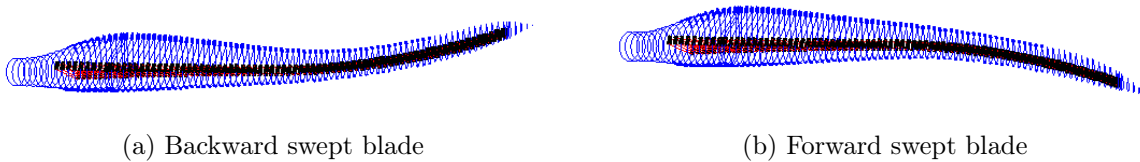


Figure 3.10: Backward vs. forward: blade shape

Simulations were performed on a 2 MW onshore machine using the design tool that will be discussed in Chapter 4. Only fatigue loads have been analyzed here, together with an estimate of the annual energy production (AEP). Two cases have been considered for both shapes, with tip sweeps of 2 and 3 m respectively. A sample of DEL moments at blade root and hub is reported in Fig. 3.11, clearly showing that load reduction effectively occurs with backward sweep, while forward sweep results in an increase in fatigue stress due to the twist-to-stall mechanism.

On the other hand, changes in AEP are shown in Fig. 3.12; as expected, the use of swept blades entails losses in energy capture, which are amplified when using forward sweep. Notice that all percentage differences are referred with respect to the baseline, which corresponds to the unswept blade.

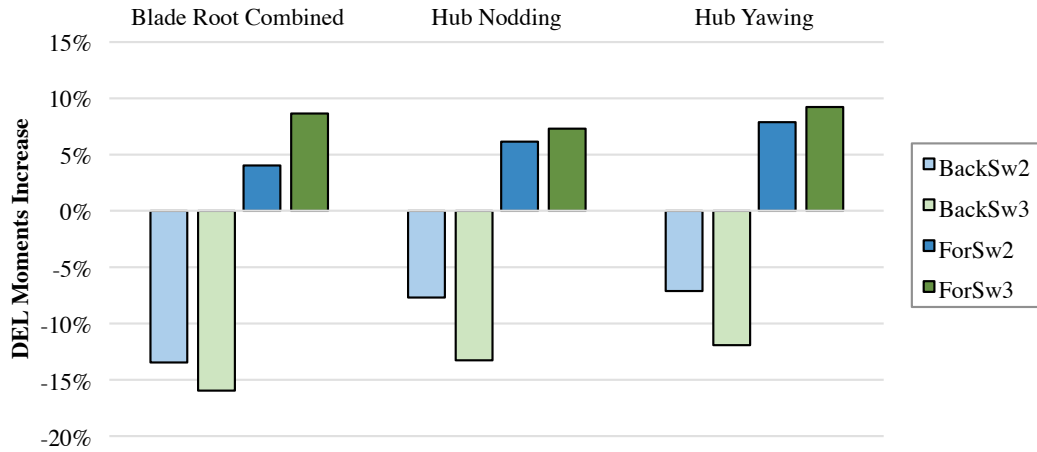


Figure 3.11: Backward vs. forward: fatigue DEL variations with respect to baseline for a sample of fatigue loads at blade root and hub

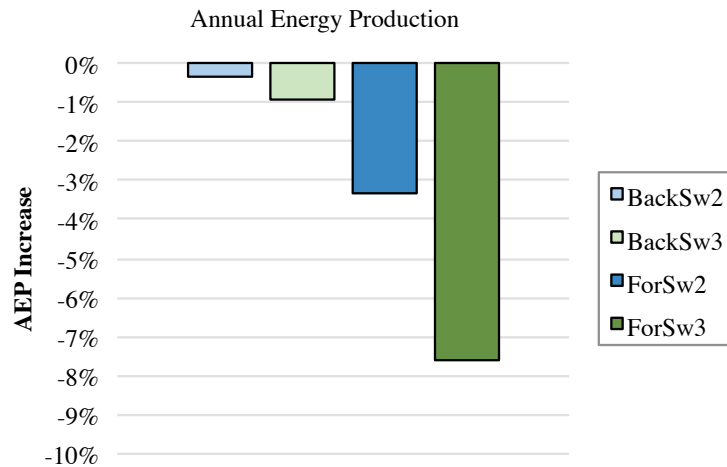


Figure 3.12: Backward vs. forward: AEP variations with respect to baseline

3.3.3 Preliminary sensitivity analysis

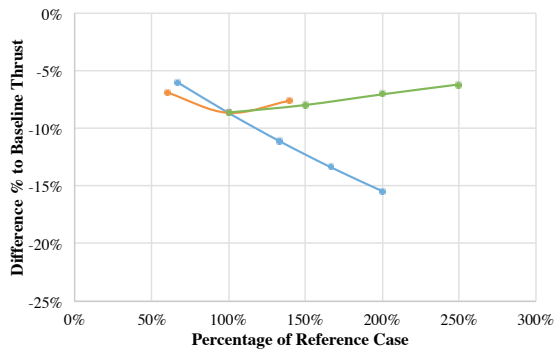
A sensitivity analysis has been performed to understand the influence of each sweep curve parameter of Eq. 3.1 on some key design variables, such as energy production, loads and amount of blade tip displacement. This preliminary analysis informed the decisions made in the design studies (Chapters 5 and 6) for the selection of the considered sweep cases.

The sensitivity analysis was conducted based on the unswept 2 MW wind turbine, which is taken as baseline. The length of the straight blades is 45 m. Moreover, a reference swept configuration was defined as a starting point for all the variations. Each sweep curve parameter, namely tip sweep d_{tip} , sweep start x_{start} , and sweep exponent γ , was varied individually and the values considered in this study are reported in Table 3.1.

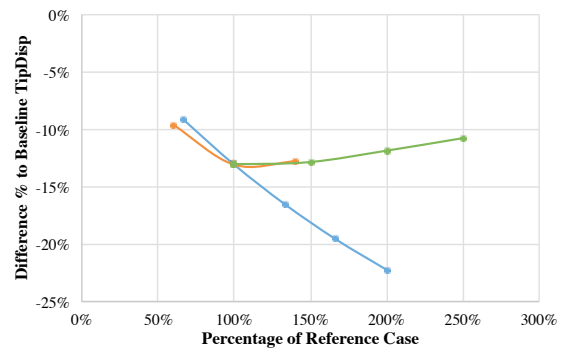
	Tip sweep d_{tip} [m]	Sweep start x_{start} [m]	Sweep exp γ [-]
Reference case	0.9	22.5	2
Variations	0.6	13.5	3
	1.2	31.5	4
	1.5		5
	1.8		

Table 3.1: Reference swept blade and variations of each sweep curve parameter

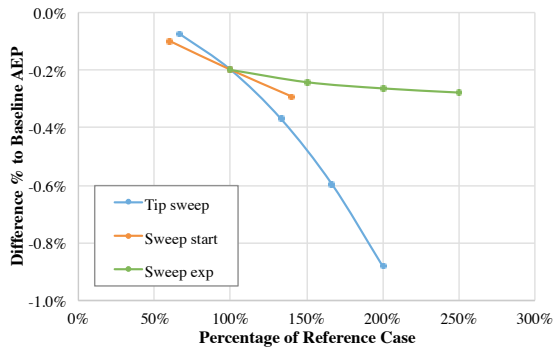
The results of the sensitivity analysis are shown in the plots below (Fig. 3.13). The percentage difference with respect to baseline (straight blade rotor) is reported on the vertical axis, whereas on the horizontal axis there is the percentage difference of each sweep parameter with respect to the reference case. Trends for annual energy production, tip displacement, ultimate thrust on the hub, and extreme torsional moment at the blade root are represented. Loads were computed by running dynamic simulations for DLC 1.3 [15], since it is usually the load case corresponding to the highest peak loads.



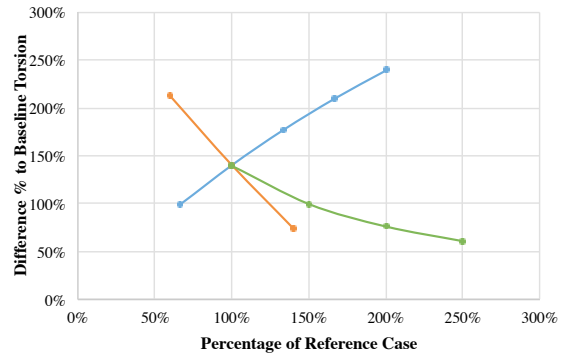
(a) Ultimate Thrust



(b) Tip Displacement



(c) Annual Energy Production



(d) Blade Root Torsion

Figure 3.13: Results from the sensitivity analysis

First, it is possible to make some general comments about the use of swept blades, regardless of the specific sweep parameters adopted. As expected, ultimate thrust and blade tip displacement are reduced compared to the unswept rotor, suggesting that good load alleviation can effectively be obtained from blade sweep. On the other hand, annual energy production appears to slightly decrease (within -1%) and blade root torsion is significantly higher compared to the straight blade.

Next, some conclusions on the influence of each sweep parameter may be drawn from the plots. Tip sweep is arguably the most sensitive parameter, since the impact on loads and AEP from changing tip sweep is larger compared to the other two variables. The ultimate thrust results show that increasing load reduction can be achieved with higher tip sweep, which is confirmed by the trends for tip displacement, a key design driver that is often associated to blade root loads. On the other hand, increasing tip sweep implies a drastic reduction in AEP and a substantial increase in blade torsion.

Finally, sweep start and curve exponent generally have minor effects on the considered design parameters; they seem to be relevant especially for torsional moments, because these loads may be reduced by shifting the sweep curve closer to the tip to have an overall more balanced blade. However, manufacturing blades that are more swept outboard may be constrained by the limits on curvature of the composite materials adopted.

Therefore, from the sensitivity analysis it could be concluded that tip sweep is the parameter with the largest effects on main design variables, which confirms results obtained from other parametric studies in the literature [53]. Hence, in the following design study, changes in sweep geometry for the different blade configurations have been applied mostly by varying tip sweep. Obviously, further analysis should be needed to consider more diverse combinations of the sweep parameters, but results are not expected to change considerably.

Wind turbine design algorithm

This chapter briefly describes the code used for all the simulations performed in this study, as well as the considered models to compute the cost of energy. The wind turbine simulation and design tool **Cp-Max**, which stands for **C**ode for **P**erformance **M**aximization, has been developed in the last decade by Prof. Bottasso and his collaborators at the Wind Energy Institute, Technische Universität München and at the Department of Aerospace Science and Technology, Politecnico di Milano. The overall code architecture is thoroughly described in Ref. [58] and its functions have been constantly improved to make sure that new advances in wind power technology can be properly accounted for and implemented in the simulations.

4.1 Integrated optimization of wind turbines

The design of a wind turbine is a complex multidisciplinary activity that requires the combination of high-fidelity physics-based models with robust and computationally efficient optimization processes. On the one hand, the external shape of rotor blades is mainly driven by aerodynamic considerations with the ultimate goal of maximizing wind energy capture, which can be achieved by using thin profiles with high efficiency and a low solidity rotor. On the other hand, thicker airfoils are required from structural efficiency considerations, especially around the blade root. Moreover, enough blade stiffness is needed to meet tower clearance and frequency constraints, hence an increased rotor solidity, while reducing weight and the need for high performance (and more expensive) materials.

The most suitable figure of merit driving the design optimization is typically identified as the cost of energy [59], which should be minimized in order to ensure competitive electricity generation from wind. As it will be explained more exhaustively in Section 4.4, cost of energy (CoE) depends both on annual energy production, which is associated to aerodynamic efficiency, and on the cost of the rotor, which is related to weight and materials of the blades. Therefore, it is essential to consider the subtle couplings existing between the aerodynamic and structural aspects of the problem, in order to design wind turbine rotors that aim at minimizing CoE.

Furthermore, a significant number of technological improvements has been developed over the last decades. Since any kind of innovative solution entails a cost and involves compromises among different variables, a holistic perspective of design is necessary in order to correctly appreciate the benefits of a new technology against its inherent drawbacks.

Several studies in the literature tackle the challenge of design optimization of wind turbine rotors, often distinguishing between aerodynamic and structural optimization loops. For example, some approaches are limited to the determination of the optimal aerodynamic shape of rotor blades [60, 61], while other procedures focus on the purely structural sizing problem [62, 63].

On the contrary, optimization tools that allow for the integrated design of wind turbines need to take into account all the subtle relations existing between the various design variables, in order to guarantee that the right trade-offs between performance and cost are achieved, while satisfying numerous design constraints. This can only be achieved by integrating into a single design framework all the different aspects of the wind turbine system, such as blade and tower structures, rotor aerodynamics, and control systems.

Hence, integrated design optimization allows for a fast exploration of the design space, potentially leading to significant improvements in terms of CoE. Such holistic approach has to consider a series of problems, which include the aerodynamic shape optimization of the rotor, the definition of appropriate control laws, the computation of all relevant load conditions, and the optimal structural sizing of the components, while considering the mutual couplings between the involved sub-systems as well as the presence of constraints of various nature.

The first steps toward the definition of integrated design methodologies for wind turbines were taken by Fuglsang and Madsen in 1999 [64]. Since then, integrated tools have been proposed by few institutions in the last decade. Notable examples include the code packages `RotorOpt` from LM Glasfiber [65], `FOCUS` from the Energy Center of The Netherlands [66], `HAWTOPT` from Denmark's Tekniske Universitet [67], and `WISDEM` from the National Renewable Energy Laboratory (NREL) and Sandia National Laboratories [68]. The field of multidisciplinary design optimization has been further explored by other recent studies that followed a multi-level approach [69], also for offshore environments [70], always with the target of CoE minimization.

The multidisciplinary research code `Cp-Max` has been developed in this framework. It basically integrates a high-fidelity aero-elastic simulator with optimization algorithms, and has evolved from a mostly structural sizing code to a comprehensive design optimization environment [58]. An integrated tool like `Cp-Max` can be useful for both the simulation and design of wind turbines, since it enables the analysis of an existing configuration as well as the sizing of a new machine. When it comes to rotor design, `Cp-Max` presents two major advantages.

First, the optimization procedure combines the overall sizing of the wind turbine with the detailed sizing of its aerodynamic and structural components [71]. This approach allows to take into account the complicated mutual effects among all systems of a wind turbine, which would probably be missed using simplified methods. For example, any change in the rotor diameter dramatically affects many factors, ranging from aerodynamics (hence power production) to loads (hence structural sizing and controls), from manufacturing to transportation issues. Therefore, it is crucial to choose the macroscopic parameters, such as rotor diameter and tower height, while taking into account the effects on detailed sizing of the wind turbine. Moreover, control laws are updated during the optimization process accordingly.

Second, many of the complex considerations that lead to the choice of a viable solution are formulated as design constraints to the optimization problem [72]. For example, the inclusion of a noise constraint by limiting tip speed significantly alters the regulation strategy of the wind turbine, as seen in Section 2.2.1, leading to changes in the power curve and hence affecting annual energy production. This may be mitigated by varying rotor solidity, which however has profound consequences on loads and might interact with other geometric constraints, such as the maximum chord length for ensuring road transportability of blades. Another example consists in the frequency constraint, which is related to the relative placement of the rotor natural frequencies with respect to the predominant harmonic excitations. As explained in Section 2.3.2, the insurgence of resonant conditions is to be avoided whenever possible. Additionally, while rotor weight is to be minimized, the maximum allowable stresses and strains on the blades must not be exceeded, and excessive tip deflections need to be avoided to prevent the blades from colliding with the tower during operation. Thus, in order to capture all the subtle effects involved, such design constraints need to be consistently enforced during the optimization process.

4.2 Aero-servo-elastic simulator

The core of the tool `Cp-Max` is a multi-body aero-servo-elastic simulator called `Cp-Lambda` [73], which stands for Code for Performance, Loads, Aeroelasticity by Multi-Body Dynamic Analysis. `Cp-Lambda` is a high-fidelity code able to represent the static and dynamic behavior of the machine in all relevant operating conditions experienced throughout the lifetime of a wind turbine.

The code was originally developed for rotorcraft applications and is based on a geometrically exact multi-body formulation of flexible systems with general topologies, expressed in terms of Cartesian coordinates and scaled Lagrange multipliers for the enforcement of constraints [74]. The software implements a complete library of elements, including rigid bodies, non-linear flexible beams, joints, actuators, and sensors (see Fig. 4.1). Spatial discretization of flexible components is done using the Finite Element Method (FEM), leading to a system of differential algebraic equations in the time domain. The code performs time integration by an implicit non-linearly unconditionally stable scheme, which includes high frequency dissipation by energy decay [75].

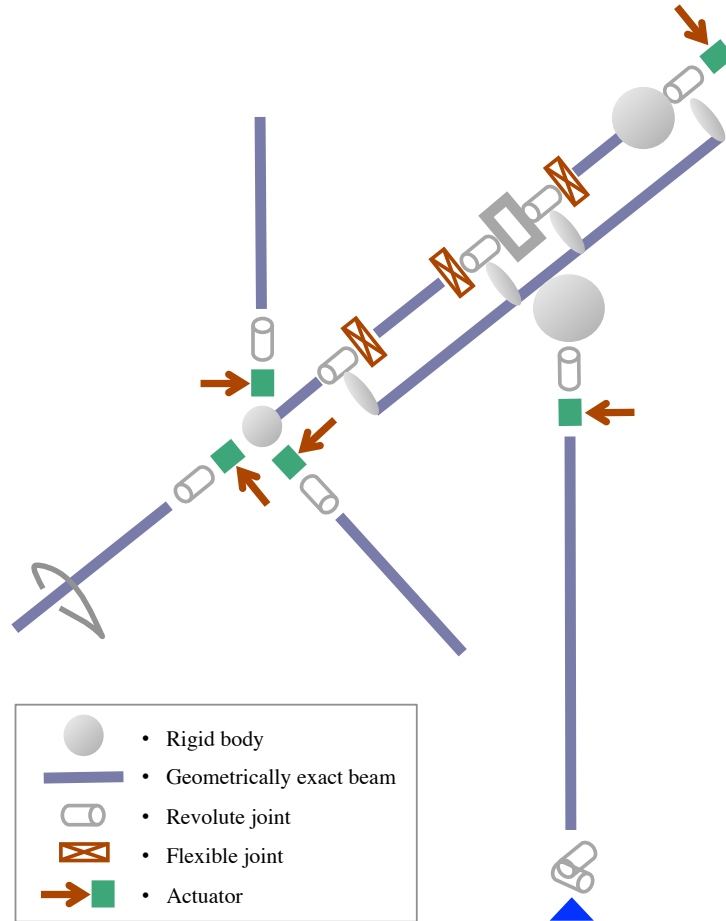


Figure 4.1: Aero-servo-elastic FEM multi-body model used by Cp-Lambda

Cp-Lambda is coupled with the Blade-Element Momentum (BEM) aerodynamic model [76], based on the annular stream-tube theory with wake swirl, including blade tip and root losses, as well as unsteady corrections, dynamic stall, and rotor-tower interference models. The BEM method assumes that a blade can be analyzed as a series of independent elements in the spanwise direction. The induced velocity at each blade element is computed through the momentum balance for a control volume containing the blade element itself. The aerodynamic characteristics are defined by lifting lines, where sectional aerodynamic coefficients are given in terms of Reynolds number and angle of attack from the airfoil data. Aerodynamic loads are computed at selected points along each lifting line, called airstations. Local airflow kinematics at each airstation include the contributions due to movement and deformation of the associated beam cross section.

The wind turbine is governed over all the operating conditions by the necessary control strategies, which are interfaced using an external routine. A Linear Quadratic Regulator (LQR) is adopted in the code [12], allowing for the automatic generation of control laws that are readily updated every time a wind turbine parameter changes. Pitch and torque are handled by controllers operating on the basis of data collected by sensor models.

4.3 General code structure

Cp-Max is built around Cp-Lambda in a MATLAB environment [77] and automatically interfaces with a number of other softwares and tools. Turbulent time histories are obtained using the open-source software TurbSim developed by NREL [78], whereas gusts are generated according to international standards [15,16]. Cp-Lambda is coupled with ANBA (Anisotropic Beam Analysis), a 2D finite-element cross-sectional analysis code implementing the anisotropic beam theory [79]. Given blade topology, geometry, and material properties, ANBA produces the six-by-six stiffness matrix, which accounts for all the possible couplings arising due to the use of anisotropic composite materials, as well as the sectional deformations associated with a certain set of loads. A similar procedure can be used for the structural sizing of the tower, which can optionally be dimensioned simultaneously to the rotor [80]. Finally, the commercial FEM solver NASTRAN [81] performs a high-fidelity structural analysis from the 3D shell mesh produced by Cp-Max, in order to capture the three-dimensional effects occurring in regions where discontinuities in the structural geometry and material properties are present.

The software Cp-Max was initially developed as an aerodynamic optimization package aiming at maximizing annual energy production by optimizing the blade chord and twist distributions. Later on, a blade structural optimization tool was implemented in Cp-Max for the minimization of rotor mass and cost. The code was further expanded into a truly integrated design tool thanks to the formulation of algorithms allowing for the simultaneous aero-structural optimization of the wind turbine rotor [58].

The overall architecture of the integrated aero-structural design procedures performed by Cp-Max is reported in Fig. 4.2. The next sections will be dedicated to the brief description of the aerodynamic and structural optimization algorithms and the integrated sizing loop.

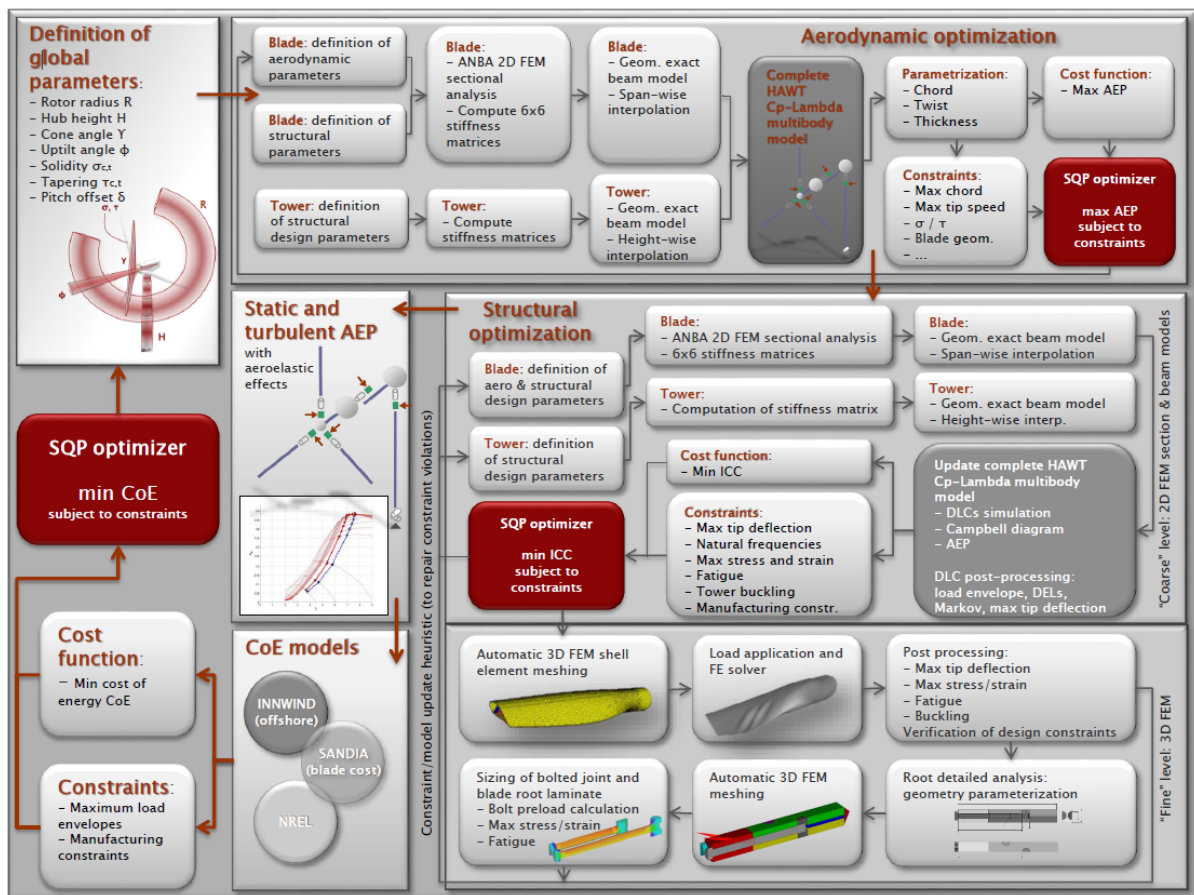


Figure 4.2: Overall architecture of the integrated aero-structural design procedure [71]

In the following, functions are expressed with the notation:

$$(O) = \text{FunctionName}(I) \quad (4.1)$$

where O are the output variables and I are the input ones.

4.3.1 Aerodynamic optimization

The rotor aerodynamic optimization consists in the computation of the optimal distributions of some aerodynamic variables, such as chord and twist angle, corresponding to maximum annual energy production (AEP). A formal description of the aerodynamic optimization problem, including the non-linear constraints to the solution, is reported below:

$$\mathbf{Function}(\mathbf{p}_a^*, AEP^*) = \text{MaxAEP}(\mathbf{p}_a, \mathbf{p}_s, \mathbf{p}_g, D) : \quad (4.2a)$$

$$AEP^* = \max_{\mathbf{p}_a}(\text{ComputeAEP}(\mathbf{p}_a, \mathbf{p}_s, \mathbf{p}_g, D)) \quad (4.2b)$$

$$\text{where } \mathbf{p}_a^* = \arg(\max_{\mathbf{p}_a}(\text{ComputeAEP})), \quad (4.2c)$$

$$\text{s.t. : } \mathbf{g}_a(\mathbf{p}_a) \leq 0. \quad (4.2d)$$

In the equation above, \mathbf{p}_a , \mathbf{p}_s , and \mathbf{p}_g are the vector arrays containing aerodynamic, structural, and global variables, respectively. In particular, function `MaxAEP` optimizes \mathbf{p}_a , consisting in the stacking of three vectors \mathbf{p}_{ac} , $\mathbf{p}_{a\theta}$, and \mathbf{p}_{at} , which control the chord, twist, and airfoil thickness distributions, respectively, obtained by spline interpolation on discrete nodal parameters. On the other hand, D is a list of given input quantities that remain constant throughout the optimization procedure:

$$D = \{P_r, C, V_{in}, V_{out}, AF, v_{tip_{max}}, L_{DLC}, \dots\} \quad (4.3)$$

including, for example, the rated power P_r , the wind turbine class C , cut-in and cut-out wind speeds V_{in} and V_{out} , the blade airfoils family AF , the maximum allowable tip speed $v_{tip_{max}}$, and the list L_{DLC} of all considered DLCs.

The optimization routine `ComputeAEP` in Eq. 4.2b is implemented in MATLAB and aims at finding the optimal set of parameters \mathbf{p}_a^* that achieves the highest possible AEP^* , while respecting the constraints \mathbf{g}_a defined in Eq. 4.2d. The optimization problem is solved by the function `fmincon`, which uses a Sequential Quadratic Programming (SQP) algorithm, computing gradients automatically by means of forward finite differences and allowing for the efficient handling of constraint equations. Such constraints can be tailored to the specific design needs and generally include limits on the maximum tip speed, maximum chord for road transportability, upper and lower bounds on rotor solidity and tapering for chord and twist distributions.

The evaluation of the cost function in `ComputeAEP` consists of several steps. First, the lifting lines describing the blade aerodynamic properties in `Cp-Lambda` are updated based on the current design parameters \mathbf{p}_a . Static simulations are run in steady wind conditions for varying values of the wind speed to evaluate the aerodynamic performance of the machine as a function of tip speed ratio λ and blade pitch angle β . Internal forces at the hub are then computed, which lead to the calculation of the thrust force and torsional moment. From these values, the power C_P and thrust C_T coefficients can be obtained, as functions of λ , β , and wind speed V , and are then stored in look-up tables. Therefore, the regulation trajectory can be computed based on the C_P table, defining the control parameters for each region in the power curve. Finally, annual energy production is obtained for each set of aerodynamic parameters \mathbf{p}_a by integrating the product of the power curve with the Weibull wind speed distribution for the given wind turbine class C . Notice that the AEP is recalculated also after the structural optimization loop using turbulent aero-elastic simulations.

4.3.2 Structural optimization

The structural optimization routine is a more computationally expensive loop that aims at obtaining the lightest structure for a set of design requirements, at frozen rotor aerodynamic configuration. The procedure is able to size the sole rotor for a given tower, the sole tower for a given rotor, or both simultaneously. The goal of the structural optimization is to identify the structural parameters \mathbf{p}_s^* associated to the minimum initial capital cost ICC^* . A formal description of the structural optimization algorithm is reported in the following:

$$\mathbf{Function} (\mathbf{p}_s^*, ICC^*) = \text{MinICC}(\mathbf{p}_a, \mathbf{p}_s, \mathbf{p}_g, D, \mathbf{\Gamma}_s) : \quad (4.4a)$$

$$\mathbf{do} \quad (4.4b)$$

$$(LQR) = \text{LQRController}(\mathbf{p}_a, \mathbf{p}_s, \mathbf{p}_g, D), \quad (4.4c)$$

$$(\mathbf{E}) = \text{LoadEnvelope}(\mathbf{p}_a, \mathbf{p}_s, \mathbf{p}_g, D, LQR), \quad (4.4d)$$

$$ICC^* = \min_{\mathbf{p}_s}(\text{ComputeICC}(\mathbf{p}_a, \mathbf{p}_s, \mathbf{p}_g, D, \mathbf{E}, \mathbf{\Gamma}_s)) \quad (4.4e)$$

$$\text{where } \mathbf{p}_s^* = \arg(\min_{\mathbf{p}_s}(\text{ComputeICC})), \quad (4.4f)$$

$$(\mathbf{\Gamma}_s^*) = \text{3DFEAnalysis}(\mathbf{p}_a, \mathbf{p}_s^*, \mathbf{p}_g, D, \mathbf{E}, \mathbf{\Gamma}_s), \quad (4.4g)$$

$$\Delta p_s = \|\mathbf{p}_s^* - \mathbf{p}_s\|, \quad \Delta ICC = \|ICC^* - ICC\|, \quad \Delta \mathbf{\Gamma}_s = \|\mathbf{\Gamma}_s^* - \mathbf{\Gamma}_s\|, \quad (4.4h)$$

$$\mathbf{p}_s = \mathbf{p}_s^*, \quad \mathbf{\Gamma}_s = \mathbf{\Gamma}_s^* \quad (4.4i)$$

$$\mathbf{while} (\Delta p_s \geq \text{tol}_{p_s}, \Delta ICC \geq \text{tol}_{ICC}, \Delta \mathbf{\Gamma}_s \geq \text{tol}_{\mathbf{\Gamma}_s}). \quad (4.4j)$$

In the equation above, \mathbf{p}_s is a vector containing the thicknesses of the structural components at a chosen number of control stations along the blade, and optionally of the tower. The blade optimization parameters include the thickness of spar caps, shear webs, shell skin, and leading and trailing edge reinforcements; the structural design variables for the tower are the outer diameter and wall thickness. The variable distributions in between the nodal values are then obtained by spline interpolation.

As shown in the simplified representation of the overall design procedure in Fig. 4.3, the structural optimization is an iterative loop. First, the regulation trajectory of the wind turbine is calculated, followed by the LQR controller gains. Next, as expressed in Eq. 4.4c, loads are computed by running all the DLCs from the list L_{DLC} using the multi-body model implemented in Cp-Lambda. Outputs of the aero-servo-elastic simulator are then post-processed in Eq. 4.4d to obtain the load envelopes \mathbf{E} , at a given number of verification sections along the blade and/or tower. Load envelopes consist in the selection of the most severe conditions for each load component corresponding to maxima and minima within all time histories of the considered set of DLCs. Extreme stress and strain distributions are evaluated by ANBA, whereas fatigue damage is estimated using a rainflow counting algorithm.

Hence, for the given load envelopes \mathbf{E} , the structural sizing routine is performed in Eq. 4.4e. From the detailed design of the structural components of rotor and tower, a bill of materials can be obtained, which in turn allows for the estimation of the cost of each component, resulting in the definition of the ICC. In particular, blade mass is computed by considering also non-structural mass contributors, such as adhesives, resin uptake, bonding plies, and the presence of a lightning protection system. At the end of this step, the minimum initial capital cost ICC^* is found, as well as the corresponding set of structural design parameters \mathbf{p}_s^* , which satisfies the design requirements $\mathbf{\Gamma}_s$. The latter is a list of inequality constraints defined as:

$$\mathbf{\Gamma}_s = \{\sigma_{\text{adm}}, \epsilon_{\text{adm}}, \delta_{\text{tipadm}}, \omega, d, \dots\} \quad (4.5)$$

and includes the admissible values for stress σ_{adm} and strain ϵ_{adm} , maximum allowable blade tip deflection δ_{tipadm} based on tower clearance, frequency constraints ω to avoid resonant conditions, bounds on fatigue damage d , and other manufacturing and technological requirements.

As it was for the aerodynamic optimization, the structural sizing routine is solved by a SQP algorithm, which is particularly indicated for problems where several constraints may be simultaneously active at convergence. In order to reduce computational effort and allow for the gradient-based solver to work properly, loads are temporarily kept constant during the optimization process. However, loads need to be updated so as to reflect variations due to the modified design of the wind turbine. The controller is also tuned whenever the design changes, so that dynamic simulations of the machine always produce consistent load conditions. This is the reason why an iterative loop is required for the structural sizing procedure: as soon as an optimal structural configuration is found by the SQP algorithm at fixed loads, the aero-elastic model of the wind turbine is updated and DLCs are simulated again with the new structural parameters. This iterative process is repeated until convergence is reached, when \mathbf{p}_s , ICC , and \mathbf{F}_s are within the predefined tolerance as in Eq. 4.4j.

Structural sizing is followed by the higher-fidelity 3D FEM analysis defined in Eq. 4.4g. This step is necessary to verify that all structural constraints are satisfied at a finer level. A 3D shell-element mesh is then created for the blade and associated with a set of load conditions. Changes in the constraint bounds are taken into account by updating \mathbf{F}_s , although effects on ICC are usually limited.

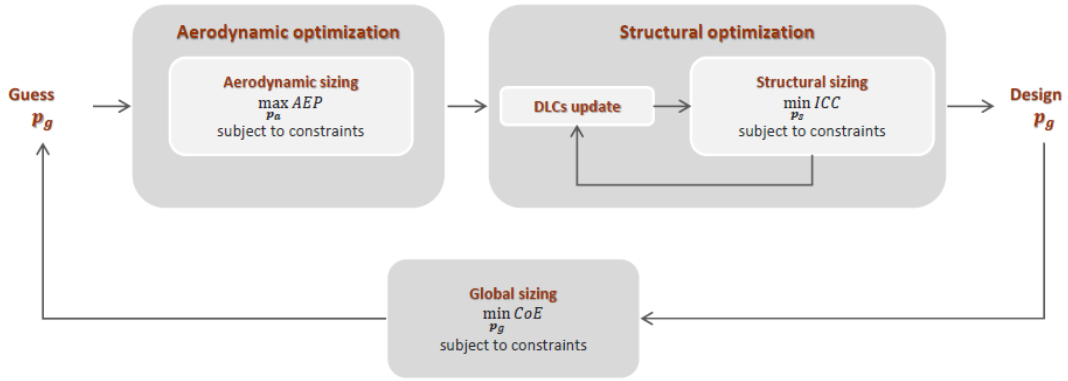


Figure 4.3: Simplified structure of the integrated aero-structural design procedure [71]

4.3.3 Global sizing

The integrated optimization is an outer loop that combines both the aerodynamic and structural optimization routines with the CoE evaluation. The goal is to find the wind turbine configuration leading to the minimum cost of energy, as shown in Fig. 4.3. The formal description of the overall sizing algorithm is reported below:

$$\mathbf{Function} (\mathbf{p}_a^*, \mathbf{p}_s^*, \mathbf{p}_g^*, CoE^*) = \text{MinCoE}(\mathbf{p}_a, \mathbf{p}_s, \mathbf{p}_g, D, \mathbf{F}_s) : \quad (4.6a)$$

$$CoE^* = \min_{\mathbf{p}_g} (\text{ComputeCoE}(\mathbf{p}_a, \mathbf{p}_s, \mathbf{p}_g, D, \mathbf{F}_s)) \quad (4.6b)$$

$$\text{where } \mathbf{p}_a^*, \mathbf{p}_s^*, \mathbf{p}_g^* = \arg(\min_{\mathbf{p}_g} (\text{ComputeCoE})), \quad (4.6c)$$

$$\text{s.t. : } \mathbf{g}_g(\mathbf{p}_g) \leq 0. \quad (4.6d)$$

The vector containing the global optimization variables \mathbf{p}_g includes rotor radius R , hub height H , rotor cone angle γ , nacelle uptilt angle ϕ , and four blade aero-structural parameters that couple the two sub-loops, namely rotor planar solidity σ_c and tapering τ_c , and blade thickness solidity σ_t and tapering τ_t .

$$\mathbf{p}_g = [R, H, \gamma, \phi, AF, \sigma_c, \tau_c, \sigma_t, \tau_t] \quad (4.7)$$

Among the global variables \mathbf{p}_g , rotor radius R is the most sensitive parameter with respect to the CoE merit figure. In fact, even a little variation in the rotor radius entails significant changes in numerous aspects of wind turbine design, such as aerodynamic performance, regulation trajectory, and structural loads. Furthermore, most of the cost items within the CoE models are scaled for the rotor radius.

Hub height H instead directly affects the tower height, hence also the magnitude of mean wind speed, although international standards [15] correlate it to the wind turbine class C only. On the contrary, a site-specific optimization is performed in **Cp-Max**, where a change in tower height has a direct impact on wind shear and average wind speed. For instance, a higher H obviously implies higher capital costs, but it also provides some benefits in terms of aerodynamic performance of the wind turbine, as wind speeds are typically higher at greater heights due to vertical shear.

Rotor cone angle γ and nacelle up tilt ϕ mainly influence the power coefficient C_P , which leads to changes in the annual energy production. In particular, AEP is reduced when the two angles increase, but this may lead to structural benefits in terms of constraints related to the maximum blade tip deflection for tower clearance. Finally, the role of the four blade aerostuctural parameters σ_c , τ_c , σ_t , and τ_t is to basically enable the integrated design procedure by coupling the aerodynamic and structural sub-loops.

The outer loop may also be subjected to non-linear constraints \mathbf{g}_g , as expressed in Eq. 4.6d, which include minimum clearance between blade tip and ground and other constraints on maximum loads.

The computation of minimum cost of energy CoE^* is performed in Eq 4.6b with the function `ComputeCoE`. Essentially, the procedure consists in a sequence of aerodynamic optimization, structural optimization, recomputation of AEP, and final evaluation of the CoE, until a minimum of the cost function is found, as shown in Eq. 4.8. In order to limit computational effort, the most intensive steps, such as DLCs simulations and the structural sizing routine in Eq. 4.4e, are run in parallel independently on multiple cores.

$$\mathbf{Function}(\mathbf{p}_a^*, \mathbf{p}_s^*, \mathbf{p}_g, CoE) = \mathbf{ComputeCoE}(\mathbf{p}_a, \mathbf{p}_s, \mathbf{p}_g, D, \mathbf{\Gamma}_s) : \quad (4.8a)$$

$$(\mathbf{p}_a^*, AEP^*) = \mathbf{MaxAEP}(\mathbf{p}_a, \mathbf{p}_s, \mathbf{p}_g, D), \quad (4.8b)$$

$$(\mathbf{p}_s^*, ICC^*) = \mathbf{MinICC}(\mathbf{p}_a^*, \mathbf{p}_s, \mathbf{p}_g, D, \mathbf{\Gamma}_s), \quad (4.8c)$$

$$(AEP^{**}) = \mathbf{ComputeAEP}(\mathbf{p}_a^*, \mathbf{p}_s^*, \mathbf{p}_g, D), \quad (4.8d)$$

$$(CoE) = \mathbf{CoEmod}(AEP^{**}, ICC^*, \mathbf{p}_a^*, \mathbf{p}_s^*, \mathbf{p}_g, D). \quad (4.8e)$$

Thus, the optimal vector of global parameters \mathbf{p}_g^* is computed, together with the associated optimal aerodynamic and structural vectors \mathbf{p}_a^* and \mathbf{p}_s^* , that achieve the minimum CoE^* . The overall wind turbine design process can be usually completed in a matter of hours or tens of hours, depending on several factors, such as the number of considered DLCs, the amount of design parameters, and the mesh refinement of the multi-body model.

4.4 Cost of energy models

Cost of energy is the most appropriate figure of merit to be minimized when it comes to providing a competitive electricity generation from wind. CoE depends, among other factors, on the aerodynamic performance and on the cost of the wind turbine. Different approaches for the definition of the optimization objective have already been assessed, but it has been demonstrated that CoE is the metric that better captures the numerous trade-offs in the design process [59].

Some studies in the literature focus on optimizing the aerodynamic efficiency of the wind turbine rotor by maximizing annual energy production. However, this approach leads to significantly inferior solutions compared to minimum CoE design, because similar aerodynamic performance can be achieved with turbine configurations that have very different masses.

Another method is to minimize the ratio between turbine mass and annual energy production, coupling the aerodynamic and structural disciplines. This choice is reasonable because the ratio resembles the definition of CoE and it assumes that costs scale proportionally with wind turbine mass, which is useful when a detailed cost model is absent. Nonetheless, this metric typically overemphasizes the role of the tower mass, which in practice has very limited effects on the total cost of the machine, as shown in Fig. 4.5 for the baseline 2 MW wind turbine.

Hence, minimum CoE is accepted as the best metric to balance aerodynamic and structural performance and produce robust designs. Cost of energy represents the sum of all costs of a fully operational wind power system over its lifetime and can be defined by the following equation:

$$\text{CoE} = \frac{\text{FCR} \cdot (\text{TCC} + \text{BOS})}{\text{AEP}} + \text{OPEX} \quad (4.9)$$

where FCR is the fixed charge rate associated to the cost of capital; TCC is the turbine capital cost, taking both rotor and tower into account; BOS is the balance-of-station cost mainly due to additional electrical equipment, foundation, transportation, and assembly; OPEX represents the annual operation and maintenance expenses; and AEP is the annual energy production. The unit of measurement of CoE is generally expressed in \$/kWh (or €/kWh).

The key elements affecting the CoE of a wind power system are reported in Fig. 4.4.

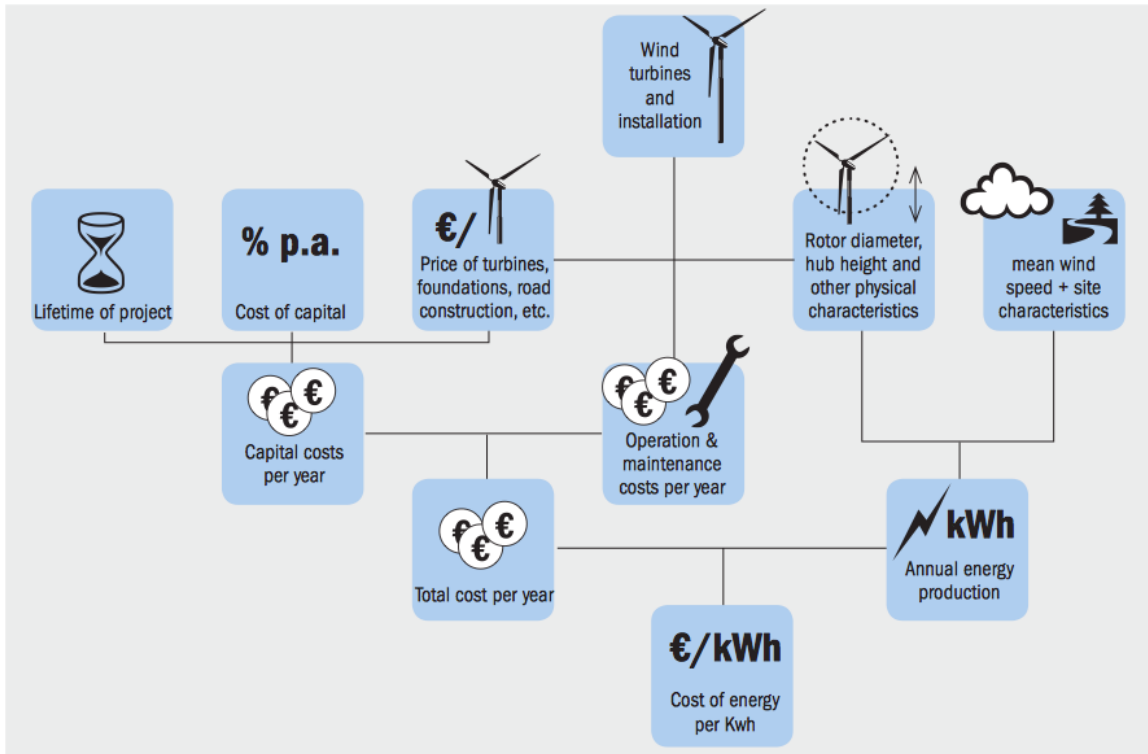


Figure 4.4: The cost of wind energy [82]

Since the cost of energy is the main parameter driving the design optimization process, it is clear that the choice of accurate CoE models is of crucial importance. In the present work, two cost models have been considered to account for the very different applicability range.

For the 2 MW wind turbine, the NREL cost model [83] has been used, which was initially developed for mid-size onshore machines like the one studied in this thesis. The NREL cost model is a spreadsheet-based tool that adopts simple scaling relationships to estimate the cost of wind turbine components and sub-systems for different sizes and configurations. In most cases, cost and mass models directly depend on the macro-parameters of the wind turbine, such as power rating, rotor diameter, tower height, or combinations of these factors.

On the other hand, for the 10 MW wind turbine, the recent INNWIND cost model [84] has been adopted, which was especially formulated for the design of large next-generation offshore machines. The INNWIND framework is based on the general approach of the NREL cost model, but it takes into account additional information relevant to offshore applications, such as water depth and distance from land.

Parallel to the two CoE models, a detailed Blade Cost Model (BCM) developed by Sandia National Laboratories [85] is implemented in the code to better account for the aero-structural trade-offs of the rotor. In particular, this model allows to overcome the simplified relations between blade mass or length and rotor cost adopted in both the NREL and INNWIND models.

The Sandia BCM is divided into three main cost items: material, labor, and equipment. Material costs take into account the mass and volume of each blade structural component according to the different materials used, such as fibers, resins, sandwich core, adhesives, paint, etc. Labor costs consist in the product between the labor hours needed for blade manufacturing, which depend on several geometrical and structural scaling factors, and the wage rate, which can be tuned according to the country where the production process takes place. Equipment costs estimate the price of mold and tooling divided by the number of blades that can be fabricated with a single set of equipment.

The addition of the swept shape analyzed in the present study entails an increase in the blade length, therefore variations in the blade costs are comprised for material and labor expenses. However, effects on transportation costs are not fully taken into consideration. Moreover, the adoption of swept blades may require particular changes in the manufacturing equipment because of their complex shape, possibly resulting in a cost of energy that is a little higher compared to what is estimated here.

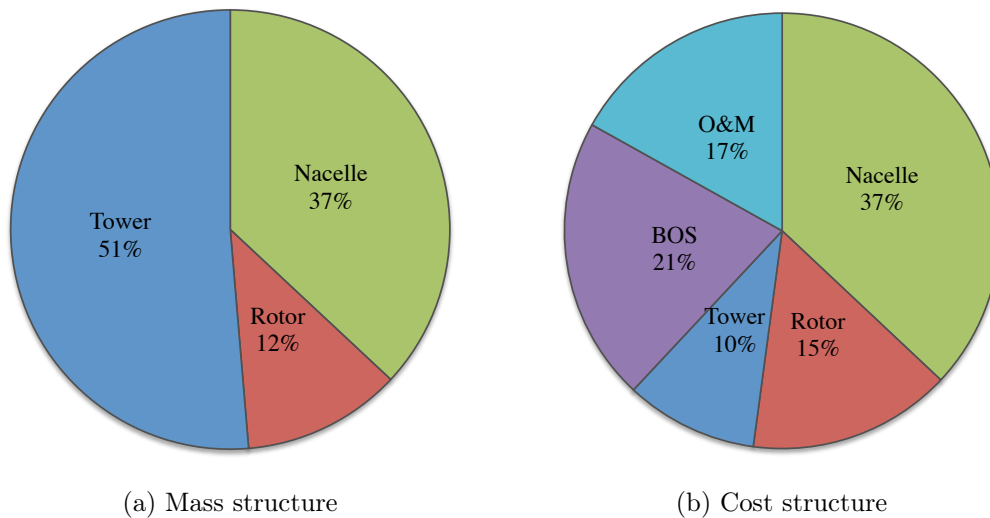


Figure 4.5: Relative contributions to total mass and total cost

4.5 Code modifications to account for sweep

Several corrections were required in order to introduce the sweep characteristic into **Cp-Max**. Major changes mainly consisted in the expansion of some model initializing functions from 2D to 3D. In fact, blade geometry had originally been defined using only the spanwise coordinate, which corresponds to the radial direction along the blade pitch axis. More recently, a second dimension had been introduced to account for blade prebend, which is a viable solution to the problem of tower clearance. Basically, blades are prebent to such an extent that they are straightened into their design configuration when the wind turbine operates at rated conditions.

Now, the code is even able to initialize and simulate blade geometries in three dimensions, hence allowing to account for both prebend and sweep simultaneously. This has been possible thanks to corrections in the MATLAB routines dedicated to the elaboration of geometric data using NURBS (Non-Uniform Rational B-Splines), which create and process curves and surfaces by means of splines and Bézier curves [86].

Introducing sweep in the blade geometry initially produced inconsistent results due to the very nature of splines, because the blade curvature actually presented oscillations in the spanwise sections with no sweep. This issue was especially problematic for backward swept blades, which are straight before the sweep starting position. A solution to the problem has been found by “cutting” non-zero values of the curve until the last unbent coordinate, hence flattening the spline and deleting all the oscillations in the sweep curvature, as represented in Fig. 4.6.

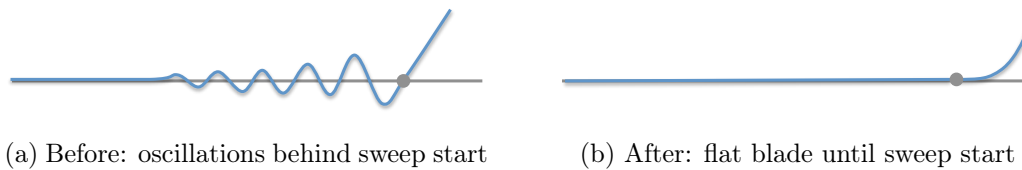


Figure 4.6: Flattening of the spline associated to the blade (magnified view close to the sweep starting position along the span)

On the other hand, the creation of boomerang-shaped blades originally presented a different issue that resulted in unrealistically high values of blade torsion at the root. In fact, the blade curvature was first produced in such a way that torsional moments acting on the blade root included effects from other forces, such as flapwise and edgewise moments. This issue has then been solved by moving the beginning of the sweep curvature slightly further along the span, leaving a straight part of the blade in the closest sections to the root. This solution effectively enabled to consider such an advanced shape in the design process, therefore allowing to show the potential of boomerang-shaped blades for the first time.

Moreover, several verification tests based on first derivative analysis have been implemented into **Cp-Max** so as to check the consistency of the blade curvature at the beginning of the simulation procedure. The goal of these tests is to avoid the creation of splines leading to unfeasible blade shapes that the code would not be able to process properly, due to the presence of too many sign-switching points or discontinuities in the curve. Whenever such an error occurs, a warning is now displayed to the user asking for corrections in the input files.

In the present study, several sweep curvatures have been defined and each of them has been aerodynamically and structurally optimized. In order to limit the inevitable loss in AEP occurring with swept blades and make a fair comparison with respect to the straight configuration, a constant rotor radius has been considered here so as to maintain the same rotor area for all cases. In fact, a similar swept area would eventually lead to a more similar AEP, reducing the gap between swept and unswept blades.

Notice that the code originally kept a fixed blade length instead of a constant rotor radius, because $C_p\text{-Max}$ had not been used to study swept blades before. As it is clearly shown in Fig. 4.7, using a swept blade with the same length of the unswept configuration would imply a reduced rotor swept area, thus a considerably decreased AEP, compared to keeping a constant rotor radius and allowing the blade length to increase.

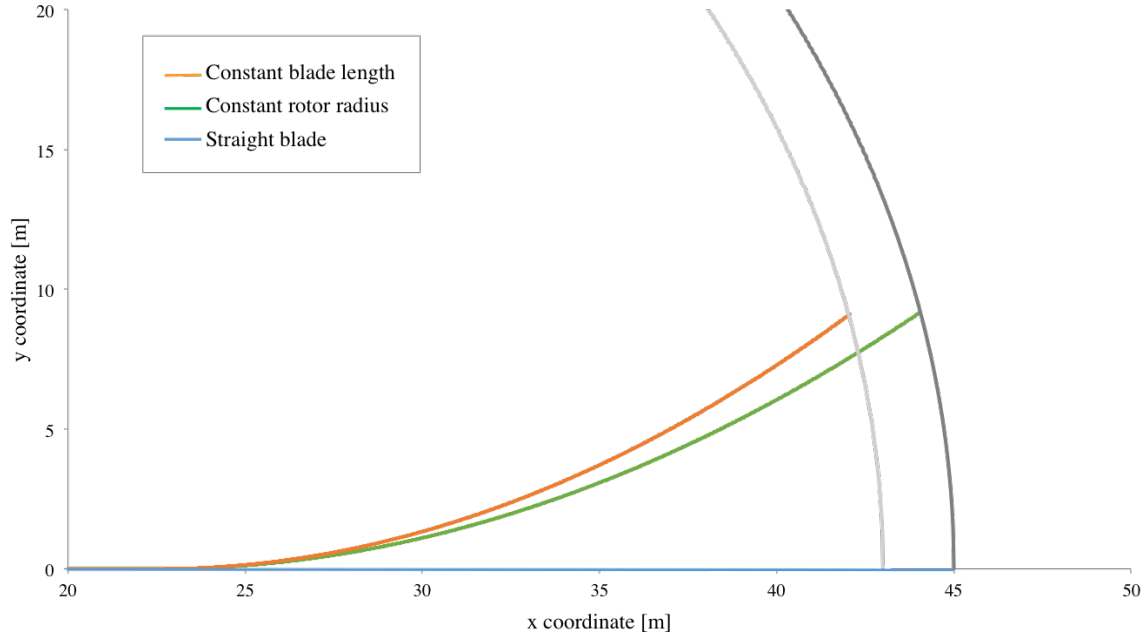


Figure 4.7: Fixed blade length vs. fixed rotor radius

The new algorithm, which allows to maintain a constant rotor radius while accounting for both sweep and prebend, is reported below.

$$TBSA = RotorDiameter/2 - BladeRoot; \quad (4.10a)$$

$$\text{for } i = 2 : \text{length}(\eta) \quad (4.10b)$$

$$x_{Radius}(i) = x_{Radius}(i-1) + \sqrt{TBSA \cdot (\eta(i) - \eta(i-1))^2 - (PB(i) - PB(i-1))^2}; \quad (4.10c)$$

$$\text{end} \quad (4.10d)$$

$$alfa = \text{asin}(SW(\text{end})/x_{Radius}(\text{end})); \quad (4.10e)$$

$$\text{for } i = 2 : \text{length}(\eta) \quad (4.10f)$$

$$x_{PA}(i) = x_{Radius}(i) \cdot \cos(alfa); \quad (4.10g)$$

$$\text{end} \quad (4.10h)$$

$$\text{for } i = 2 : \text{length}(\eta) \quad (4.10i)$$

$$BL = BL + \sqrt{(x_{PA}(i) - x_{PA}(i-1))^2 + (PB(i) - PB(i-1))^2 + (SW(i) - SW(i-1))^2}; \quad (4.10j)$$

$$\text{end} \quad (4.10k)$$

where $TBSA$ stands for *ThicknessBladeSweptArea* and corresponds to the length of the straight blade, $BladeRoot$ is the extent of the blade length that is enclosed within the hub, η is the non-dimensional coordinate along the blade span, x_{Radius} is the radial coordinate from root to tip, x_{PA} is the radial coordinate along the pitch axis, BL is the new blade length, PB is the prebend coordinate, and SW is the sweep coordinate.

The new parametric model described in Eq. 4.10 was deemed necessary to introduce consistent coordinates for sweep and prebend, because **Cp-Lambda** works and elaborates geometries in the three dimensional system, whereas most parameters in **Cp-Max** are defined by distributions along the span of the blade.

A graphical representation of the geometric variables used in the code is reported in Fig. 4.8, where the view of the blade in the plane of rotation is represented on the left, whereas the figure on the right shows the side-view of the blade. The functioning of the new algorithm may be better appreciated by looking at the figure below, which also allows to see how both prebend and sweep can effectively be taken into account at the same time.

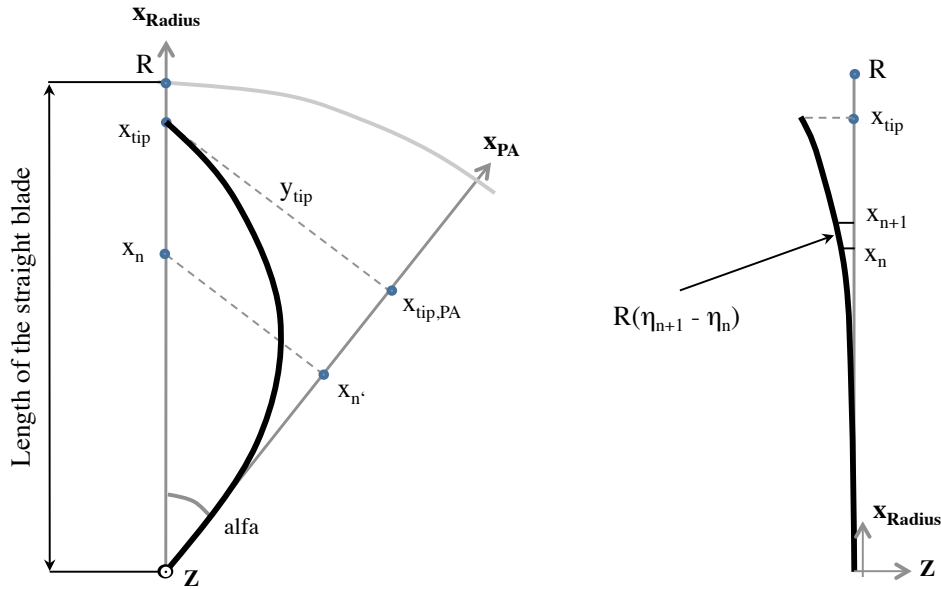


Figure 4.8: Representation of the new geometric coordinate system, showing blade sweep (left) and prebend (right) simultaneously

Parallel to the present work, a new version of **Cp-Max** has been developed with the main goal of improving the usability of the program. This was achieved by implementing graphic user interfaces that would make the definition of optimization parameters much simpler. Therefore, the models for the new code release had to be created or modified from the previous version, ensuring their functioning for all design purposes, including the study of swept blades. Great efforts have been put into the processing of output data from the new **Cp-Max** and into the integration of the originally numerous input files into a single Excel spreadsheet.

Finally, the use of swept blades generated a number of other issues in the design process, especially during the computation of loads at the considered design load cases. For example, the gains, tolerance, and initial conditions of the dynamic simulations had to be changed by adjusting the time functions of rotor speed and pitch angle, so as to ensure convergence.

Moreover, in order to properly create the control laws for swept rotors, the controller had to be adjusted for each machine; in particular, the weights of the LQR controller had to be set accordingly in order to regulate the gains of control quantities such as blade pitch and generator torque, allowing for the correct functioning of the simulations.

2 MW wind turbine

The potential of swept blades for load reduction is first assessed for an onshore 2 MW wind turbine. This chapter begins with the description of the baseline configuration for this machine, which is considered as reference for the swept rotors analyzed in the present study. An initial load analysis is performed in Section 5.2 in order to understand the extent of load alleviation for different sweep geometries, including boomerang-shaped blades. Both ultimate loads and fatigue are computed for design load cases corresponding to normal operation. Moreover, trends for maximum tip displacement are discussed. The study continues with the design optimization of a set of swept rotors in Section 5.3, which is conducted with the integrated design algorithm described in Chapter 4. Twist distribution is optimized for each configuration and structural sizing is performed using a reduced number of design load cases, taking into account the most relevant design constraints. The potential benefits deriving from blade sweep are further evaluated through the optimized design of larger rotors in Section 5.4. Lastly, the design of wind turbine rotors with a combination of sweep and prebend is considered in Section 5.5.

5.1 Baseline wind turbine

The 2 MW machine is a class 3A onshore three-bladed wind turbine, with a variable-speed rotor and collective pitch control. Blades are made of standard glass fiber reinforced plastic (GFRP) with two spar caps, two shear webs, a skin layer and extra unidirectional reinforcements at the leading (LE) and trailing edges (TE). The main parameters of the baseline wind turbine are reported in Table 5.1.

Data	Value	Data	Value
Wind class	IEC 3A	Rated power	2 MW
Hub height	80.0 m	Rotor diameter	92.4 m
Hub diameter	2.4 m	Max tip speed	72 m/s
Rotor cone	2.0 deg	Nacelle uptilt	6.0 deg
Blade mass	8730 kg	Tower mass	125 ton
Cut-in wind speed	4 m/s	Cut-out wind speed	25 m/s

Table 5.1: Configuration of the baseline 2 MW wind turbine

The optimal configuration for this wind turbine was found using **Cp-Max** prior to this study. The corresponding chord and twist distributions are shown in Fig. 5.1. The blades are equipped with DU airfoils [87] positioned as listed in Table 5.2, while the blade topology and its structural configuration are described in Table 5.3.

In the design optimization problem, the aerodynamic parameter vector \mathbf{p}_a includes 13 variables, which describe twist at 5 stations along the blade span, and chord and airfoil positions at 4 stations, while the structural vector \mathbf{p}_s parameterizes 7 structural components at 11 spanwise locations.

Airfoil name	Span position
Circle	0.0%
Circle	2.2%
DU00-W2-401	19%
DU00-W2-350	26%
DU97-W-300	35%
DU91-W2-250	48%
DU93-W-210	69%
DU95-W-180	89%
DU95-W-180	100%

Table 5.2: Spanwise positioning of the airfoils for the 2 MW wind turbine

Structural component	From (% span)	To (% span)	Material type
External shell	0	100	Stitched triaxial fiberglass
Spar caps	10	98	Unidirectional fiberglass
Shear webs	10	98	Stitched biaxial fiberglass
TE and LE reinforcements	10	80	Unidirectional fiberglass
Sandwich core	5	95	Balsa

Table 5.3: Blade topology for the 2 MW wind turbine

Extreme moments on the load envelope resulting from dynamic simulations performed for a reduced set of DLCs are reported in Table 5.4 with the corresponding load case. These ultimate loads, together with the fatigue moments in Table 5.5, represent the reference for all the swept configurations that will be introduced later. The considered load cases – including DLCs 1.1, 1.3, 2.1, 2.3, 6.1, 6.2, and 6.3 – represent normal operating conditions, extreme turbulent wind conditions, extreme gusts combined with electric faults, and the occurrence of a 50-year storm at different values of yaw angle [15]. The choice of a reduced set of DLCs is an effective way to limit computational costs while accounting for all significant situations. A more comprehensive set should be run on the final design in order to verify that all design driving loads were included in the process. Furthermore, in the present study, an additional reduction in computational cost is achieved by using a single turbulent seed in the dynamic simulations.

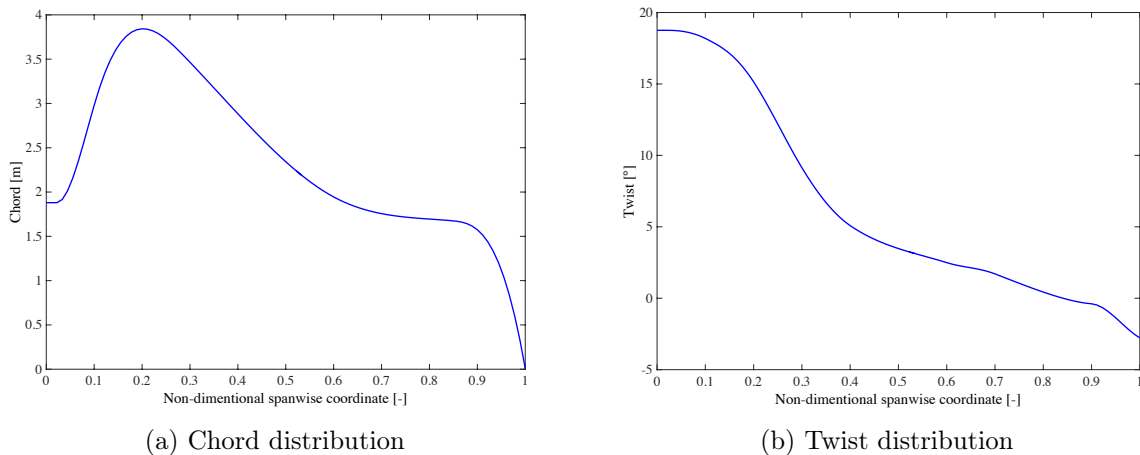


Figure 5.1: Chord and twist distribution for the baseline 2 MW wind turbine

Ultimate moment	Value [kNm]	Design Load Case
Blade root torsion	209	DLC6.2 @ -180degYM
Blade root edge	3885	DLC1.3 @ 25m/s
Blade root flap	7278	DLC1.3 @ 15m/s
Blade root combined	7314	DLC1.3 @ 15m/s
Hub nodding	4746	DLC1.3 @ 17m/s
Hub yawing	4796	DLC1.3 @ 23m/s
Tower top rolling	3442	DLC1.3 @ 15m/s
Tower root side-side	22958	DLC1.3 @ 25m/s
Tower root fore-aft	53171	DLC1.3 @ 15m/s

Table 5.4: Ultimate loads for the baseline 2 MW wind turbine

Fatigue moment	Value [kNm]
Blade root torsion	48
Blade root edge	3433
Blade root flap	2950
Blade root combined	2995
Hub nodding	2645
Hub yawing	2390
Tower top rolling	688
Tower root side-side	8866
Tower root fore-aft	14981

Table 5.5: Fatigue loads for the baseline 2 MW wind turbine

In this machine, the highest ultimate loads at the blade root come from DLCs corresponding to normal operation. As an example, the load ranking for combined moment¹ is reported in Fig. 5.2, with the horizontal axis showing the DLCs associated to the different maximum loads.

A passive load alleviation technique like blade sweeping may be beneficial in this case to reduce the extreme loads during normal functioning, whereas peak loads at storm conditions (DLC 6.2) are not expected to vary significantly with the sweep curvature.

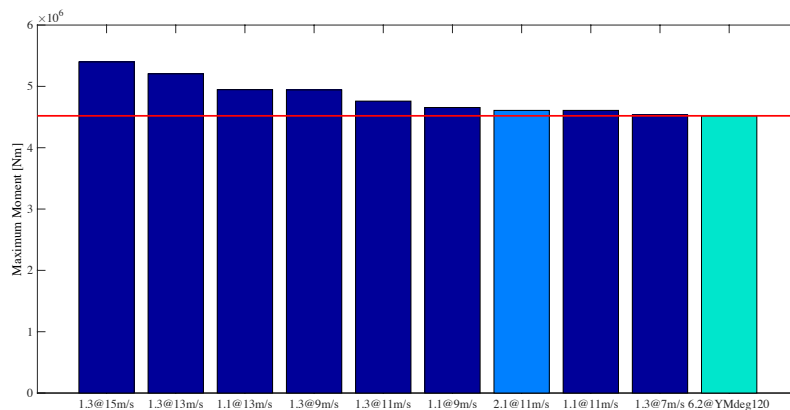


Figure 5.2: Load ranking for blade root combined moment (baseline 2 MW machine)

¹Combined moment couples the effects of flapping and edging loads at the blade root

5.2 Detailed load analysis

A detailed load analysis was conducted in order to understand the amount of load reduction for different backward swept blades, without taking into consideration the consequences on power output and cost of energy at this stage. This preliminary study has informed the choices made during the design optimization process described in Section 5.3.

In this analysis, both ultimate loads and fatigue damage are taken into account. Moments and forces are calculated only for the design load cases corresponding to normal operation, that is DLC 1.1, in order to verify if loads can be effectively alleviated with swept blades. More exhaustive simulations will be performed in the actual design of swept rotors, using an expanded set of DLCs and accounting for all design constraints, as well as the effects on energy production. Moreover, this study is useful to understand if boomerang-shaped blades actually allow for more aeroelastically balanced rotors, limiting the inherent increase in blade root torsional stress while maintaining the other loads at similar values.

The blade shapes considered in the load analysis are reported in Fig. 5.3. These curves have been obtained from the sweep equations introduced in Section 3.3.1. Notice that the term $Sweep(d_{tip})$ corresponds to backward swept blades with a tip sweep of d_{tip} , whereas the term $ForwSweep(d_{tip})$ has been adopted here for boomerang-shaped blades. Light colors are associated with the former, whereas the latter are characterized by darker colors.

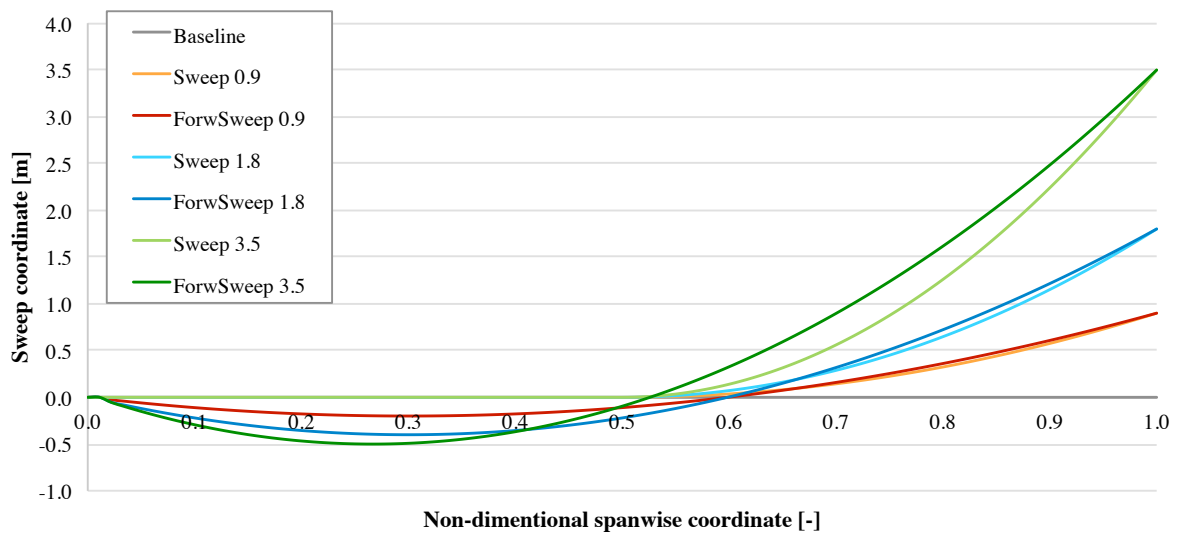


Figure 5.3: Sweep curves considered for the load analysis

5.2.1 Maximum tip displacement

Tip displacement is an important design driver and it is connected to the tower clearance constraint. A reduction in maximum tip deflection suggests that the blade stiffness can be decreased by a certain amount, hence there are margins for mass reduction. Moreover, tip displacement is a quantity that is directly related to the combined moment at the blade root, therefore it may provide some insights into the potential for load mitigation.

The plot in Fig. 5.4 reports a comparison of tip displacement between the baseline rotor and the considered sweep cases. Results have been obtained from dynamic simulations performed for DLC 1.3 at 15 m/s, that is a load condition at which maximum tip displacement typically occurs in this machine. It is clearly shown how a lower tip displacement is effectively achieved by increasing tip sweep, which means that there is actual margin for mass and load reductions. Moreover, introducing forward sweep in the inner sections by using boomerang-shaped blades does not really alter this trend, since results for the same tip sweep are very similar.

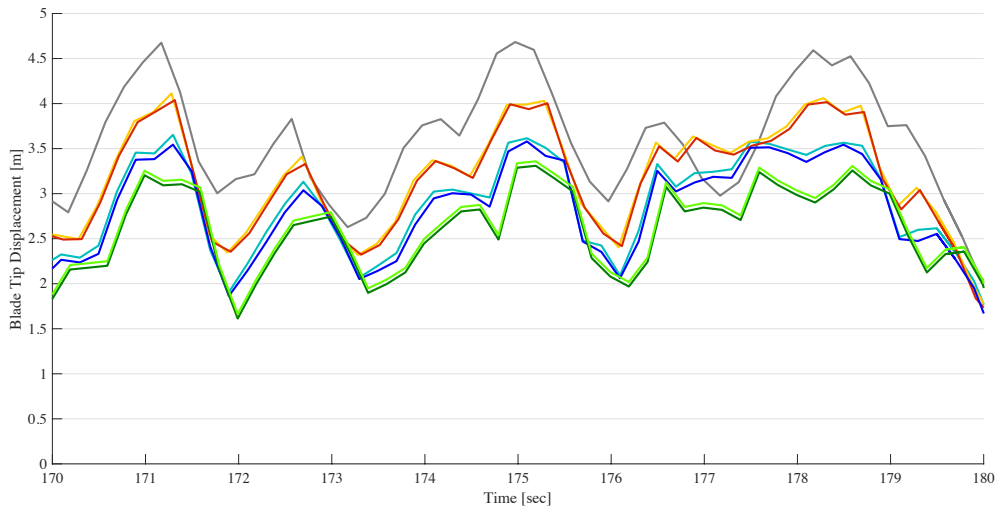


Figure 5.4: Load analysis: tip displacement comparison

5.2.2 Ultimate loads

The results for ultimate loads refer to dynamic simulations corresponding to DLC 1.1. The plots in Fig. 5.5 report the percentage difference of extreme loads with respect to the baseline case, that is the unswept rotor, for the swept blades represented in Fig. 5.3.

Generally, it can be seen that loads are lower for increasing tip sweep in most cases for moments and forces at blade root, hub, and tower root. As expected from the considerations discussed earlier in Section 3.3.1, the only exception is constituted by blade root torsional moment (see Fig. 5.5b), which grows significantly due to sweeping, especially for blades with larger curvature.

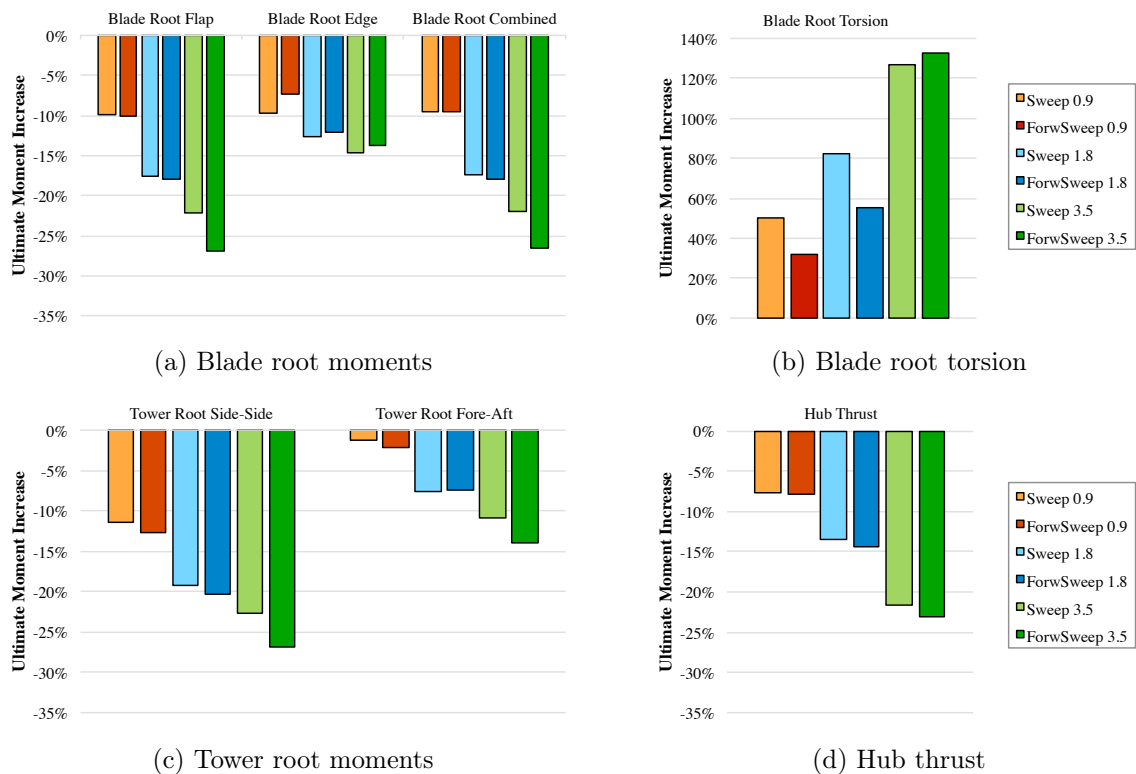


Figure 5.5: Load analysis: ultimate loads comparison (reference: baseline)

However, it is shown that adopting boomerang-shaped blades may allow for a more limited increase, provided that their shape is carefully designed. In fact, blade root torsion for the *ForwSweep 3.5* configuration is slightly higher compared to the simple backward swept case *Sweep 3.5* with the same tip sweep, possibly because the amount of forward sweep in the inboard sections is not sufficient to compensate for the larger tip sweep and produce a more balanced blade. Notice that the other load reduction trends are not altered considerably.

Even though the increase in torsional stress at the blade root is evident, this load is in absolute terms more than one order of magnitude smaller than the other blade loads, as it could have already been observed by looking at Table 5.4 for the baseline machine. Therefore its impact on the whole wind turbine design is expected to be limited, apart from likely negative effects on the pitch control mechanism.

5.2.3 Fatigue loads

As far as fatigue is concerned, the concept of Damage Equivalent Load (DEL) introduced in Section 2.3.1 is used. Fatigue DEL is defined as the constant amplitude load that for an arbitrary number of load cycles would produce the same fatigue damage as the variable amplitude load spectrum, that is all actual loads combined. This concept makes it much easier to compare different design configurations, as it converts a long history of random fatigue loads into one simpler number.

As an example, the DEL for blade root combined moment is shown in Fig. 5.6. For all sweep cases, DEL quantities have been computed for each wind speed between cut-in and cut-out conditions. As for ultimate loads, also fatigue appears to decrease significantly with larger tip sweep. Furthermore, results present good trends as a function of wind speed, since the largest load alleviation occurs where the blades are more loaded, that is around rated conditions in the range of 11–13 m/s.

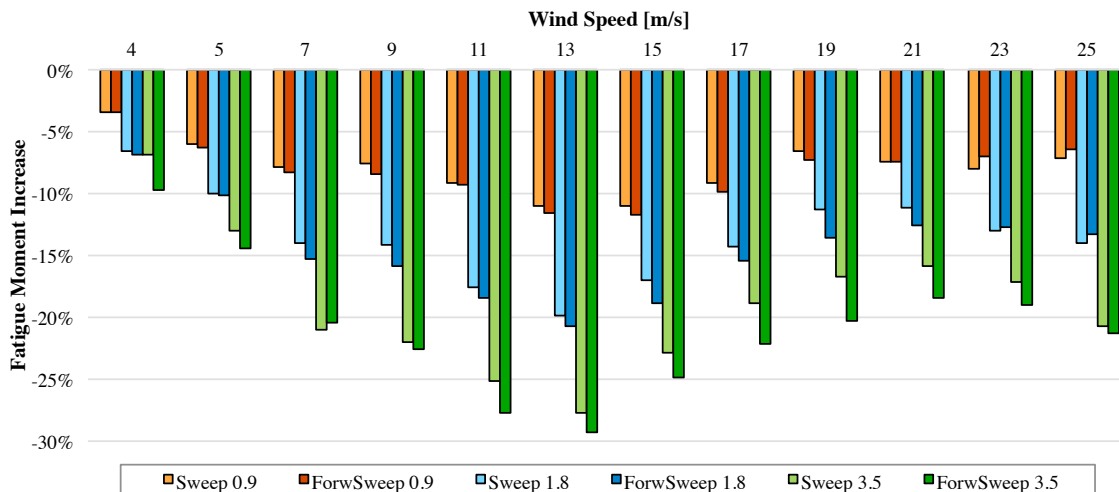


Figure 5.6: Load analysis: blade root combined moment DEL comparison (reference: baseline)

Additionally, a Weibull-averaged DEL has been computed for several loads of interest, by cumulating fatigue DEL for the whole range of operating wind speed. A Weibull-averaged DEL allows to further simplify the comparison among the different configurations, since it translates the DEL values corresponding to the various wind speeds into a single quantity. Results are shown in Fig. 5.7. Trends are very similar to the ones obtained for ultimate loads, with an even larger general load reduction (especially at tower root and hub) and a more limited increase in blade torsion.

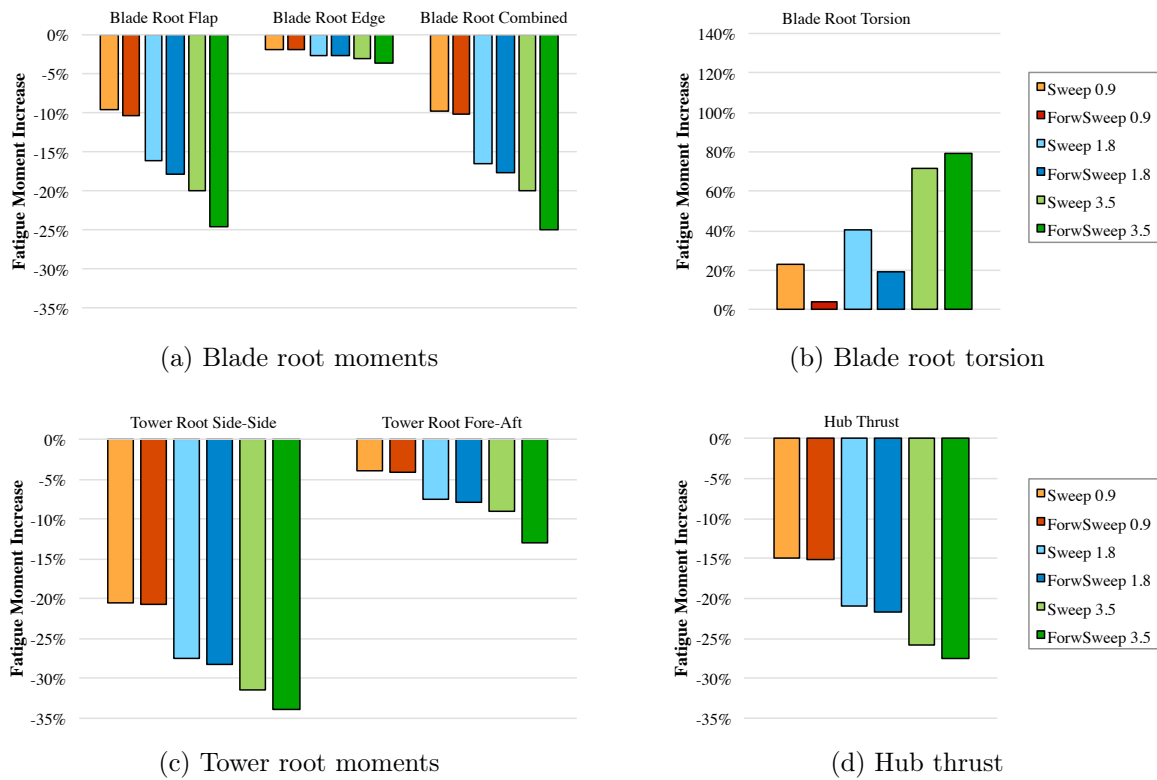


Figure 5.7: Load analysis: Weibull DEL comparison (reference: baseline)

5.2.4 Conclusions of the load analysis

This initial load analysis demonstrated that tip displacement and most of the loads may be effectively reduced with swept blades. In particular, a larger tip sweep results in greater load alleviation. Similar conclusions are drawn for fatigue and extreme loads. Only blade root torsion increases with sweep, but its magnitude is still much smaller compared to the other loads, and should not affect the overall design substantially. It is observed that ultimate blade torsion is more difficult to reduce compared to fatigue.

However, it is important to consider that the sweep configurations discussed so far do not represent realistic blades. In fact, the swept shape was simply added to the baseline geometry, without performing any twist optimization and structural redesign. This means that blade stiffnesses and components thicknesses have not varied from the straight blade ones.

Hence, a complete redesign of the wind turbine rotors with swept blades is required so as to properly analyze the potential benefits of this passive load alleviation technique. The results from the optimized design are described in the following section.

5.3 Design optimization

The rotor design optimization is conducted using the multidisciplinary design tool *Cp-Max*, described in Chapter 4. A partial aerodynamic optimization is first performed to find the optimal twist distribution for each swept blade configuration, followed by the detailed sizing of the structural components. Several design constraints have been kept under continuous control to ensure a correct rotor design. Finally, cost of energy and its principal elements, namely blade cost and annual energy production, are computed and compared with the baseline case. In the present study, the tower structure has not been optimized in order to focus on the consequences of sweeping the blades and avoid interferences from external factors.

The blade shapes analyzed here are different from the ones considered in the load analysis and they are shown in Fig. 5.8. Notice that now the term $sw(d_{tip})$ refers to backward swept blades, while the term $fsw(d_{tip})$ is used for boomerang-shaped blades.

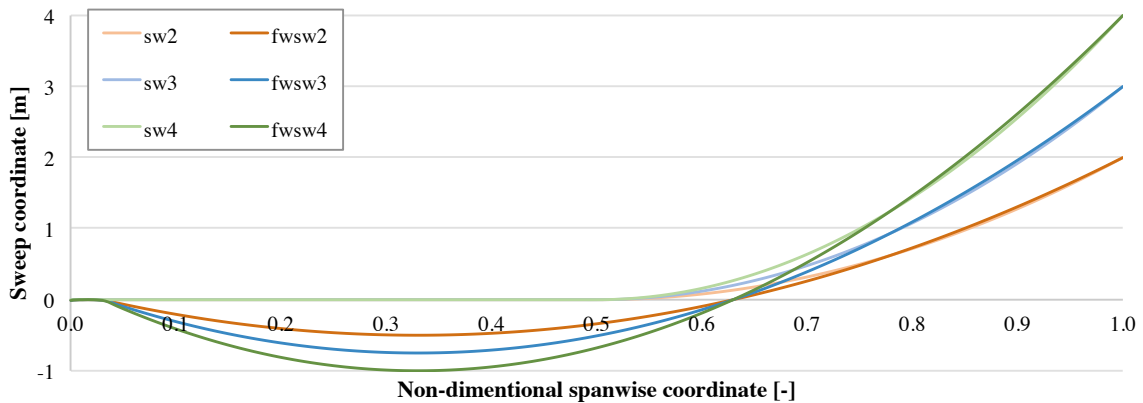
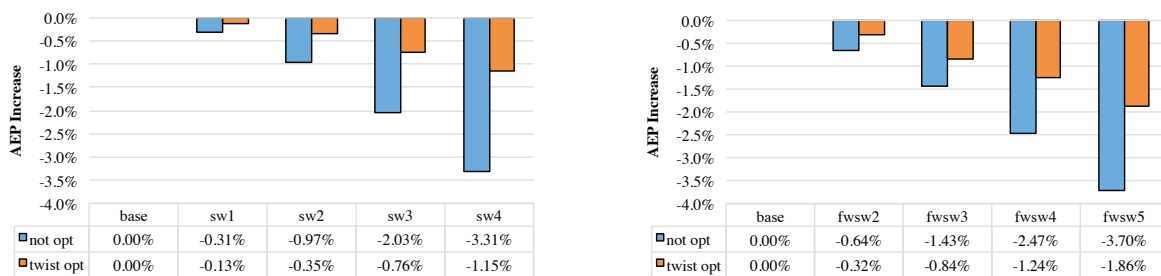


Figure 5.8: Sweep curves considered for the design optimization of the 2 MW machine

5.3.1 Optimal twist distribution

First, the aerodynamic optimization was performed as described in Section 4.3.1 in order to compute the optimal twist distribution for each sweep case, while the chord and airfoil thickness distributions were not varied in the present study. From Fig. 5.9 it is clear how the decrease in annual energy production is successfully limited by optimizing twist, instead of keeping it the same as for the baseline configuration. This way, the loss in AEP deriving from blade sweeping can be reduced by more than 50%, even though the energy produced is always lower compared to the unswept rotor. An example of the optimized twist angles for two sweep cases is reported in Fig. 5.10, together with the baseline distribution.



(a) Backward swept blades

(b) Boomerang-shaped blades

Figure 5.9: AEP loss before and after twist optimization (reference: baseline)

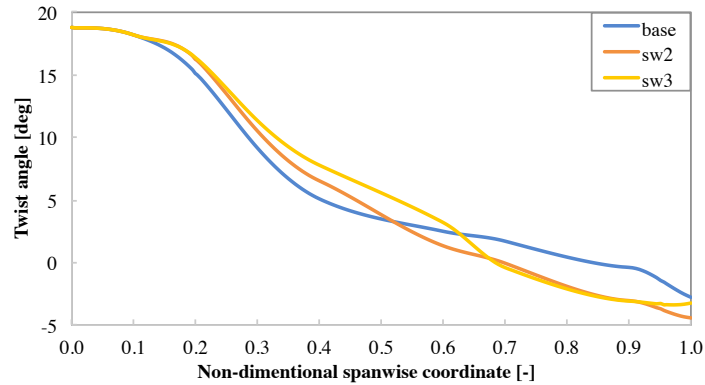


Figure 5.10: Aerodynamic optimization: optimal twist distribution

5.3.2 Ultimate loads

As far as structural redesign is concerned, the optimization procedure described in Section 4.3.2 is followed. Structural sizing is performed simulating the reduced set of design load cases defined in Section 2.3.3, which is meant to represent all significant situations that typically occur during the lifetime of a wind turbine.

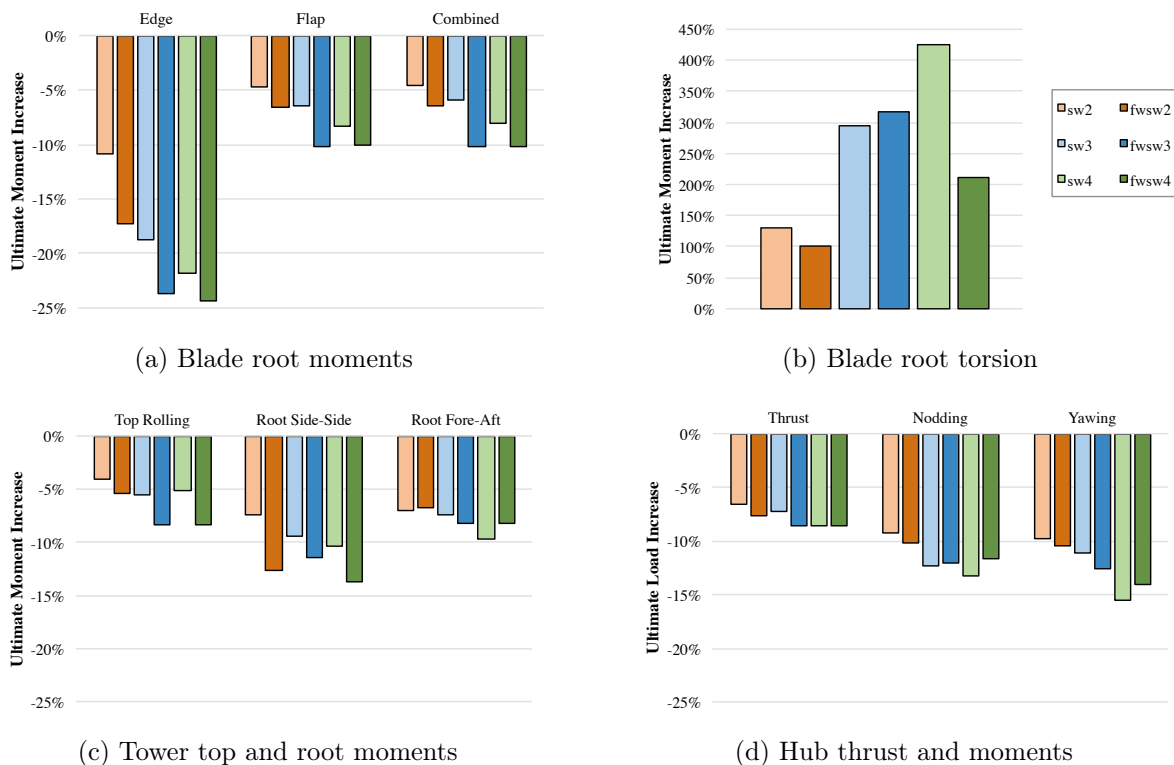


Figure 5.11: Structural optimization: ultimate loads comparison (reference: baseline)

Ultimate loads are analyzed first and the results are reported in Fig. 5.11. Apart from blade torsion, extreme loads are effectively reduced at blade root, hub and tower. For most loads, swept blades show a reduction of around 5–10% with respect to the unswept configuration, while the edgewise moment at the blade root is considerably alleviated. Generally, it seems that larger tip sweeps still lead to greater load decrease, although the difference is not as important as shown by the load analysis. Moreover, boomerang-shaped blades appear to be beneficial with respect to some extreme loads compared to simple backward swept blades.

As expected from aeroelastic considerations and from the results of the load analysis, torsional moments at the blade root increase as soon as sweep is introduced. This time, the rise in torsion is even more pronounced because the internal structural components have been redesigned, usually resulting in thinner elements that present smaller torsional stiffness. Adding forward sweep in the inboard sections of the blade possibly allows to limit this inherent increase, provided that the complex blade shape is properly designed. For example, from Fig. 5.11b it is possible to see that the boomerang shape for the *fsw4* case is designed such that ultimate torsion can be halved compared to the backward swept blade with the same tip sweep of 4 m. On the contrary, ultimate torsion for the *fsw3* configuration is slightly higher than for *sw3*, although the former design allows to further reduce other loads at the same tip sweep, such as blade root combined moment, which is generally more relevant when it comes to rotor mass reduction.

Actually, during the dynamic simulations, DLC 6.2 has been particularly problematic and hardly converged for several sweep cases, often showing inconsistent results. However, it is important to consider that as far as blade root torsion is concerned, only operating conditions should be taken into account, since the main consequence of an increase in blade torsion is mostly related to the pitching mechanism, which is not active during a storm.

5.3.3 Fatigue loads

Results for fatigue show some similarities to the ones obtained for ultimate loads but generally present a larger reduction. The Weibull-averaged DEL for some loads of interest is reported in Fig. 5.12. Fatigue damage related to the combined moment at blade root is substantially alleviated for all cases, around 15–20% lower than baseline. The same holds for tower root fore-aft moments and loads on the hub. The increase in blade torsion is much more limited in terms of fatigue, up to around twice the value for the unswept rotor in the worst case. Boomerang-shaped blades are shown to successfully limit this increase for all configurations, and they seem to further alleviate the edgewise moment at the blade root and the hub loads.

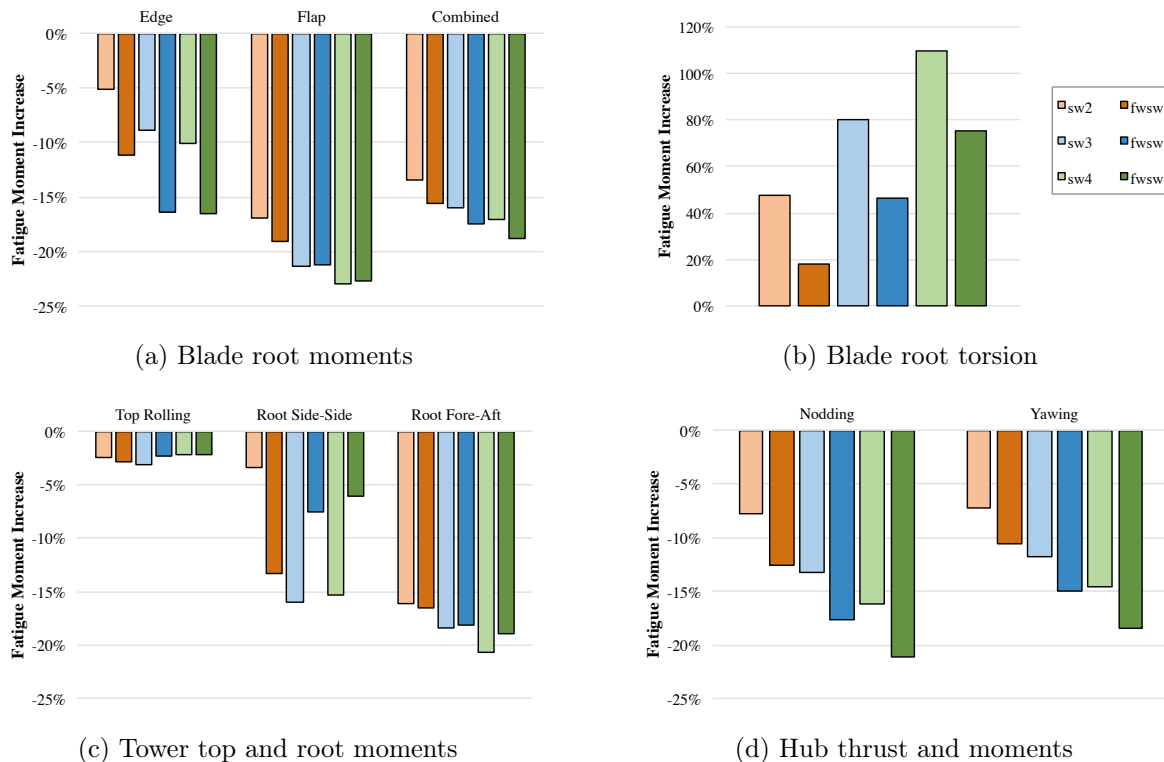


Figure 5.12: Structural optimization: fatigue loads comparison (reference: baseline)

5.3.4 Design constraints analysis

The load ranking analysis reveals that ultimate loads during normal operation (DLCs 1.x) can be effectively reduced using the considered swept rotors, while peak loads corresponding to storm conditions (DLCs 6.x) do not vary significantly with sweep curvature, hence they move up in the ranking. Still, the highest ultimate loads occur during normal operation and this may suggest that there is some more margin of improvement for reducing operational loads with swept blades.

However, frequency and tip deflection constraints are now active and driving the design for almost all cases, thus limiting the advantages deriving from sweep on this machine. Therefore, load reduction can hardly be further enhanced with larger tip sweep. Table 5.6 reports the status of each design constraint for all optimized blade designs. In particular, the frequency placement constraint is a measure to avoid resonant conditions and demands that the flapping frequency is at least 16% higher than the blade-passing frequency (or third fundamental harmonic, $3P$).

For almost all models, the frequency placement and the maximum tip deflection constraints are active at convergence, hence the rotor design process is driven by the blade flapwise bending stiffness. Additionally, the fatigue damage constraint is found to be active for the shell skin and shear webs in the blade middle sections, which are the regions with the largest chord values.

Case	Flap freq.	Max tip defl.	Fatigue
sw2	N	A	A: skin from 20% to 50% span A: webs at 50% span
sw3	A	A	A: skin from 20% to 30% span A: webs at 20% and 50% span
sw4	A	A	A: skin at 20% span A: webs at 20% and 60% span
fsw2	A	A	A: skin from 20% to 30% span
fsw3	A	A	A: skin at 20% span A: webs at 20% span
fsw4	A	A	A: skin at 20% span A: webs at 20% span

Table 5.6: Constraint status for the optimal designs (A = active; N = non-active)

5.3.5 CoE comparison

The final results from the design optimization of swept rotors are represented in the plots below. Fig. 5.13a shows that blade weight can be reduced by around 5% with backward swept blades, and just below 10% by adopting a boomerang shape. However, savings in rotor cost are more limited because, although structural thicknesses are generally reduced thanks to load alleviation, the longer blades together with more complex geometries require additional manufacturing expenses.

The trends for annual energy production are reported in Fig. 5.13b; static AEP refers to steady wind conditions, whereas turbulent AEP is computed by integrating the power output obtained during DLC 1.1, hence considering the control system and the dynamic response of the machine to turbulence. As already discussed in Section 3.3, swept blades entail losses in aerodynamic performance due to the reduction in angle of attack. As a result, reduced blade costs are counterbalanced by a slightly lower power output, which implies a little increase in the cost of energy for all cases compared to the unswept rotor. This happens because the impact of AEP variations on the CoE is much greater than changes in the rotor cost, meaning that even a significant reduction in blade weight may be overcome by a small loss in power production. Overall, the CoE increase is always below 1%, as shown in Fig. 5.14.

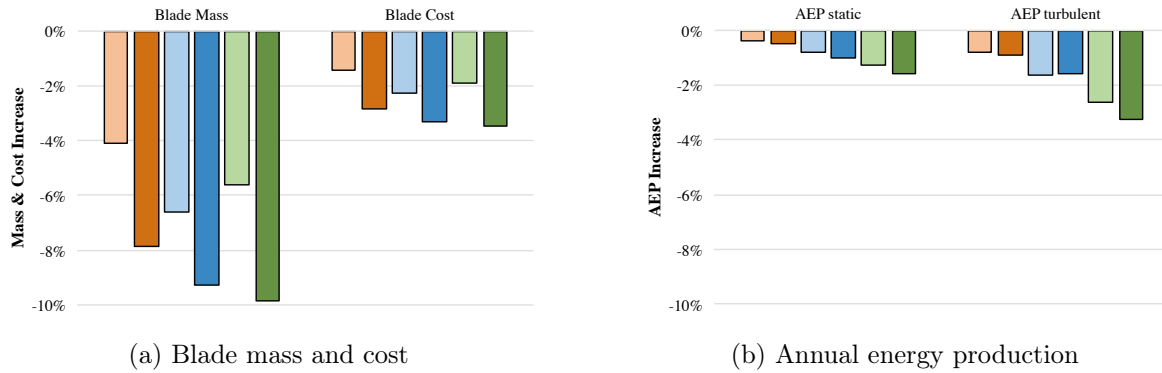


Figure 5.13: Design optimization: mass, cost and AEP comparison (reference: baseline)

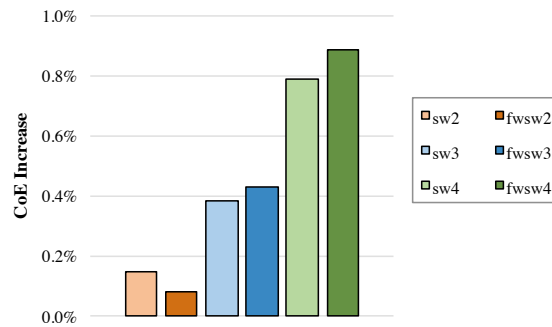


Figure 5.14: Design optimization: cost of energy comparison (reference: baseline)

5.3.6 Conclusions of the design optimization

Results from the design optimization of the 2 MW wind turbine show that loads can successfully be alleviated by adopting swept blades, leading to benefits in terms of blade mass. However, the rotor cost is only slightly reduced, not enough to compensate for the lower performance in terms of power production, hence resulting in higher cost of energy.

Positive outcomes may be obtained by expanding the swept area, so that the annual energy production, which mainly depends on the rotor radius, increases significantly. At the same time, swept blades are used to maintain comparable loads to the ones occurring on the original machine, resulting in a wind turbine that has a lower cost of energy within the same load envelope. This possibility is studied in the next section.

5.4 Larger rotor design

The idea at the basis of the larger rotor study is to increase blade length a little in order to gain in energy capture, while keeping similar loads to the baseline 2 MW wind turbine by adding sweep, with the ultimate goal of achieving a reduction in terms of cost of energy. The effects on the same types of loads that were analyzed in the previous section have been investigated here, for both fatigue and extreme loads.

In the present analysis, a tip sweep of 3 m has been considered for all cases, because the *sw3* model from Section 5.3 presented significant load alleviation with a relatively little loss in energy production, producing a good trade-off between the two competing aspects in rotor design. Three configurations have been aerodynamically and structurally optimized using *Cp-Max*, with blades longer by 3, 5, and 10% respectively, compared to the original rotor. These new rotors have been named *sw3_r(x%)* and are represented in Fig. 5.15.

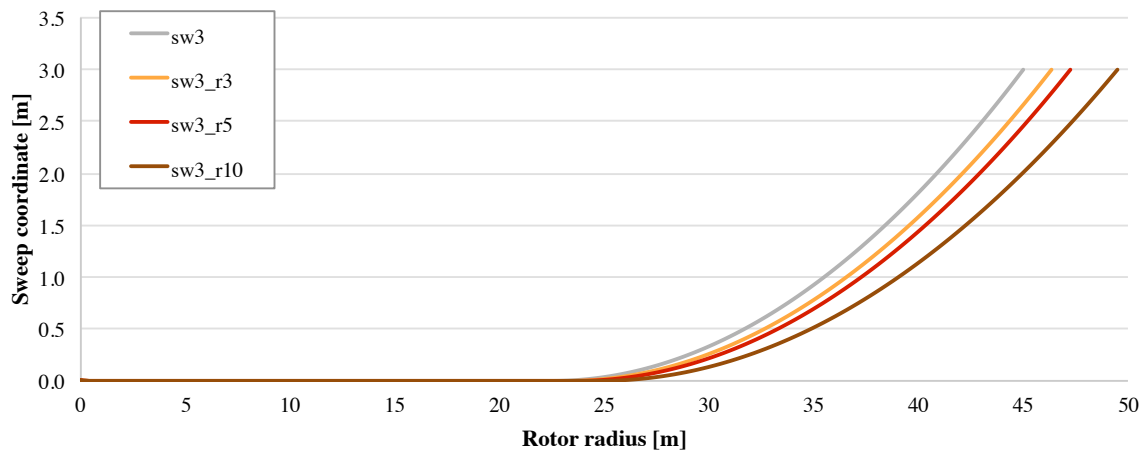


Figure 5.15: Sweep curves considered for the larger rotor study

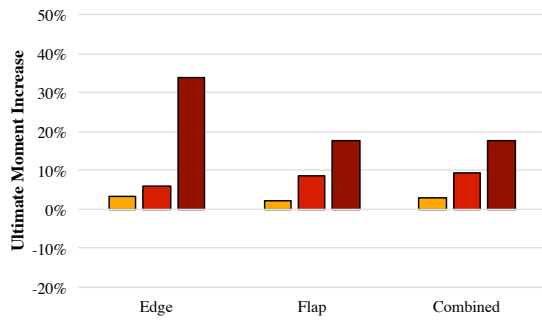
5.4.1 Ultimate loads

Results obtained for the ultimate loads in the three configurations with longer blades are reported in Fig. 5.16, taking the original unswept rotor described in Section 5.1 as reference. In fact, it is shown that extreme loads might actually be limited to comparable values, particularly for blades only slightly longer.

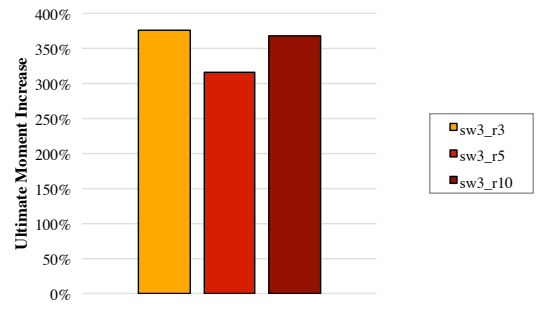
The 3% longer blade provides ultimate moments that are akin to baseline, even showing a reduction of loads at the hub and tower. The *sw3_r5* case also displays rather similar results at the same locations, while blade root moments are up to 10% higher. On the other hand, a 10% longer blade produces much greater loads, especially at the blade root with an increase of more than 15%. Obviously, blade root torsional stress is much larger compared to the shorter straight blade and the associated load is rather close for each longer swept configuration due to the same amount of tip sweep.

5.4.2 Fatigue loads

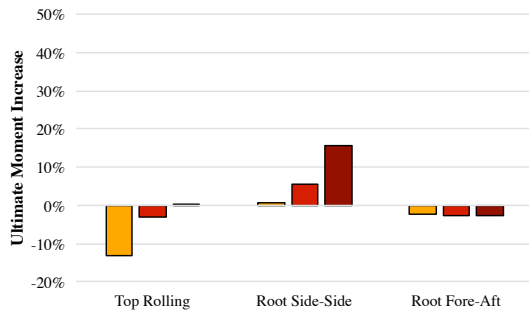
Similar results are obtained for fatigue DEL, as shown in Fig. 5.17, with the most remarkable increase on the blade root edging moment, which occurs because this load, among other factors, depends heavily on the weight of the blades. On the other hand, fatigue from flapwise moments is reduced, except for the longest configuration. Otherwise, trends for fatigue loads are somewhat similar to the ones observed for peak loads.



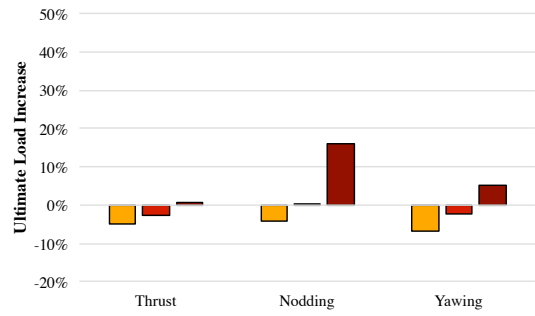
(a) Blade root moments



(b) Blade root torsion

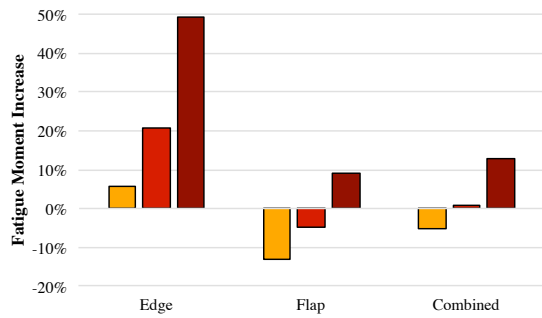


(c) Tower top and root moments

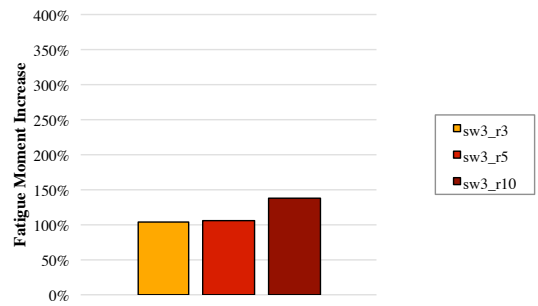


(d) Hub thrust and moments

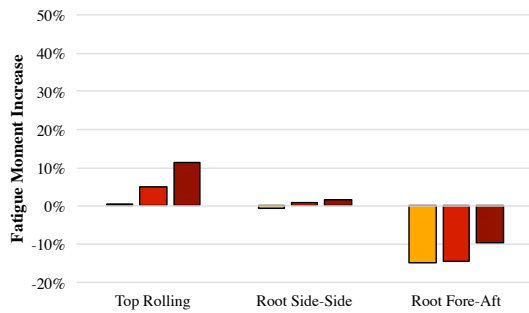
Figure 5.16: Larger rotor optimization: ultimate loads comparison (reference: baseline)



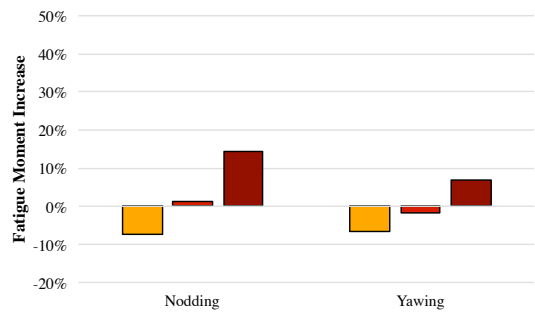
(a) Blade root moments



(b) Blade root torsion



(c) Tower top and root moments



(d) Hub thrust and moments

Figure 5.17: Larger rotor optimization: fatigue loads comparison (reference: baseline)

5.4.3 CoE comparison

Finally, cost of energy and its principal factors, namely blade cost and energy production, have been computed and compared with the baseline rotor. Thanks to the expanded swept area, the AEP obviously rises; however, blade mass also increases due to the greater blade length, particularly in the 10% longer case. In fact, prior to this study, the structural configuration of the blades had to be reinforced with a thicker shell skin near the root so as to account for the increased blade length, leading to a higher initial rotor mass. An exception is represented by the 3% longer blade, which weighs and costs approximately the same as the original one.

In terms of CoE, all configurations are found to be beneficial, because the higher AEP impacts the most on the CoE estimate, as already mentioned in Section 5.3.5. Therefore, the largest reduction occurs for the longest rotor, at a price of much heavier (+35%) blades. On the other hand, the 5% longer rotor achieves around 0.4% reduction in cost of energy with a 10% increase in blade mass, overall maintaining similar loads to the original machine. Lastly, the 3% larger rotor presents some benefits in CoE at nearly the same blade mass.

In the end, it is important to notice that the choice of a larger rotor mainly depends on the design margins for the specific machine and on the specific requirements that are to be satisfied by the designer. For example, if a wind turbine rotor has to be substituted after a certain number of years while keeping the same underlying structures, a viable solution may be to replace it with swept blades that are longer than the original ones; this might enhance the energy capture capability of the wind turbine for the same power rating, without the need to change the tower and most of the supporting systems thanks to similar load conditions. Of course, this design possibility has to be carefully pondered in order to ensure the full satisfaction of all design requirements.

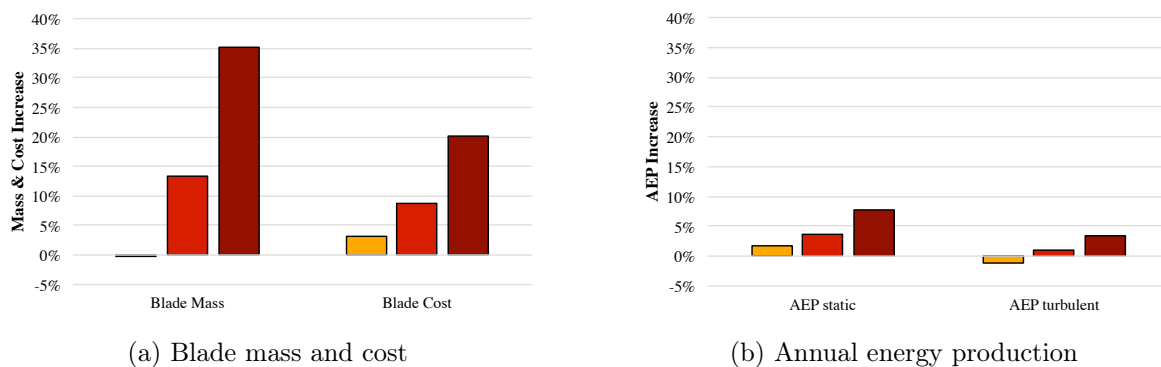


Figure 5.18: Design optimization: mass, cost and AEP comparison (reference: baseline)

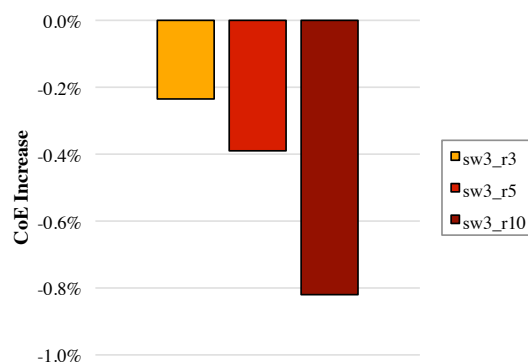


Figure 5.19: Design optimization: cost of energy comparison (reference: baseline)

5.4.4 Comparison with larger unswept rotor

For a more complete analysis of expanded swept rotors, it is interesting to compare the variations of some loads of interest when longer swept blades are used, with respect to straight blades of the same length. The plots reported below show the change in both peak loads and fatigue for the combined moment at blade root (Fig. 5.20), the nodding moment (Fig. 5.21) and the yawing moment at the hub (Fig. 5.22). The reference is always the original 45 m long unswept rotor.

Only the 3% and 5% longer blades have been considered here, since the 10% case generally resulted in a significant increase in loads and mass. Compared to a longer straight blade, which is subjected to higher moments with respect to the original (shorter) blade, sweep allows for a substantial alleviation in the loads.

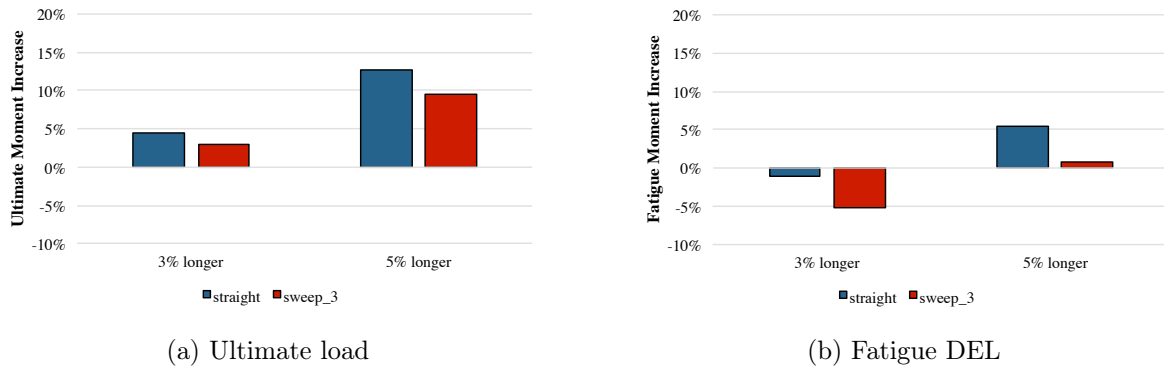


Figure 5.20: Comparison with larger unswept rotor: blade root combined moment (reference: baseline)

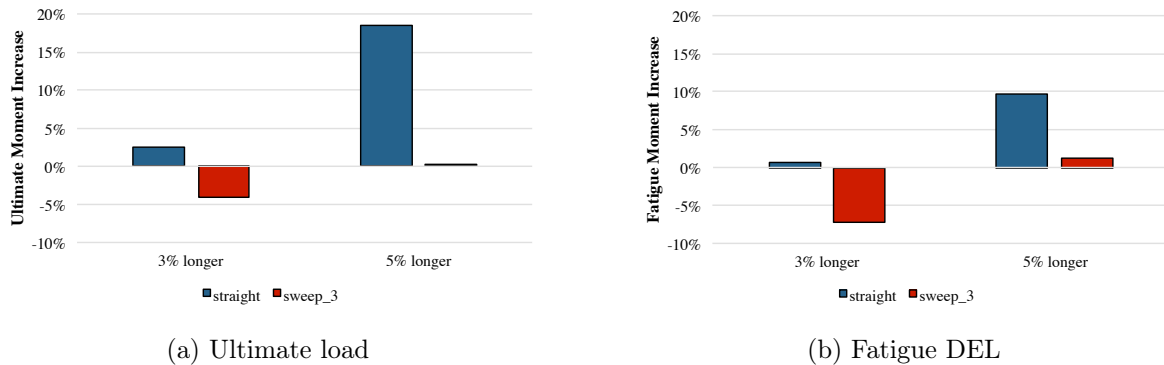


Figure 5.21: Comparison with larger unswept rotor: hub nodding moment (reference: baseline)

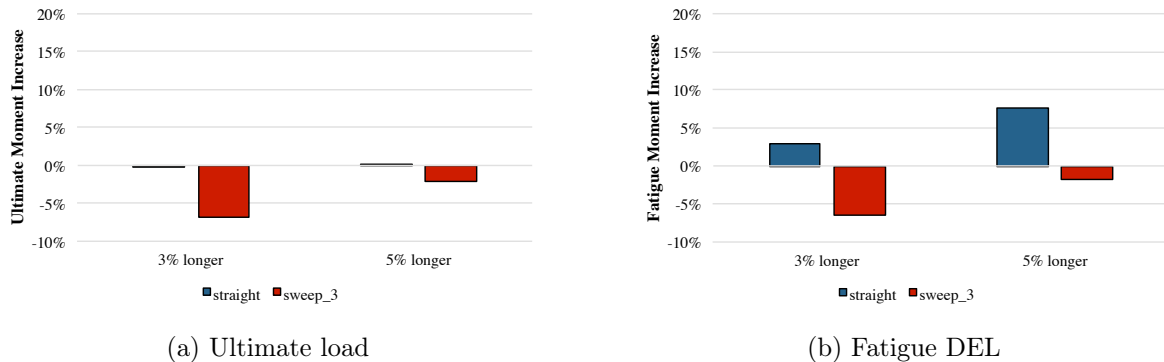


Figure 5.22: Comparison with larger unswept rotor: hub yawing moment (reference: baseline)

5.5 Combined swept-prebent rotor design

An initial analysis on the potential benefits deriving from the combination of sweep with prebend has been performed, too. Within C_p -Max, prebend is optimally designed using the procedure recently integrated into the code [88], in order to have the blade flat in the uptilted rotor plane at rated wind conditions. Swept-prebent blades may be a viable solution to produce very light and flexible rotors thanks to the increased tower clearance.

In the present study, five configurations are compared with the baseline 2 MW wind turbine described in Section 5.1:

- prebent blades with a tip prebend of 1.8 m (*base_PB*);
- swept blades with a tip sweep of 2 and 3 m, respectively (*sw2* and *sw3*);
- prebent-swept blades with a tip sweep of 2 and 3 m, respectively (*sw2_PB* and *sw3_PB*).

For all cases of interest, the blade prebend amounts to 1.8 m at the tip. From Fig. 5.23a, it is clear that sweep can indeed reduce the loads compared to a blade with prebend only; moreover, a combined configuration could lead to significant load alleviation. However, the great reduction in blade mass (more than 15%) and cost (around 5%) is achieved mostly thanks to prebend and the difference here is much more limited, as shown in Fig. 5.23b.

When it comes to energy harvesting performance, the AEP gets worse for all cases, especially the ones including sweep (see Fig. 5.24). Nonetheless, the important decrease in blade cost with combined sweep-prebend allows for a lower CoE compared to the straight blade, although better results are obtained using blades with prebend only. Of course, the feasibility of manufacturing and transportation of such complex shapes may be a limiting factor to be considered.

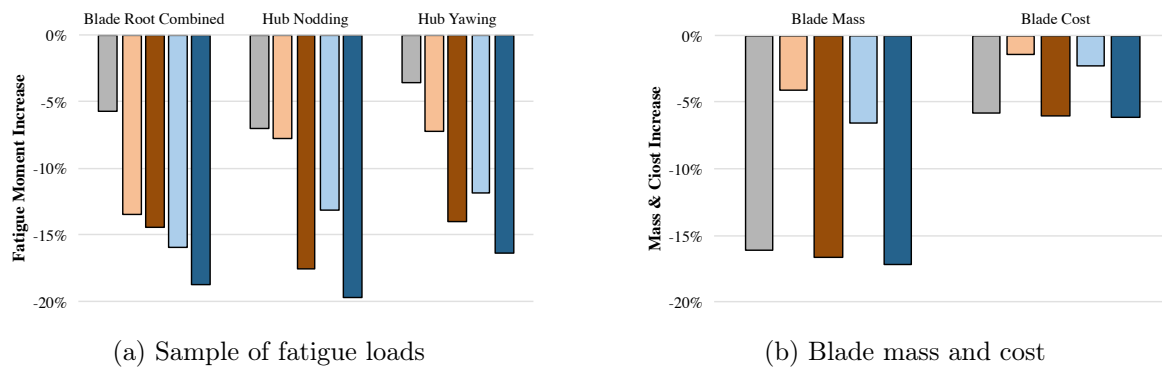


Figure 5.23: Combined sweep and prebend: fatigue and blade mass comparison (reference: baseline)

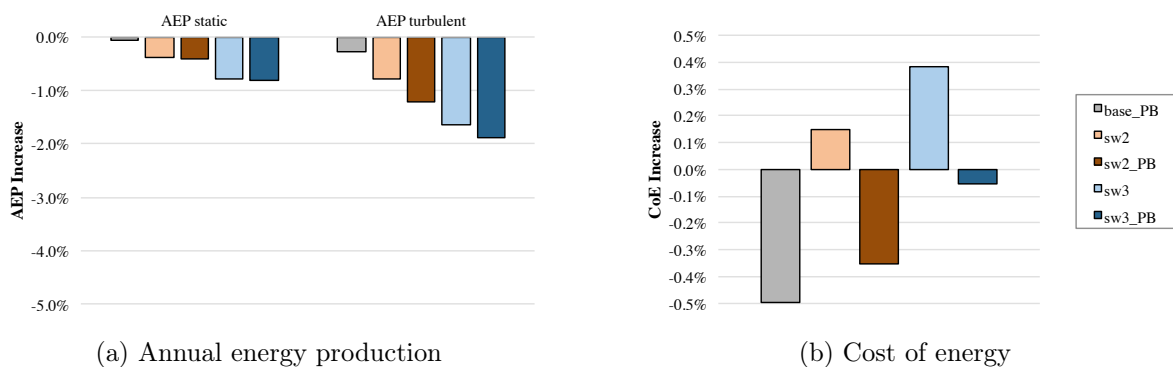


Figure 5.24: Combined sweep and prebend: AEP and CoE comparison (reference: baseline)

10 MW wind turbine

Swept blades have been tested also on a 10 MW offshore conceptual machine, which is representative of next generation wind turbines. This large scale machine has been developed as an evolution of the original DTU 10 MW wind turbine proposed by Ref. [89]. Initial results from the optimized design of some swept rotor configurations are discussed in Section 6.2.

6.1 Baseline wind turbine

The baseline 10 MW machine is a class 1A offshore three-bladed wind turbine and its main parameters are reported in Table 6.1. Notice that in offshore applications the noise constraint is less important, hence the maximum speed of the blade tip can increase from 75 to 90 m/s. Following the approach of the original DTU 10 MW wind turbine, the system is modelled without any of the support structures typically needed in offshore applications and the foundation is assumed to be a standard onshore one.

Data	Value	Data	Value
Wind class	IEC 1A	Rated power	10.0 MW
Hub height	119.0 m	Rotor diameter	178.3 m
Hub diameter	5.6 m	Max tip speed	90 m/s
Rotor cone	4.65 deg	Nacelle uptilt	5.0 deg
Blade mass	49732 kg	Tower mass	617.5 ton
Cut-in wind speed	4 m/s	Cut-out wind speed	25 m/s

Table 6.1: Configuration of the baseline 10 MW wind turbine

Blades are equipped with FFA airfoils [90] located as listed in Table 6.2 and they have two spar caps, three shear webs, and unidirectional composite reinforcements at the leading edge, trailing edge and also in the root region, that are required due to the much heavier structure. The blade topology is described more in detail in Table 6.3.

Airfoil name	Span position
Circle	0.00%
Circle	1.74%
FFA-W3-480	20.80%
FFA-W3-360	29.24%
FFA-W3-301	38.76%
FFA-W3-241	71.87%
FFA-W3-241	100%

Table 6.2: Spanwise positioning of the airfoils for the 10 MW wind turbine

Structural component	From (% span)	To (% span)	Material type
External shell	0	100	Stitched triaxial fiberglass
Spar caps	1	99.8	Unidirectional fiberglass
Shear webs	5	99.8	Stitched biaxial fiberglass
Third shear web	22	95	Stitched biaxial fiberglass
TE and LE reinforcements	10	95	Unidirectional fiberglass
Root reinforcements	0	22	Unidirectional fiberglass
Shell and web core	5	99.8	Balsa

Table 6.3: Blade topology for the 10 MW wind turbine

The aerodynamic optimization vector \mathbf{p}_a is made of 13 variables, which describe twist at 5 stations along the blade span, and chord and airfoil positions at 4 stations. The structural vector \mathbf{p}_s is composed by 69 variables parameterizing 9 structural components at 14 spanwise locations.

For the 10 MW offshore machine, wind conditions are adjusted for the different class following the IEC certification guidelines [15], assuming an average wind speed at the hub height of 10 m/s, while the 50-year storm wind speed is set to 50 m/s.

In the present study, only DLCs 1.1 and 1.3 have been simulated due to issues with the convergence of dynamic simulations, especially the ones corresponding to storm conditions. A more complete set of design loads cases will be needed for the final design of this wind turbine, but the reduced set of DLCs considered here is expected to provide useful insights into the effects of various rotor configurations. Ultimate loads on the load envelope for the straight blade wind turbine are reported in Table 6.4, while fatigue DEL are listed in Table 6.5. These values are taken as reference for the swept configurations optimized in the next section.

Ultimate moment	Value [kNm]	Design Load Case
Blade root torsion	717	DLC1.3 @ 15m/s
Blade root edge	40302	DLC1.3 @ 17m/s
Blade root flap	71532	DLC1.3 @ 13m/s
Hub nodding	33839	DLC1.3 @ 23m/s
Hub yawing	33768	DLC1.3 @ 21m/s
Tower top rolling	22427	DLC1.3 @ 11m/s
Tower root side-side	154554	DLC1.3 @ 25m/s
Tower root fore-aft	368226	DLC1.3 @ 13m/s

Table 6.4: Ultimate loads for the baseline 10 MW wind turbine

Fatigue moment	Value [kNm]
Blade root torsion	478
Blade root edge	38769
Blade root flap	28120
Hub nodding	14030
Hub yawing	14189
Tower top rolling	4194
Tower root side-side	75812
Tower root fore-aft	126819

Table 6.5: Fatigue loads for the baseline 10 MW wind turbine

6.2 Design optimization

As for the onshore wind turbine, the rotor design optimization is conducted using the multi-disciplinary design suite **Cp-Max**. First, the twist distribution is optimized for each swept blade configuration. Next, the structural optimization of the rotor is performed. Again, the tower has not been optimized in order to consider only the effects of sweeping the blades on rotor design.

The sweep parameters characterizing the three configurations analyzed here are reported in Table 6.6 and the related sweep curvatures are shown in Fig. 6.1. This time, only backward swept blades are considered.

Configuration name	d_{tip} [mm]	x_{start} [%radius]	γ [-]	y_{min} [mm]
sw3	3000	50%	2	0
sw5	5000	50%	2	0
sw7	7000	35%	2	0

Table 6.6: Sweep curve parameters for the 10 MW wind turbine swept blades

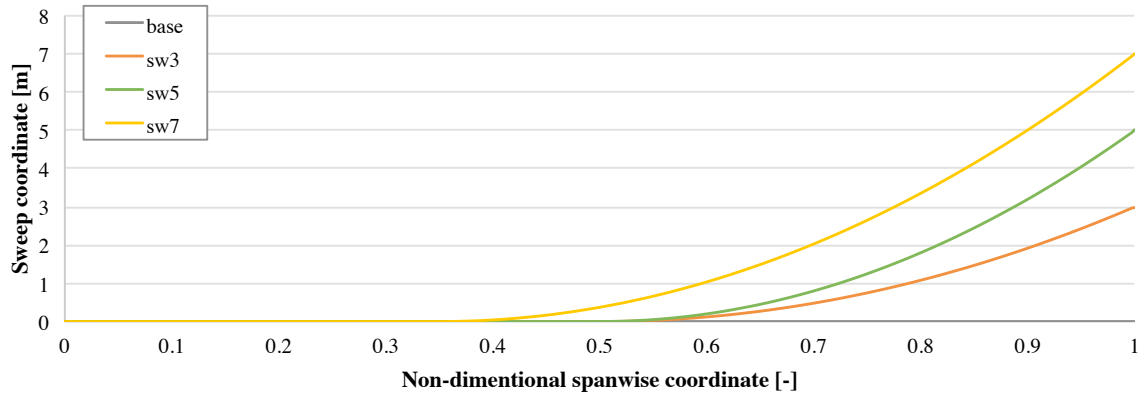


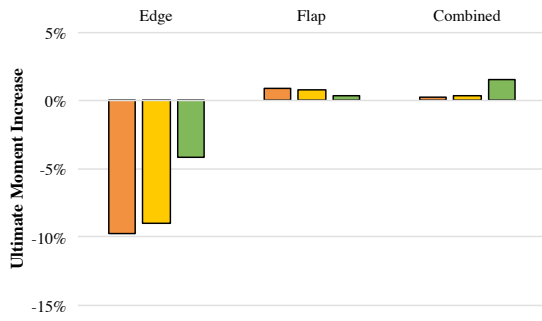
Figure 6.1: Sweep curves considered for the design optimization of the 10 MW machine

6.2.1 Ultimate loads

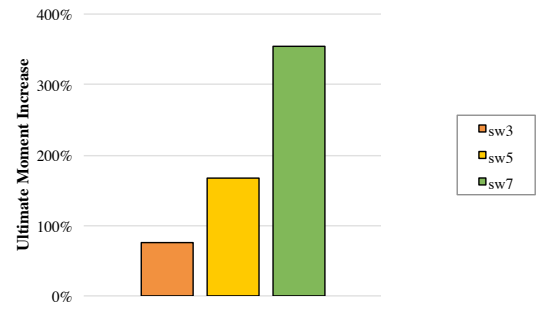
Results for ultimate loads are reported in Fig. 6.2. Extreme moments are not always reduced by sweep: for instance, the magnitude of flapwise bending at the blade root is nearly the same or even slightly higher with respect to baseline, and the same happens at the tower top. Nodding and yawing moments at the hub decrease compared to baseline, even though trends do not vary considerably with sweep curvature. The ultimate edgewise moment at the blade root is shown to be effectively reduced for all cases, while the increase in blade root torsion is somehow proportional to the amount of sweep at the blade tip.

6.2.2 Fatigue loads

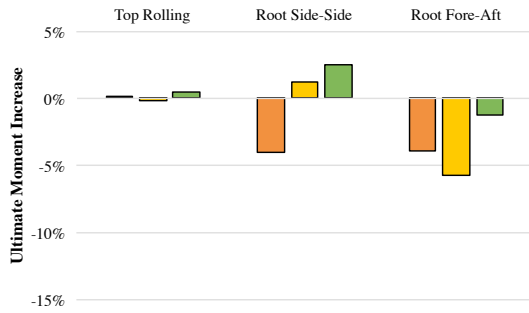
Compared to ultimate loads, results reported in Fig. 6.3 show that better load alleviation occurs in terms of fatigue, with percentage decreases generally around 5%. The only exception is constituted by edging DEL at the blade root for the most swept rotor, probably because this blade is very heavy and edgewise bending strictly depends on gravity forces. Again, the increase in blade root torsion is more limited for fatigue, as it was for the 2 MW wind turbine.



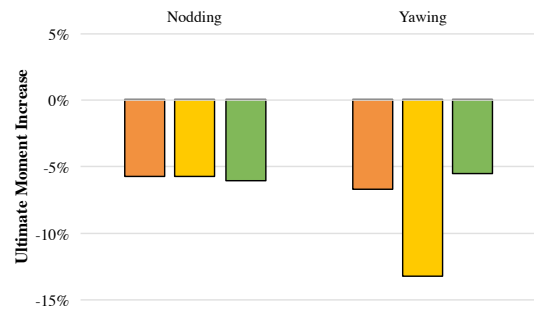
(a) Blade root moments



(b) Blade root torsion

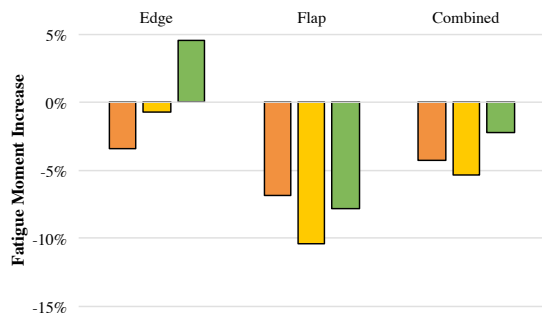


(c) Tower top and root moments

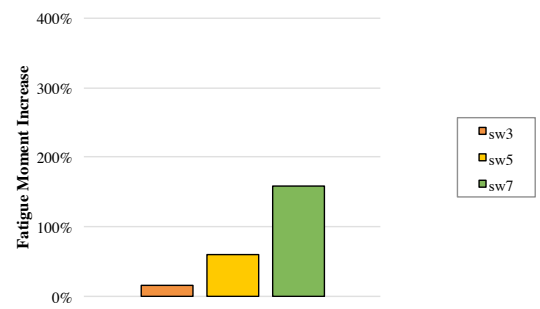


(d) Hub thrust and moments

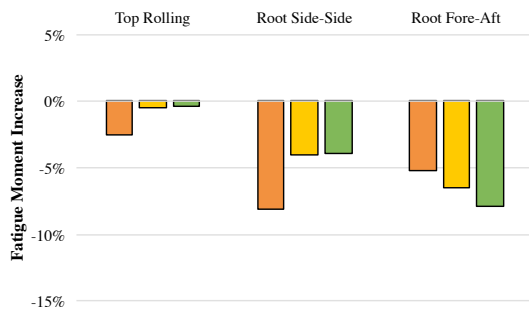
Figure 6.2: Structural optimization: ultimate loads comparison (reference: baseline)



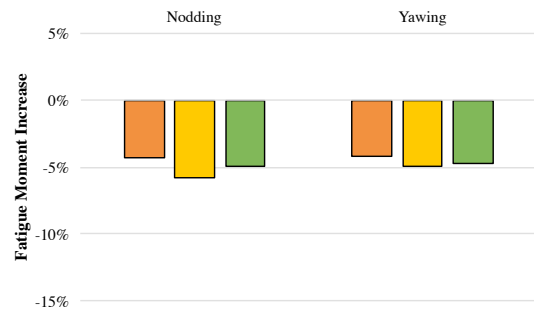
(a) Blade root moments



(b) Blade root torsion



(c) Tower top and root moments



(d) Hub thrust and moments

Figure 6.3: Structural optimization: fatigue loads comparison (reference: baseline)

6.2.3 CoE comparison

The limited extent of load alleviation that is obtained from the considered swept blades on the 10 MW wind turbine does not allow to reduce mass significantly (see Fig. 6.4). Actually, the *sw5* blade has a cost that is approximately the same as the baseline machine, whereas the configuration with the largest tip sweep presents a 10% heavier blade. Energy production performance is worse than for the unswept rotor, however the AEP loss is more limited than the one occurring in the onshore wind turbine, possibly thanks to the much larger size. Nonetheless, even for this machine CoE slightly increases when using swept blades, with higher values for larger tip sweeps, as seen in Fig. 6.5.

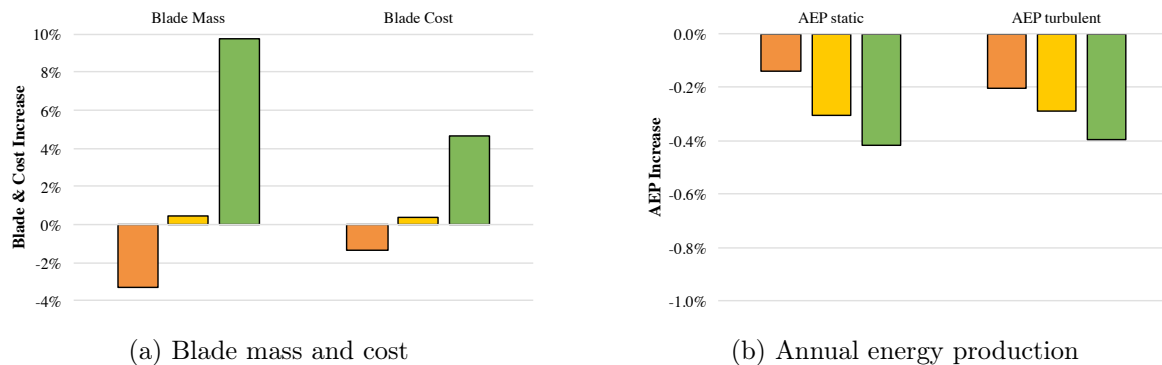


Figure 6.4: Design optimization: mass, cost and AEP comparison (reference: baseline)

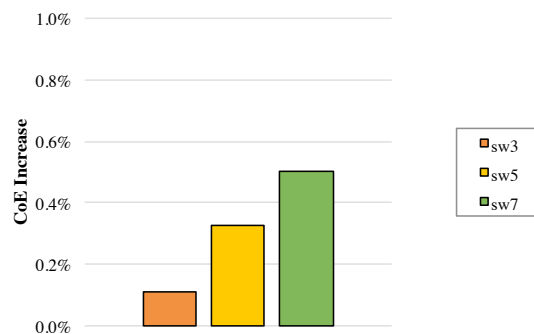


Figure 6.5: Design optimization: cost of energy comparison (reference: baseline)

6.2.4 Conclusions of the design optimization

Results from the optimized design of three backward swept rotors for the 10 MW offshore machine suggest that load alleviation capability may be more limited on this machine and no substantial blade mass reduction is observed. Overall, no evident relationship between load mitigation and tip sweep is found for this machine, possibly due to more complex effects resulting from the much greater blade length that characterizes rotors of this size. In this sense, since load alleviation is rather comparable for all considered sweep curvatures, the most interesting case is arguably the one with the smallest tip sweep as it shows a relatively good mass reduction, which may entail some benefits in such a large scale wind turbine.

However, it must be noted that the study on the 10 MW machine is still at a preliminary stage and there is a great need to further investigate the consequences of sweeping the blades to better quantify losses in AEP, benefits from load relief and the overall impact on CoE.

Conclusion

This thesis focused on the design of swept wind turbine rotors, conducted with an integrated design tool that allows for the simultaneous optimization of blade aerodynamics and structures.

The study began with the sweep curve parametrization, which enabled to account for the swept shape in the simulations. A preliminary analysis demonstrated that tip sweep is the most sensitive parameter affecting key design variables, thus major changes in the sweep curvature were applied mostly by varying the amount of tip sweep. Moreover, it was shown that forward swept blades are not interesting for load alleviation purposes, hence they were not further analyzed.

A more general sweep equation was introduced in order to consider the possibility of creating so-called boomerang shapes, which consist in adding a certain extent of forward sweep in the inboard sections of the blades to make them more aeroelastically balanced.

The potential benefits of this passive load alleviation technique were assessed for two different applications: a 2 MW onshore wind turbine and a 10 MW offshore conceptual machine.

The core of the thesis consisted in the load analysis and successive redesign of the onshore machine, which were possible thanks to the multidisciplinary code `Cp-Max`. The optimization procedure started with the computation of the optimal twist distribution and was followed by the detailed structural sizing of the rotor, while automatically updating the control laws and verifying all significant design constraints at each optimization loop. A reduced set of relevant design load cases was considered so as to evaluate both ultimate loads and fatigue at different locations of the machine, namely blade root, hub, and tower extremes.

On the basis of the results obtained for the 2 MW wind turbine, it is possible to draw the following conclusions about the use of swept blades:

- Operational loads may be substantially mitigated with respect to the unswept rotor with the same diameter. Greater load relief is generally achieved for larger tip sweep.
- Blade root torsion inherently increases when using backward swept blades, but this drawback can be restrained by adopting properly designed boomerang-shaped blades, while the other loads are maintained similar at the same amount of tip sweep.
- Blade mass can be effectively reduced thanks to the lower loads under which the machine is operating, whereas benefits in terms of rotor cost are more limited mainly due to the additional manufacturing expenses required for the more complex blade shape.
- Energy capture performance below rated conditions gets slightly worse due to the reduction in angle of attack originating from the bend-twist coupling effects driving load alleviation.
- Cost of energy, which is the main figure of merit to be considered for wind turbine design, is significantly affected by the loss in annual energy production and therefore increases a little compared to the straight rotor configuration, if the same blade length is kept.
- Sweep may be beneficial because it allows to use larger rotors, thereby gaining in energy harvesting capability while maintaining comparable loads to the original machine, ultimately leading to advantages in terms of cost of energy.

Additionally, an initial analysis of combined swept-prebent blades was performed. This solution was found to produce a very light and flexible wind turbine rotor thanks to the load alleviation deriving from sweep and the increased margin in tower clearance obtained with prebend.

As far as the design of swept rotors for the 10 MW offshore machine is concerned, the analysis conducted seems to suggest that load relief capability is more limited, especially for ultimate loads. However, the results obtained from this initial study need to be integrated by a more comprehensive investigation of the load reduction potential on next generation wind turbines, possibly evaluating more sweep curvatures and maybe introducing boomerang-shaped blades also on the 10 MW machine, since transportability issues are less problematic in offshore applications. Moreover, it would be interesting to analyze the effects of expanded swept rotors on the cost of energy for wind turbines of this size.

7.1 Outlook

The results obtained in this thesis may be taken as a starting point for various kinds of analyses. A larger number of sweep curvatures should be designed, possibly varying not only tip sweep, but also the other two main parameters of the curve, namely the sweep exponent and the span coordinate for sweep curvature start. Additionally, a more detailed study on boomerang-shaped blades should be performed as they may entail significant benefits in terms of mass and load reduction, especially limiting the inherent increase in blade root torsion.

An automatic routine for the optimization of sweep may be implemented in the code, as it would allow to keep the swept shape in the overall optimization process, without the need to manually modify sweep to find the best rotor design. This might be achieved by simultaneously expanding the rotor diameter and limiting the load increase in order to make sweep advantageous in terms of cost of energy, compared to the unswept blade. However, an additional design variable would be required to account for loads in the global optimization loop as well as in the cost model, which represents the main complication against the development of the automatic routine.

Other studies that may be conducted starting from the outcomes of this work include the analysis of combined bend-twist coupling technologies, for instance integrating sweep with off-axis fiber orientation and/or spar cap offset, in order to get even greater load and mass reductions that might lead to benefits in terms of cost of energy, possibly without the need to increase the rotor diameter with respect to the original configuration.

Finally, more advanced cost models may be required to account for the consequences of sweeping blades more properly, especially taking into consideration all the possible undesirable effects on manufacturing complexity and road transportability.

LIST OF FIGURES

2.1	IEA World Energy Scenarios	3
2.2	Global annual installed wind capacity, 2000-2015	4
2.3	Global cumulative installed wind capacity, 2000-2015	4
2.4	Net electricity generating installations in the EU, 1995-2015	4
2.5	Clean energy investments in Europe, 2015	5
2.6	Growth in size of modern wind turbines	6
2.7	Main components of an upwind HAWT	6
2.8	Power coefficient as a function of TSR and β for a given wind turbine	8
2.9	Example of a wind turbine power curve	9
2.10	Example of a Campbell diagram for a wind turbine	11
3.1	Active and passive load control techniques	15
3.2	Illustration of the variable length blade concept	16
3.3	Illustration of aerodynamic drag devices	17
3.4	Response of bend-twist coupled blades to bending loads	18
3.5	Coupling mechanisms in composite plates and beams	19
3.6	Representation of the blade sectional topology with spar cap offset	20
3.7	The swept blade concept	21
3.8	Backward swept blade geometry	22
3.9	Boomerang-shaped blade geometry	23
3.10	Backward vs. forward: blade shape	23
3.11	Backward vs. forward: fatigue DEL variations with respect to baseline	24
3.12	Backward vs. forward: AEP variations with respect to baseline	24
3.13	Results from the sensitivity analysis	25
4.1	Aero-servo-elastic FEM multi-body model	29
4.2	Overall architecture of the integrated aero-structural design procedure	30
4.3	Simplified structure of the integrated aero-structural design procedure	33
4.4	The cost of wind energy	35
4.5	Relative contributions to total mass and total cost	36
4.6	Flattening of the spline associated to the blade	37
4.7	Fixed blade length vs. fixed rotor radius	38
4.8	Representation of the new geometric coordinate system	39
5.1	Chord and twist distribution for the baseline 2 MW wind turbine	42
5.2	Load ranking for blade root combined moment (baseline 2 MW machine)	43
5.3	Sweep curves considered for the load analysis	44
5.4	Load analysis: tip displacement comparison	45
5.5	Load analysis: ultimate loads comparison	45
5.6	Load analysis: blade root combined moment DEL comparison	46
5.7	Load analysis: Weibull DEL comparison	47
5.8	Sweep curves considered for the design optimization of the 2 MW machine	48
5.9	AEP loss before and after twist optimization	48

5.10	Aerodynamic optimization: optimal twist distribution	49
5.11	Structural optimization 2 MW WT: ultimate loads comparison	49
5.12	Structural optimization 2 MW WT: fatigue loads comparison	50
5.13	Design optimization 2 MW WT: mass, cost and AEP comparison	52
5.14	Design optimization 2 MW WT: cost of energy comparison	52
5.15	Sweep curves considered for the larger rotor study	53
5.16	Larger rotor optimization 2 MW WT: ultimate loads comparison	54
5.17	Larger rotor optimization 2 MW WT: fatigue loads comparison	54
5.18	Design optimization 2 MW WT: mass, cost and AEP comparison	55
5.19	Design optimization 2 MW WT: cost of energy comparison	55
5.20	Comparison with larger unswept rotor: blade root combined moment	56
5.21	Comparison with larger unswept rotor: hub nodding moment	56
5.22	Comparison with larger unswept rotor: hub yawing moment	56
5.23	Combined sweep and prebend: fatigue and blade mass comparison	57
5.24	Combined sweep and prebend: AEP and CoE comparison	57
6.1	Sweep curves considered for the design optimization of the 10 MW machine	61
6.2	Structural optimization 10 MW WT: ultimate loads comparison	62
6.3	Structural optimization 10 MW WT: fatigue loads comparison	62
6.4	Design optimization 10 MW WT: mass, cost and AEP comparison	63
6.5	Design optimization 10 MW WT: cost of energy comparison	63

LIST OF TABLES

2.1	Wind turbine classes	12
3.1	Reference swept blade and variations of each sweep curve parameter	25
5.1	Configuration of the baseline 2 MW wind turbine	41
5.2	Spanwise positioning of the airfoils for the 2 MW wind turbine	42
5.3	Blade topology for the 2 MW wind turbine	42
5.4	Ultimate loads for the baseline 2 MW wind turbine	43
5.5	Fatigue loads for the baseline 2 MW wind turbine	43
5.6	Constraint status for the optimal designs	51
6.1	Configuration of the baseline 10 MW wind turbine	59
6.2	Spanwise positioning of the airfoils for the 10 MW wind turbine	59
6.3	Blade topology for the 10 MW wind turbine	60
6.4	Ultimate loads for the baseline 10 MW wind turbine	60
6.5	Fatigue loads for the baseline 10 MW wind turbine	60
6.6	Sweep curve parameters for the 10 MW wind turbine swept blades	61

BIBLIOGRAPHY

- [1] IEA, “Technology roadmap, wind energy,” International Energy Agency, Tech. Rep., 2013.
- [2] UNFCCC, “Paris agreement on climate change,” http://http://unfccc.int/paris_agreement/items/9485.php, December 2015.
- [3] IEA, “Energy technology perspectives,” International Energy Agency, Tech. Rep., 2010.
- [4] GWEC, “Global wind energy outlook 2016,” Global Wind Energy Council, Tech. Rep., 2016.
- [5] EWEA, “Wind in power, 2015 european statistics,” European Wind Energy Association, Tech. Rep., 2016.
- [6] WindEurope, “Making transition work,” WindEurope, Tech. Rep., 2016.
- [7] EWEA, “Design limits and solutions for very large wind turbines,” UpWind Report, Tech. Rep., 2011.
- [8] J. F. Manwell, J. G. McGowan, and A. L. Rogers, *Wind Energy Explained: Theory, Design and Application*, 2nd ed. John Wiley & Sons, 2009.
- [9] energy.gov, “The inside of a wind turbine,” <http://http://www.energy.gov/eere/wind/inside-wind-turbine-0>.
- [10] E. Hau, “Wind turbines: fundamentals, technologies, application, economics,” *Springer: Berlin, Germany*, 2006.
- [11] R. Wilson and P. Lissaman, “Applied aerodynamics of wind power machines,” Oregon State Univ., Corvallis (USA), Tech. Rep., 1974.
- [12] C. Bottasso, A. Croce, Y. Nam, and C. Riboldi, “Power curve tracking in the presence of a tip speed constraint,” *Renewable energy*, vol. 40, no. 1, pp. 1–12, 2012.
- [13] G. Leloudas, W. Zhu, J. Sørensen, W. Shen, and S. Hjort, “Prediction and reduction of noise from a 2.3 mw wind turbine,” *Journal of Physics: Conference Series*, vol. 75, no. 1, 2007.
- [14] B. Harris, *Fatigue in composites: science and technology of the fatigue response of fibre-reinforced plastics*. Woodhead Publishing, 2003.
- [15] *Wind Turbines - Part I: Design Requirements*, 3rd ed., International Standard IEC 61400-1, 2005.
- [16] *Guidelines for the Certification of Wind Turbines*, Germanischer Lloyd, 2010.
- [17] C. van Dam, D. Berg, and S. Johnson, “Active load control techniques for wind turbines,” Sandia National Laboratories, Tech. Rep., 2008.
- [18] E. Bossanyi, “Individual blade pitch control for load reduction,” *Wind Energy*, vol. 6, no. 2, pp. 119–128, 2002.

- [19] M. Geyler and P. Caselitz, "Individual blade pitch control design for load reduction on large wind turbines," in *European Wind Energy Conference*, 2007, pp. 82–86.
- [20] T. van Engelen, "Design model and load reduction assessment for multi-rotational mode individual pitch control," in *European Wind Energy Conference*, 2006.
- [21] E. Bossanyi, B. Savini, M. Iribas, M. Hau, B. Fischer, D. Schlipf, T. Engelen, M. Rossetti, and C. Carcangiu, "Advanced controller research for multi-mw wind turbines in the upwind project," *Wind Energy*, vol. 15, no. 1, pp. 119–145, 2012.
- [22] M. Hand and M. Balas, "Blade load mitigation control design for a wind turbine operating in the path of vortices," *Wind Energy*, vol. 10, no. 4, pp. 339–355, 2007.
- [23] M. Dawson, "Variable length wind turbine blade," Energy Unlimited, Inc., Tech. Rep., 2006.
- [24] J. Korsgaard, "Flexible blade length concept reduces cost of offshore wind energy by up to 10 percent," in *EWEA Offshore*. LM Wind Power, 2015.
- [25] T. Barlas and G. van Kuik, "Review of state of the art in smart rotor control research for wind turbines," *Progress in Aerospace Sciences*, vol. 4, no. 1, pp. 1–27, 2010.
- [26] S. Basualdo, "Load alleviation on wind turbine blades using variable airfoil geometry," *Wind Engineering*, vol. 29, no. 2, pp. 169–182, 2005.
- [27] T. Buhl, M. Gaunaa, and C. Bak, "Potential load reduction using airfoils with variable trailing edge geometry," *Journal of Solar Energy Engineering*, vol. 127, pp. 503–516, 2005.
- [28] T. Barlas, V. Pettas, D. Gertz, and M. H.A., "Extreme load alleviation using industrial implementation of active trailing edge flaps in a full design load basis," in *Journal of Physics: Conference Series*, vol. 753, no. 4, 2016.
- [29] E. Mayda, C. van Dam, and D. Yen-Nakafuji, "Computational investigation of finite width microtabs for aerodynamic load control," *AIAA Conference Wind Energy Symposium*, 2005.
- [30] S. Johnson, J. Baker, C. Van Dam, and D. Berg, "An overview of active load control techniques for wind turbines with an emphasis on microtabs," *Wind Energy*, vol. 13, no. 2-3, pp. 239–253, 2010.
- [31] E. Moreau, "Airflow control by non-thermal plasma actuators," *Journal of Physics D: Applied Physics*, vol. 40, no. 3, 2007.
- [32] J. Lin, "Review of research on low-profile vortex generators to control boundary-layer separation," *Progress in Aerospace Sciences*, vol. 38, no. 4, pp. 389–420, 2002.
- [33] R. Gasch, *Windkraftanlagen*. B. G. Teubner, Stuttgart, 1996.
- [34] D. Lobitz, P. Veers, and P. Migliore, "Enhanced performance of hawts using adaptive blades," Sandia National Laboratories, Tech. Rep., 1996.
- [35] V. Fedorov, C. Berggreen, S. Krenk, and K. Branner, "Bend-twist coupling effects in wind turbine blades," *Dissertation, Technical University of Denmark*, vol. 474, 2012.
- [36] D. Lobitz, P. Veers, and D. Laino, "Performance of twist-coupled blades on variable speed rotors," *ASME Wind Energy Symposium*, 2000.
- [37] P. Veers, G. Bir, and D. Lobitz, "Aeroelastic tailoring in wind-turbine blade applications," in *Proceedings, Windpower*, vol. 98, 1998, pp. 291–304.

- [38] D. Lobitz, P. Veers, G. Eisler, D. Laino, P. Migliore, and G. Bir, “The use of twist-coupled blades to enhance the performance of horizontal axis wind turbines,” *SAND2001-1003, Sandia National Laboratories, Albuquerque, NM*, 2001.
- [39] L. GE Wind Energy, “Advanced wind turbine program next generation turbine development project: June 17, 1997–April 30, 2005,” National Renewable Energy Laboratory (NREL), Golden, CO., Tech. Rep., 2006.
- [40] M. Capellaro and M. Kühn, “Boundaries of bend twist coupling,” in *The Science of Making Torque from Wind*, 2010.
- [41] D. Griffin, “Evaluation of design concepts for adaptive wind turbine blades,” *SAND2002-2424, Sandia National Laboratories Contractor Report*, 2002.
- [42] M. Capuzzi, A. Pirrera, and P. Weaver, “Structural design of a novel aeroelastically tailored wind turbine blade,” *Renewable Energy*, vol. 95, pp. 7–15, 2015.
- [43] C. Bottasso, F. Campagnolo, A. Croce, and C. Tibaldi, “Optimization-based study of bend–twist coupled rotor blades for passive and integrated passive/active load alleviation,” *Wind Energy*, vol. 16, no. 8, pp. 1149–1166, 2013.
- [44] S. Scott, M. Capuzzi, D. Langston, E. Bossanyi, G. McCann, P. Weaver, and A. Pirrera, “Gust response of aeroelastically tailored wind turbines,” in *Journal of Physics: Conference Series*, vol. 753, no. 4, 2016.
- [45] A. Croce, L. Sartori, M. Lunghini, L. Clozza, P. Bortolotti, and C. Bottasso, “Lightweight rotor design by optimal spar cap offset,” in *Journal of Physics: Conference Series*, vol. 753, no. 6, 2016.
- [46] A. Croce, F. Gualdoni, P. Montinari, C. Riboldi, and C. Bottasso, “Inertial and aerodynamic tuning of passive devices for load alleviation on wind turbines,” in *Journal of Physics: Conference Series*, vol. 753, no. 10, 2016.
- [47] C. Bottasso, A. Croce, F. Gualdoni, and P. Montinari, “Load mitigation for wind turbines by a passive aeroelastic device,” *Journal of Wind Engineering and Industrial Aerodynamics*, vol. 148, pp. 57–69, 2016.
- [48] S. Larwood and M. Zuteck, “Swept wind turbine blade aeroelastic modeling for loads and dynamic behavior,” *AWEA windpower*, no. 1–17, 2006.
- [49] B. Liebst, “Wind turbine gust load alleviation utilizing curved blades,” *Journal of Propulsion and Power*, vol. 2, no. 4, pp. 371–377, 1986.
- [50] M. Zuteck, *Adaptive blade concept assessment: curved planform induced twist investigation*. Citeseer, 2002.
- [51] Knight and C. W. Group, “Sweep-twist adaptive rotor blade: final project report,” Sandia National Laboratories, Tech. Rep., 2010.
- [52] D. Verelst and T. Larsen, “Load consequences when sweeping blades - a case study of a 5 mw pitch controlled wind turbine,” Danmarks Tekniske Universitet, Risø Nationallaboratoriet for Bæredygtig Energi, Tech. Rep., 2010.
- [53] S. Larwood, C. van Dam, and D. Schow, “Design studies of swept wind turbine blades,” *Renewable Energy*, vol. 71, pp. 563–571, 2014.

- [54] Siemens, “Living energy: The magazine for international energy leadership,” http://https://w3.siemens.com.cn/energy/cn/zh/news/energy-introduction/Documents/LE_Issue9_En.pdf, July 2013.
- [55] C. Pavese and T. Kim, “Implementation of passive control strategies through swept blades,” in *10th EAWE PhD Seminar on Wind Energy in Europe*, 2014, pp. 92–95.
- [56] Y. Ding and X. Zhang, “An optimal design method of swept blades for hawts,” *Journal of renewable and sustainable energy*, vol. 8, no. 4, 2016.
- [57] J. de Vaal, T. Nygaard, and R. Stenbro, “Developing a passive load reduction blade for the dtu 10 mw reference turbine,” in *Journal of Physics: Conference Series*, vol. 753, 2016.
- [58] C. Bottasso, P. Bortolotti, A. Croce, and F. Gualdoni, “Integrated aero-structural optimization of wind turbines,” *Multibody System Dynamics*, pp. 1–28, 2015.
- [59] S. Ning, R. Damiani, and P. Moriarty, “Objectives and constraints for wind turbine optimization,” *Journal of Solar Energy Engineering*, vol. 139, no. 4, 2014.
- [60] J. Méndez and D. Greiner, “Wind blade chord and twist angle optimization by using genetic algorithms,” in *Proceedings of the Fifth International Conference on Engineering Computational Technology*, vol. 6, 2006, pp. 12–15.
- [61] W. Xudong, W. Shen, W. Zhu, J. Sørensen, and C. Jin, “Shape optimization of wind turbine blades,” *Wind Energy*, vol. 12, no. 8, pp. 781–803, 2009.
- [62] M. Jureczko, M. Pawlak, and A. Mezyk, “Optimisation of wind turbine blades,” *Journal of materials processing technology*, vol. 167, no. 2, pp. 463–471, 2005.
- [63] D. Laird, “Numad: blade structural analysis,” *Wind Turbine Blade Workshop, Sandia National Laboratories*, 2008.
- [64] P. Fuglsang and M. H.A., “Optimization method for wind turbine rotors,” *Journal of Wind Engineering and Industrial Aerodynamics*, vol. 80, no. 1, pp. 191–206, 1999.
- [65] L. Fuglsang, “Integrated design of turbine rotors,” *European Wind Energy Conference & Exhibition*, 2008.
- [66] N. Duineveld, “Structure and possibilities of the focus design package,” *Dutch WInd Workshops, TU Delft*, 2008.
- [67] M. Døssing, “Optimization of wind turbine rotors-using advanced aerodynamic and aeroelastic models and numerical optimization,” Ph.D. dissertation, Technical University of Denmark, Risø National Laboratory for Sustainable Energy, 2011.
- [68] K. Dykes, A. Ning, R. King, P. Graf, G. Scott, and P. Veers, “Sensitivity analysis of wind plant performance to key turbine design parameters: A systems engineering approach,” in *32nd ASME Wind Energy Symposium, National Harbor, Maryland*, 2014.
- [69] K. Maki, R. Sbragio, and N. Vlahopoulos, “System design of a wind turbine using a multi-level optimization approach,” *Renewable Energy*, vol. 43, pp. 101–110, 2012.
- [70] T. Ashuri, M. Zaaijer, J. Martins, G. van Bussel, and G. van Kuik, “Multidisciplinary design optimization of offshore wind turbines for minimum levelized cost of energy,” *Renewable Energy*, vol. 68, pp. 893–905, 2014.
- [71] P. Bortolotti, C. Bottasso, and A. Croce, “Combined preliminary–detailed design of wind turbines,” *Wind Energy Science*, vol. 1, pp. 71–88, 2016.

- [72] C. Bottasso, F. Campagnolo, and A. Croce, “Multi-disciplinary constrained optimization of wind turbines,” *Multibody System Dynamics*, vol. 27, no. 1, pp. 21–53, 2012.
- [73] C. Bottasso and A. Croce, *Cp-Lambda: User’s Manual*, Dipartimento di Scienze e Tecnologie Aerospaziali, Politecnico di Milano, 2010.
- [74] O. Bauchau, A. Epple, and C. Bottasso, “Scaling of constraints and augmented lagrangian formulations in multibody dynamics simulations,” *Journal of Computational and Nonlinear Dynamics*, vol. 4, no. 2, 2009.
- [75] O. Bauchau, C. Bottasso, and L. Trainelli, “Robust integration schemes for flexible multi-body systems,” *Computer Methods in Applied Mechanics and Engineering*, vol. 192, pp. 395–420, 2003.
- [76] M. Hansen, *Aerodynamics of wind turbines*, 3rd ed. Routledge, 2015.
- [77] *MATLAB*, The MathWorks Inc., 3 Apple Hill Drive, Natick, MA 01760-2098, USA.
- [78] B. Jonkman and L. Kilcher, *TurbSim User’s Guide*, NREL, 2012.
- [79] V. Giavotto, M. Borri, P. Mantegazza, G. Ghiringhelli, V. Carmaschi, G. Maffioli, and F. Mussi, “Anisotropic beam theory and applications,” *Computers & Structures*, vol. 16, no. 1-4, pp. 403–413, 1983.
- [80] C. Bottasso, F. Campagnolo, A. Croce, S. Dilli, F. Gualdoni, and M. Nielsen, “Structural optimization of wind turbine rotor blades by multilevel sectional/multibody/3d-fem analysis,” *Multibody System Dynamics*, vol. 32, no. 1, pp. 87–116, 2014.
- [81] *NASTRAN 2012 Quick Reference Guide*, MSC Software, 2012.
- [82] EWEA, “The economics of wind energy,” European Wind Energy Ass., Tech. Rep., 2009.
- [83] L. Fingersh, M. Hand, and A. S. Laxson, “Wind turbine design cost and scaling model,” *NREL Technical Report*, 2006.
- [84] INNWIND.EU, “Deliverable 1.23, pi-based assessment of innovative concepts (methodological issues),” INNWIND.EU, Tech. Rep., 2014.
- [85] D. Griffith and W. Johanns, “Large blade manufacturing cost studies using the sandia blade manufacturing cost tool and sandia 100-meter blades,” *Sandia National Laboratories Technical Report*, 2013.
- [86] L. Piegl and W. Tiller, *The NURBS book*, 2nd ed. Springer, 1997.
- [87] N. Timmer and R. van Rooij, “Summary of the delft university wind turbine dedicated airfoils,” *Journal of Solar Energy Engineering*, vol. 125, 2003.
- [88] L. Sartori, P. Bortolotti, A. Croce, and C. Bottasso, “Integration of prebend optimization in a holistic wind turbine design tool,” in *Journal of Physics: Conference Series*, vol. 753, no. 4, 2016.
- [89] C. Bak, F. Zahle, R. Bitsche, T. Kim, A. Yde, L. Henriksen, M. Hansen, J. Blasques, M. Gaunaa, and A. Natarajan, “The dtu 10-mw reference wind turbine,” *Danish wind power research*, 2013.
- [90] A. Björck, “Coordinates and calculations for the ffa-w1-xxx, ffaw2-xxx and ffa-w3-xxx series of airfoils for hawt,” *The Aeronautical Research Institute of Sweden*, 1990.